UNIVERSITÀ
DEGLI STUDI
DI PADOVA

Sede Amministrativa: Università degli Studi di Padova

Dipartimento di GEOSCIENZE

SCUOLA DI DOTTORATO DI RICERCA IN SCIENZE DELLA TERRA
CICLO: XXVI

RECONCILING SEDIMENTOLOGY AND NUMERICAL MODELLING TO INVESTIGATE TECTONICALLY-DRIVEN DEPOSITION AND LANDSCAPE EVOLUTION WITHIN UPLAND INCISED VALLEYS: THE PLIOCENE – PLEISTOCENE AMBRA VALLEY-FILL (TUSCANY, ITALY)

Direttore della Scuola: Prof. Massimiliano Zattin

Supervisore: Dr. Massimiliano Ghinassi

Co-supervisore: Dr. Tristan Salles

Dottorando: Valeria Bianchi

Regola #26

“Tutto è bene quel che finisce”

Rules #26

“All is well that ends”

Table of contents

ABSTRACT

Sedimentation in the upstream reaches of incised valleys is predominantly fluvial and mostly out from any relative sea level fluctuations. Here, the dynamics of facies distribution respond to an interaction of tectonics and climate. Tectonics can directly influence fluvial aggradation and degradation through local changes in gradient, both longitudinal and transverse to the valley slope.

This paper deals with a –Pliocene – Pleistocene fluvial valley fill developed in the northeastern shoulder of the Siena Basin (Northern Apennines, Italy). Valley fill aggradation resulted from the interaction of autogenic dynamics and extensional tectonics manifested by normal and oblique-slip faults parallel and near orthogonal to the valley axis, which generated rises of local fluvial base level.

This thesis coupled a classical field approach, which aims at analysing the interaction between longitudinal and lateral alluvial plain tectonic tilting and fluvial sedimentation, and numerical modelling, which focuses on the temporal and spatial validation of tectonic forcing on the studied valley fill and on the effects of uplift rate on variable-discharge systems.

Longitudinal tilting was generated by a transverse, upstream-dipping normal fault that controlled aggradation of fining-upward strata-sets both upstream and downstream of the fault zone. Aggradation in the upstream sector occurred as a backfilling process and predated that in the downstream one, where sediment was stored as a downfilling. Lateral tilting, spacing out the aggradations, was governed by the interaction between fault-generated subsidence and the topographic confinement of progradational, flank-sourced alluvial fans. Both longitudinal and lateral tilting anomalies are easily recorded in sedimentary succession generated by high-discharge system disturbed by high uplift rates.

RIASSUNTO

Nel tratto prossimale di un sistema di valle incisa la sedimentazione fluviale risulta indipendente dalle variazioni eustatiche; pertanto la distribuzione delle diverse facies sedimentarie rispecchia principalmente l'interazione tra tettonica e clima. Una tettonica sindeposizionale può portare ad aggradazione o degradazione di depositi fluviali a causa di variazioni locali di gradiente sia longitudinale che trasversale dello *slope* della valle.

Questo lavoro focalizza sulla successione di riempimento Plio-Pleistocenico di una valle sviluppatasi sul margine N-E del Bacino di Siena (Appennino Settentrionale, Italia). L'aggradazione di questa successione è il risultato dell'interazione tra dinamiche autogeniche ed allogeniche, manifestate da faglie normali con componente obliqua che presentano un'orientazione variabile da parallela ad ortogonale alla direzione dell'asse della valle e sono causa di un sollevamento localizzato rispetto al livello di base fluviale.

La tesi integra un tradizionale approccio di campagna, finalizzato all'analisi dell'interazione tra il tilting longitudinale e laterale della piana alluvionale e la sedimentazione fluviale, con un'analisi basata su modellizzazione numerica, che risulta volta a convalidare il controllo spazio-temporale della tettonica sulla sedimentazione e ad analizzare gli effetti del diverso tasso di sollevamento su sistemi fluviali a diversa portata.

Il tilting longitudinale della piana alluvionale è generato da una faglia normale immergente sopracorrente, la cui attività induce l'aggradazione di depositi con trend granulometrico tipo *fining-upward* sia sopracorrente che sottocorrente rispetto alla zona di faglia. A monte della zona di faglia, l'aggradazione avviene principalmente tramite un processo di backfilling e precede l'accumulo nelle aree sottocorrente, che si verifica secondo un processo di downfilling. Il tilting laterale è causato da subsidenza localizzata ed induce lo spostamento laterale del principale sistema di drenaggio, che risulta anche influenzato da apporti provenienti dai fianchi della valle.

CHAPTER 1

INTRODUCTION

1.1 OVERVIEW

This study – dealing with fluvial successions accumulated in inland valleys under the influence of localised tectonic disturbance – aims at defining the tectono-sedimentary dynamics in relation to the architecture of resulting alluvial successions. A Pliocene – Pleistocene fluvial succession exposed along the northern margin of the Siena Basin (Northern Apennines, Italy) was analysed with a multidisciplinary approach based on the integration of sedimentological and geophysical data with numerical modelling.

1.2 STATE OF THE ART

1.2.1 Incised valleys

During the flourishing of hydrocarbon exploration, the interest in ancient valley fills significantly increased due to their high economic potential as productive reservoirs (Zaitlin & Schulz, 1984; Posamentier & Vail, 1988; Posamentier *et al.*, 1988; Howard & Whitaker, 1990; Van Wagoner *et al.*, 1990; Dolson *et al.*, 1991; Shanley & McCabe, 1991; Brown, 1993; Wright & Marriott, 1993; Dalrymple *et al.*, 1994). A large percentage of global siliciclatic reservoirs are hosted within incised-valley systems (Brown, 1993), and a clear understanding of their internal architecture and facies distribution is, therefore, crucial for reservoir detection and development (Boyd *et al.*, 2006). Van Wagoner *et al.* (1990) suggested some key criteria for the identification of incised valleys: i) the occurrence of a significant erosional surface cutting older strata; ii) the association of

fluvial or estuarine strata on marine deposits; iii) the existence of a significant basinward shift in facies, with subaerial exposure on interfluves (see also Zaitlin *et al.*, 1994; Boyd *et al.*, 2006). Nonetheless, modern analogues for incised valleys as described by Van Wagoner *et al.* (1990), are commonly buried beneath Holocene delta plains or are submerged on the shelves, and no longer have a morphological expression. Incised valleys are complex sedimentary environments, since their genesis and development are widely controlled by factors (Fig. 1.1), whose influence varies depending on the distance from the palaeocoastline (Wright & Marriott, 1994; Dalrymple *et al.*, 1994; Boyd *et al.*, 2006).

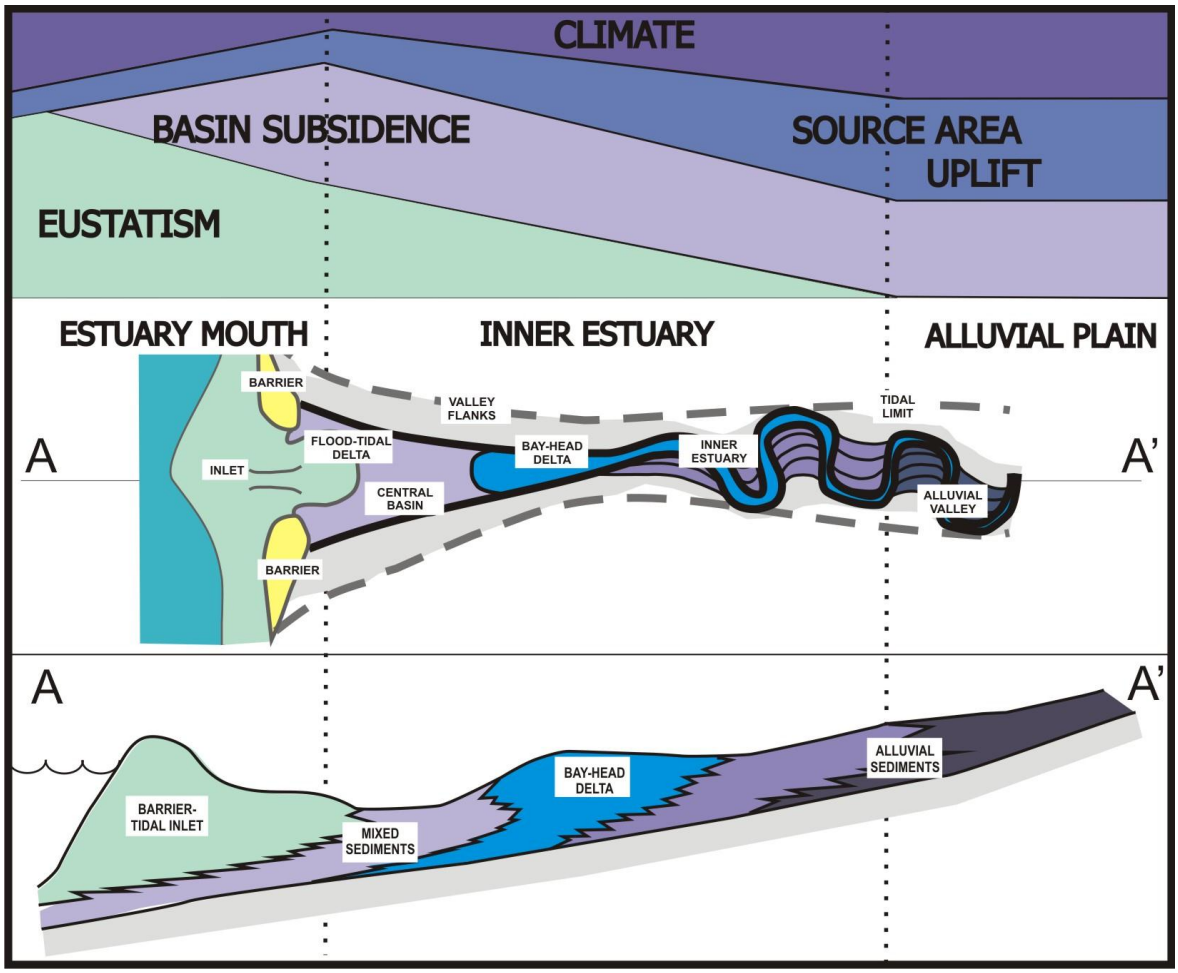

Figure 1.1: Schematic representation on forcing distribution along an incised valley depending on the distant of the palaeo-coastline and manifesting different type of sedimentation. Modified after Shanely & McCabe (1991), Dalrymple *et al.* (1994).

Even though different types of valley-fill successions have been described and different classifications have been proposed (Aslan & Blum, 1999; Blum & Tornqvist, 2000; Dalrymple, 2006; Simms *et al.*, 2006; Gibling *et al.*, 2011), the distance from the palaeocoastline is a key parameter (Fig. 1.1) that distinguishes marine-controlled reaches downstream from fluvial-influenced reaches upstream (Zaitlin *et al.*, 1994; Gibling *et al.*, 2011). Downstream valley reaches are cut and filled in response to relative sea-level fluctuations (Fig. 1.2A; Allen & Posamentier, 1993; Dalrymple *et al.*, 1994; Li *et al.*, 2006; Simms *et al.*, 2006; Breda *et al.*, 2009), whose influence can control inland sedimentation (Fig. 1.2B) up to 400 km from the coast (Blum & Tornqvist, 2000; Gibling *et al.*, 2011). In contrast, the upstream valley reaches (i.e. inland valleys) are characterised by: i) solely fluvial sedimentation (Dalrymple *et al.*, 1994; Zaitlin *et al.*, 1994); ii) a coarse-grained infill

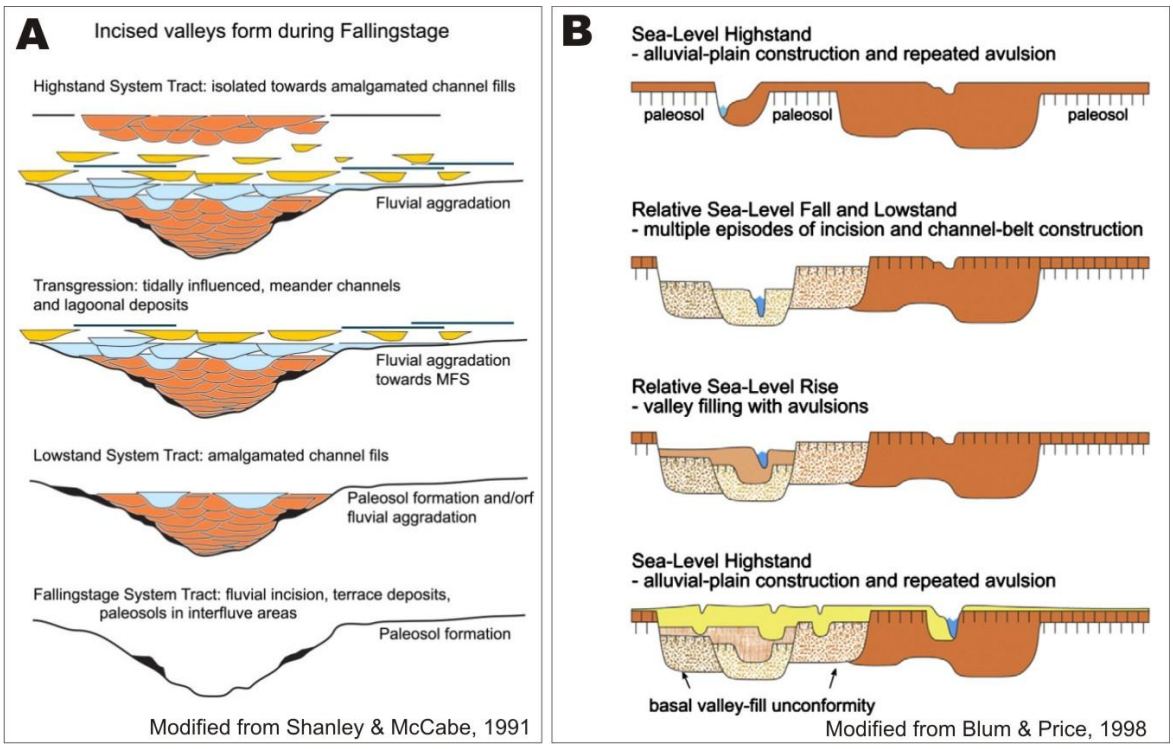

Figure 1.2: A) Sequence stratigraphic sketch on downstream valley reaches cut and filled in response to relative sea-level oscillations. B) Sequence stratigraphic sketch on upstream valley reaches, characterised by a dominant fluvial sedimentation, cut and filled by several factors, as tectonic, climate and relative sea-level fluctuation.

(Vincent, 2001; Fielding *et al.*, 2007); iii) an infilling occurring beyond the influence of relative-sea level oscillations (Currie, 1997; Legarreta & Uliana, 1998; Martinsen *et al.*, 1999); iv) a development under the complex interaction between tectonics, climate and drainage evolution (Shanley & McCabe, 1991, 1994; Blum & Tornqvist, 2000; Holbrook, 2001; Gibling *et al.*, 2011).

Seaward reaches are widely described in terms of the classical estuary model (Dalrymple *et al.*, 1994; Boyd *et al.*, 2006; Gibling, 2006; Simms et al., 2006; Blum & Womack, 2009; Blum *et al.*, 2013), whereas minor attention has been given to the landward reaches (Gibling *et al.*, 2011).

1.2.2 Inland valleys and tectonics

Inland valleys are poorly understood because their infill is either rarely preserved due to erosion, or when present, it is hard to distinguish in the stratigraphic record because of the similar sediment composition between intra-valley and extra-valley deposits (Gibling *et al.*, 2011). Although they are poorly documented, fillings of Quaternary upstream valleys appear to archive precious information about the tectonic evolution of inland areas (Gibling *et al.*, 2011; Blum *et al.*, 2013). The effects of tectonics on fluvial sedimentation have been described for modern rivers (Schumm, 1986; Guiseppe & Heller, 1998; Holbrook & Schumm, 1999) and laboratory experiments (Ouchi, 1985; Lague *et al.*, 2003; Hickson *et al.*, 2005; Turowski *et al.*, 2006), concluding that rivers are extremely sensitive to tectonic modifications, both in terms of morphology and channel behaviour. The fluvial response to tectonic disturbance can be manifested in terms of: i) changes of geomorphic features and fluvial style (Twidale, 1971; Ouchi, 1985;; Blum & Tornqvist, 2000; Gibling *et al.*, 2011); ii) modification of the equilibrium profile

(Dalrymple, 2006); iii) alternation between aggradation and degradation (Shanley & McCabe, 1991; Holbrook & Schumm, 1999); iv) channel avulsion (Bryant *et al.*, 1995).

Large and mature structural highs, such as the U.S. Colorado and Tibetan plateaus, may denote an easy identification of warpings (Holbrook & Schumm, 1999). Small and/or incipient epeirogenic warpings that are hidden by the landscape may be difficult to detect in modern settings, and present an even bigger challenge to be recognised in ancient ones (Holbrook & Schumm, 1999). Several studies focused on the effects of subsidence on fluvial dynamics (Leeder, 1978; Hickson *et al.*, 2005), but only few of them took into account the effects of localised uplift and relative valley-slope perturbation (Burnett & Schumm, 1983; Ouchi 1985; Pazzaglia & Brandon, 2001). Rapid uplift (>10 mm/y) of specific valley segments can result in valley flooding (e.g. New Madrid earthquake, Russ, 1982) or dramatic avulsions (e.g. Indus Valley, Dales, 1966; Hole, 2011). The effects of these localised uplifts on valley-fill aggradation are poorly known (Holbrook & Schumm, 1999), and this gap is even more relevant when we consider the fossil record (Guiseppe & Heller, 1998; Holbrook & White, 1998; Vincent, 2001), where the effects of other forcings could hide the tectonic signature.

1.3 GOALS OF THE STUDY

Scarce knowledge on tectonically-influenced fluvial successions raises queries concerning the dynamics of their accumulation and development of stratal architectures: i) how does tectonic activity control fluvial aggradation within upstream valley reaches? ii) how do tectonically-controlled fluvial valley-fills differ from those controlled by relative sea-level fluctuations?

The present work contributes to unravelling these issues by analysing a Pliocene – Pleistocene fluvial valley-fill through the integration of sedimentological and geophysical data with numerical modelling. The succession is exposed along the northern margin of the Siena Basin, one of the main Neogene-Quaternary depressions (Fig. 1.3) that developed on the Northern Apennines (Italy) as superficial response to a lithospheric scale extension (Carmignani *et al.*, 1994, 1995, 2001; Brogi, 2008; Barchi, 2010). The studied valley-fill accumulated beyond the influence of relative sea-level changes (Aldinucci *et al.*, 2007), and its upper part developed from the interaction between the southward-draining fluvial system and two normal faults, named here Ambra River and Terre Rosse faults.

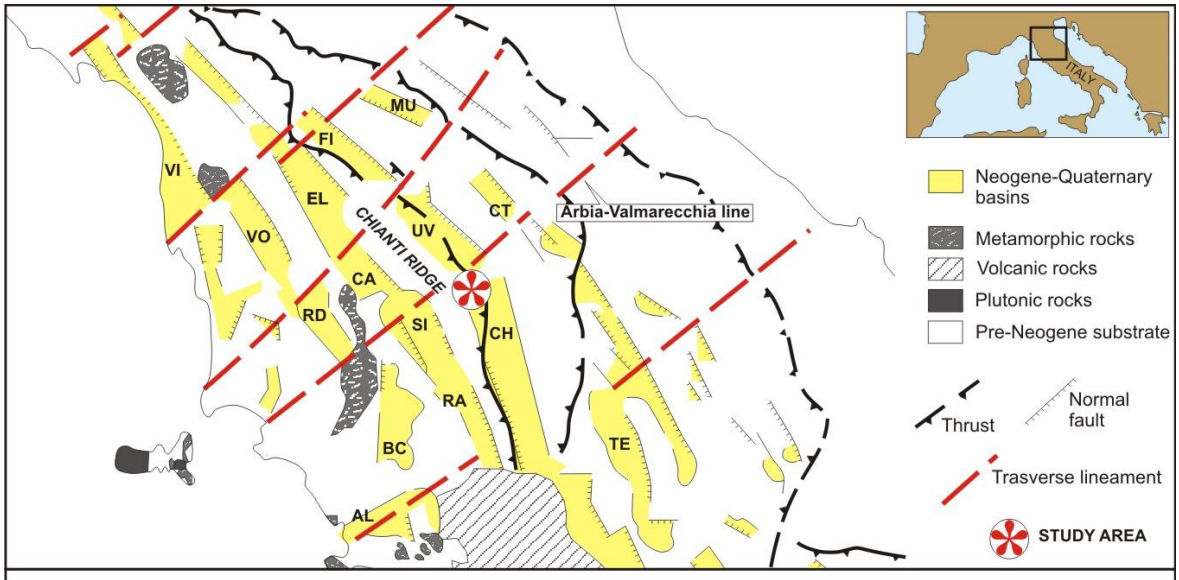

Figure 1.3: Simplified geological sketch of the Northern Apennines showing the Neogene-Quaternary basins bounded by bedrock ridges and main tectonic features.

The present work was carried out in two steps. The first one was based on a "classical" sedimentological and stratigraphic approach aimed at: i) analysing the effects

of tectonics on the spatial distribution of aggradation and degradation processes; ii) exploring the role of tectonics on fluvial sedimentation within a confined setting; iii) investigating the relationship between tectonics and valley avulsion. The second step focused on numerical modelling of landscape evolution, a newly developed approach to geosciences (e.g., Dietrich *et al.*, 2003; Bonnet & Crave, 2003; Braun & van der Beek, 2004; Willgoose, 2005; Paola *et al.*, 2009; Tucker & Hancock, 2010), which aimed to: i) calibrate time and modes of aggradation for the study succession; ii) compare the results with the classical models used to explain fluvial morphodynamics in tectonically active areas; iii) develop generic models and analyse the impact of fluvial discharge and uplift rate on developing fluvial architectures.

1.4 THESIS OUTLINE

The present work is presented through five chapters.

Chapter 2 and **Chapter 3** deal with the sedimentology and stratigraphy of the study area, respectively. Chapter 2 summarises the results of a high-resolution field mapping, which was required to outline geometries and facies distribution within the main sedimentary units forming the valley-fill succession. The results of this work were published in Journal of Maps (Bianchi *et al.*, 2013. DOI: 10.1080/17445647.2013.829412) and include a geological map at 1:20:000 scale which is attached to the present thesis. Chapter 3 goes deeper into the stratigraphic issues to analyse and discuss the study succession in terms of sedimentology, structural geology and geophysics. The main body of this chapter has been submitted to Sedimentology (Bianchi et al., SED – 2014 – OM – 013).

Chapter 4 discusses a numerical modelling simulation for the study succession and some generic models that analyse similar tectono-sedimentary scenarios. This chapter will provide material for a further publication, which is currently in preparation.

Chapter 5 summarises the main results of this thesis.

CHAPTER 2

GEOLOGICAL MAP OF PLIOCENE-PLEISTOCENE DEPOSITS OF THE AMBRA AND OMBRONE VALLEYS (NORTHERN SIENA BASIN, TUSCANY, ITALY)

2.1 OVERVIEW

This chapter is a journal paper published in Journal of Maps. Geological setting of the Plio-Pleistocene Ambra palaeovalley (Northern Apennines, Italy) is presented, with particular emphasis to the spatial distribution of the valley-fill deposits. This paper illustrates a detailed geological map of an area of about 20 km^2. The map was published at a 1:20.000 scale and is attached to this thesis. It aims at refining the stratigraphy of the Pliocene - Pleistocene deposits exposed along the eastern margin of Siena Basin, and highlight the relationship between tectonic activity and the sedimentary evolution of the northern Siena Basin during Pliocene-Pleistocene time span.

2.2 PAPER

VALERIA BIANCHI[1], MASSIMILIANO GHINASSI[1], MAURO ALDINUCCI[2], NICOLA BOSCAINI[3], IVAN MARTINI[4], GIORGIA MOSCON[1], MARCELLA RONER[1]

[1]*Dept. of Geosciences, University of Padova, via Gradenigo 6, 35131 Padova, Italy.*

[2]*Weatherford Petroleum Consultants A.S., Folke Bernadottesvei 38 5147 Fyllingsdalen, Bergen, Norway.*

[3]*Via J. F. Kennedy 14, Sant'Ambrogio di Valpolicella, 37010 Verona, Italy*

[4]*Dept. of Environment, Earth and Physical Sciences, University of Siena, via Laterina 8, 53100 Siena, Italy.*

2.2.1 Abstract

The study area is located across the Chianti Ridge (Tuscany, Italy), between the Upper Valdarno Basin and the Siena Basin. This area covers about 25 km^2, forming a narrow belt oriented N–S and drained by the Ambra and Ombrone Rivers, which flow northward and southward, respectively. Field mapping was carried out at 1:10,000 scale through an allostratigraphic-sedimentological approach. The study deposits represent the infill of a SW-draining paleovalley, cut both in pre-Neogene bedrock and marine Pliocene deposits of the Siena Basin. The valley-fill succession consists of two main allounits, named here as V1 and V2. V1 comprises gravelly to sandy fluvial deposits, whereas V2 deposits show noticeable downvalley variability. V2 consists of poorly-drained floodplain deposits in the northern sector of the paleovalley, whereas gravel and sand-bed river deposits fill its southern part. Alluvial-fan and palustrine deposits are also associated with V2 fluvial facies. A normal fault trending NW–SE is the main structural feature of the area. This fault cuts the V2 unit lowering the upstream reach and is thought to have promoted the marked facies changes observed in the fluvial deposits of unit V2.

Keywords: fluvial deposits, incised valley, Siena Basin.

2.2.2 Introduction

The study area (Fig. 2.1A), located on the northern margin of the Siena Basin (Tuscany, Italy), has been the target of geological studies since the beginning of the 80's. Specifically, Costantini *et al.* (1982) focused on the deposits exposed in the southern part of the study area in the framework of their relationship with the Pliocene Siena Basin, whose alluvial nature was firstly recognized by Magi (1992). Furthermore, the

geomorphological features of the Ambra Valley and its relationships with the Pleistocene depositional evolution of Upper Valdarno Basin (Fig. 2.1A) were discussed by Costantini *et al.* (1995). More recently, Aldinucci *et al.* (2007) interpreted the alluvial deposits cropping out in the southern part of the study area as the Plio–Pleistocene infill of an incised-valley. This interpretation was also reported by Lazzarotto *et al.* (in press) in the frame of the geological mapping project of Carta Geologica d'Italia (Foglio 297-Asciano. ISPRA)

Although increasing attention has been paid to the alluvial post-Middle Pliocene deposits of this area, their spatial distribution and internal architecture is still poorly known, as well as their sedimentary history.

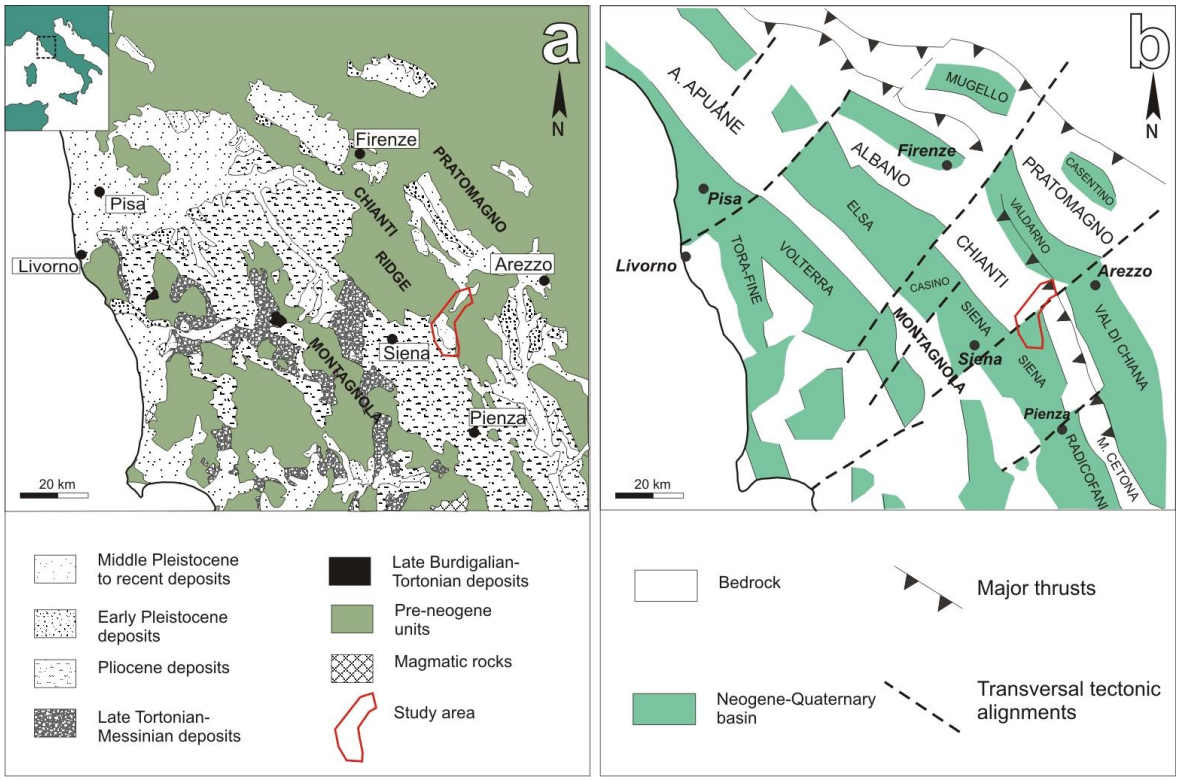

Figure 2.1: Northern Apennines. A) Geological sketch map of Tuscany; B) Schematic structural map of the area shown in A.

The present study was carried out through detailed field mapping, according to sedimentological and allostratigraphic principles, in order to refine the stratigraphy of the Pliocene - Pleistocene deposits exposed along the eastern margin of Siena Basin. This

work aims also at clarifying the relationship between tectonic activity and the sedimentary evolution of the northern Siena Basin during Pliocene-Pleistocene time span. The study area is located in central Tuscany (about 70 km south of Florence), between the Upper Valdarno Basin and the Siena Basin (Fig. 2.1A and B). It represents a N-S oriented belt along the so-called "Arbia-Val Marecchia line" (one of the main tectonic transverse lineaments of the Northern Apennines, Liotta, 1991; Pascucci *et al.*, 2007), and extending from the north-eastern margin of the Siena Basin into the Chianti Ridge (Fig. 2.1A) (Brogi, 2011a). The northern and southern parts of this area are presently drained by the Ambra and Ombrone Rivers, respectively. Specifically, the Ambra River flows northward, towards Upper Valdarno Basin, whereas the Ombrone River drains southward and belongs to the catchment of the Siena Basin (Fig. 2.1A).

2.2.3 Geological Setting

The Northern Apennines are a Tertiary fold-and-thrust belt resulting from the interaction between the Adria and Corsica–Sardinian microplates, in the framework of the larger-scale collision of Africa with Eurasia (Carmignani *et al.*, 2001 and references therein). The Northern Apennines tectonic pile consists of several stacked tectonic units representing different paleogeographical zones, ranging from western (internal) oceanic areas (Ligurian units) to eastern continental domains (Tuscan and Umbria-Marche units), with an intervening area of transitional crust (Subligurides units). The geological history of the Northern Apennines reflects a compressional-extensional orogenic cycle (Elter *et al.*, 1975; Carmignani *et al.*, 1994, 1995; Liotta *et al.*, 1998; Brogi, 2008; Barchi, 2010), with compression dating back to the Late Cretaceous - Paleocene and following the closure of the Ligurian-Piedmont Ocean in the inner Northern Apennines (i.e. southern Tuscany).

The extensional tectonics started in the Early (Tyrrhenian area, Carmignani *et al.*, 1995) – Middle (southern Tuscany, Brogi & Liotta, 2008) Miocene and coexisted with the compressional tectonics in the outer Northern Apennines. This extensional tectonics gave rise to detachment basins, which were successively dissected by high-angle normal faults showing listric geometries (Dallmayer & Liotta, 1998; Brogi *et al.*, 2003; Brogi, 2008; Brogi, 2011b) and leading to the modern "horst and graben" configuration (Fig. 2.1B). This extensional basin pattern was described in detail by Martini & Sagri (1993). These authors distinguished between "peripheral" and "central" basins, which were located close to the Apenninic divide and the Tyrrhenian Sea, respectively. The central basins were filled by upper Miocene – Middle Pliocene deposits, whereas the peripheral ones experienced a Pliocene – Pleistocene continental sedimentation.

Neogene – Quaternary basins (Fig. 2.1B) are separated by bedrock ridges trending NW–SE (e.g. Chianti Ridge) and transversal lineaments trending NE–SW (e.g. so called "Arbia-Val Marecchia line"; Liotta, 1991; Pascucci *et al.*, 2007). Although their origin is still debated, transversal lineaments are thought to represent the link between areas with different rate of extension and shortening (Castellarin *et al.*, 1986; Liotta, 1991; Pascucci *et al.*, 2007).

The fill of the Upper Valdarno Basin comprises fluvio-lacustrine deposits up to 550 m thick, subdivided into four main unconformity-bounded stratigraphic units (Fidolini et al., 2013a; Ghinassi et al., 2013). The Siena Basin (Brogi, 2011a) was filled with about 1000 m of Miocene continental deposits unconformably overlain by about 600 m of Pliocene alluvial to shallow marine deposits (Costantini *et al.*, 1982; Martini *et al.*, 2011, 2013). The stratigraphic architecture of Pliocene deposits is relatively poorly known, except for some areas, recently investigated according to allostratigraphic and sequence-stratigraphic

principles (Arragoni *et al.*, 2012; Martini *et al.*, 2011, 2013). Specifically, according to Martini *et al.* (2011) the Pliocene deposits of the northern basin margin (alluvial-to-inner shelf marine sediments) are organised in four allostratigraphic units. Marine sedimentation ended in the latest Piacenzian, when an overall uplift of southern Tuscany resulted in subaerial exposure and sedimentation of Pleistocene alluvial deposits (Costantini *et al.*, 1982; Martini & Sagri, 1993).

2.2.4 Methods

The present work provides a high-resolution map (1:20,000) covering about 25 km2, from the area of Capannole village to the neighbourhood of Rapolano Terme village, and focuses on the continental deposits accumulated from the earliest Late Pliocene (Piacenzian) to the Middle Pleistocene (Ionian). Field mapping was performed at 1:10,000 scale using the "Carta Tecnica Regionale" topographic map (sections: 287080, 287120, 287150, 287160, 288050, 288090, 288130, 297030, 297040, 297070, 297080, 297110 and 297120). Field mapping was carried out through an allostratigraphic-sedimentological approach, based on facies analysis principles. The mapped deposits represent different sedimentary environments (i.e. facies associations) that were subdivided in allounits, namely stratigraphic units bounded by both unconformities and correlative-conformity surfaces (North American Commission on Stratigraphic Nomenclature, 1983). Facies association mapping was adopted since it is a powerful tool to define depositional history and basin-scale geometry of sedimentary successions (Ghinassi *et al.*, 2009; Martini *et al.*, 2011, 2013; Arragoni *et al.*, 2012). Allounits are preferred to depositional sequences (Vail *et al.*, 1977), UBSU (Salvador, 1987) or synthems (Chang, 1975; International Subcommission on Stratigraphic Classification, 1987; Salvador, 1994) because of their

wide applicability in narrow confined basins characterized by erosional, non depositional and correlative-conformity surfaces, either in marginal or depocentral areas.

2.2.5 Stratigraphy

The studied deposits overlie unconsolidated, alluvial to shallow-marine Zanclean to Piacenzian sediments of the Siena Basin and pre-Neogene bedrock (i.e. Ligurian, Subligurian and Tuscan units).

2.2.5.1 Pre-Neogene bedrock

Ligurian units are represented by siliciclastic (Santa Fiora Fm., Cretaceous–Paleocene) and calcareous (Mt. Morello Fm., Eocene) turbiditic deposits (Abbate & Sagri, 1982; Abbate *et al.*, 1986; Boccaletti *et al.*, 1990; Lazzarotto *et al.*, in press). The Santa Fiora Formation is made of grayish mud-siltstone strata intercalated by limestone and fine calcarenitic. The Monte Morello Formation is composed of grayish to brownish limestone and marl-limestone strata, with intercalations of marl and calcarenites layers.

Subligurian units are characterized by turbiditic deposits of the Paleocene–Eocene Argille e Calcari di Canetolo Fm. (Bruni *et al.*, 2007) and Oligocene Arenarie di Mt. Senario Fm. (Lazzarotto *et al.*, in press). The first formation is constituted by grayish to brownish mud-siltstone strata interbedded with grayish calcarenites and sandstone. The second one consists of yellowish coarse sandstone strata intercalated with conglomeratic-sandstone intervals and thin argillite layers.

The Tuscan Units are represented solely by the Macigno Fm. (Chattian–Aquitanian), consisting of thick strata of turbiditic sandstone with mudstone intercalations. At the base of the formation several layers of calcarenites can occur

(Cornamusini *et al.*, 2012).

2.2.5.2 Zanclean-Piacenzian deposits (Siena basin)

The Pliocene (Zanclean–Piacenzian) alluvial to shallow-marine deposits are organized in four allostratigraphic units (Martini *et al.*, 2011), which are grouped under a single label in the frame of the present study.

The Pliocene succession consists of alluvial deposits (De Castro & Pilotti, 1933; Manganelli *et al.*, 2007; 2011; Martini *et al.*, 2011), passing upward into nearshore (deltaic-non deltaic) deposits often rich in molluscan assemblages (Manganelli *et al.*, 2010).

2.2.5.3 Gelasian–Calabrian deposits (Valley fill)

The examined succession comprises two allounits (V1 and V2) and represents the infill of a U-shaped elongate depression that was cut both in the bedrock and Pliocene deposits. For the sake of clarity, the description of the study area will focus on two sectors: North of Castello di Montalto and South of Castello di Montalto. In the southern sector V1 and V2 are stacked one upon the other although the bodies' axis are not aligned vertically, whereas in the northern sector these allounits are vertically stacked. V1 comprises mainly gravelly deposits and rare mud, whereas V2 consists of sand and mud with subordinate gravel. Field evidence and well-core data show that allounits V1 and V2 are at least 60 and 25 m thick, respectively.

Paleocurrent measurements from both these units show that the main transport direction was toward SW (i.e. toward the Siena Basin).

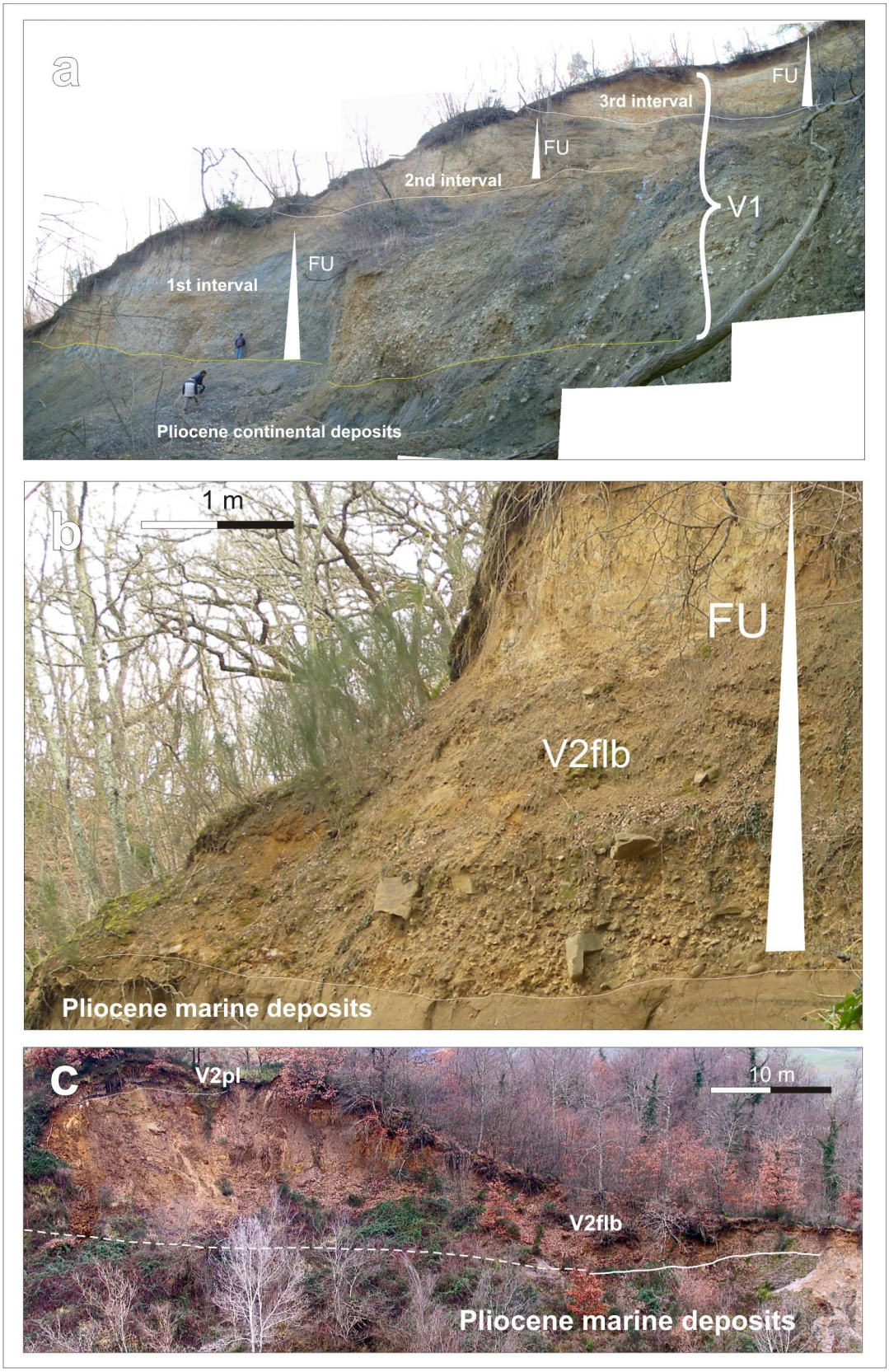

Figure 2.2: Stratigraphy of the study alluvial deposits. A) Pliocene continental deposits unconformably overlain by allounit V1, which shows three main fining upward (FU) intervals, the main unconformity is marked by yellow line; B) Fining-upward fluvial gravel of unit V2flb, unconformably overlaying Pliocene marine deposits; C) Sandy fluvial deposits of unit V2flb deposits, covered by palustrine V2pl facies and overlain Pliocene marine deposits.

2.2.5.3.1 Allounit V1

Allounit V1 crops out in the southern sector, but has also been identified in the northern sector through well-core data. It is composed of alternating intervals of gravel, sand and subordinate mud, showing a well-defined fining-upward trend (Fig. 2.2A). The gravelly intervals consist of amalgamated channelized bodies with minor intercalations of lens shape gravelly sand (Fig. 2.3B). Gravel is clast-supported, poorly sorted and locally contains abundant sandy matrix. Clasts are rounded and some of them show abraded litophaga traces, highlighting reworking from Pliocene marine deposits below.

The sandy to muddy intervals (Figs 2.2A and 2.3A) are characterized by strong pedogenesis, with organic-rich mud horizons and scattered continental gastropods (Pomatia elegans and Retinella sp; Aldinucci *et al.*, 2007). All these fine-grained intervals disappear moving northward, making the gravelly intervals amalgamate.

The basal gravelly part of each interval is interpreted as fluvial bars of a gravel-bed river system (Lunt & Bridge, 2004; Lunt *et al.*, 2004; Bridge & Lunt, 2006), whereas the muddy to sandy deposits represent a floodplain environment (Reading, 1996; Jones *et al.*, 2001; Bridge, 2003). Continental gastropods suggest these deposits are younger than Piacenzian in age.

2.2.5.3.2 Allounit V2

Allounit V2 consists of a wide spectrum of deposits with different stacking pattern North and South of Castello di Montalto.

North of Castello di Montalto, allounit V2 (up to 25-30 m thick) is dominated by massive, brownish to grayish silt-grained pedogenized deposits characterized by plant remains, roots and organic-enriched layers (V2fla; Fig. 2.3C). Isolated and rare sandy

deposits occur as lens-shaped bodies, floored by gravel-rich coarse sand. These deposits are ascribed to a poorly-drained floodplain environment (V2fla) (Miall, 1996; Nemec, 1996; Jones *et al.*, 2001; Bridge, 2003).

South of the Castello di Montalto, allounit V2 is composed of 15 m thick, channelized and cross-stratified gravel (V2flb; Figs 2.2B and 2.3D), passing downstream into channelized trough cross stratified gravelly sand (V2flb; Fig. 2C). Both these units are covered by organic-rich mud (V2pl; Fig. 2.3E), which is up to 6 m thick and contains abundant freshwater gastropods (e.g. *Bithynia tentaculata*). The gravelly deposits are interpreted as fluvial bars within a gravel bed river setting (Lunt & Bridge, 2004; Lunt *et al.*, 2004; Bridge & Lunt, 2006), whereas the sandy ones as fluvial bars of a sand-bed river system (Thorne *et al.*, 1985; Smith 1986; Bridge, 2003). The overlying muddy interval accumulated in a palustrine setting (Esu *et al.*, 1993; Miall, 1996; Nemec, 1996).

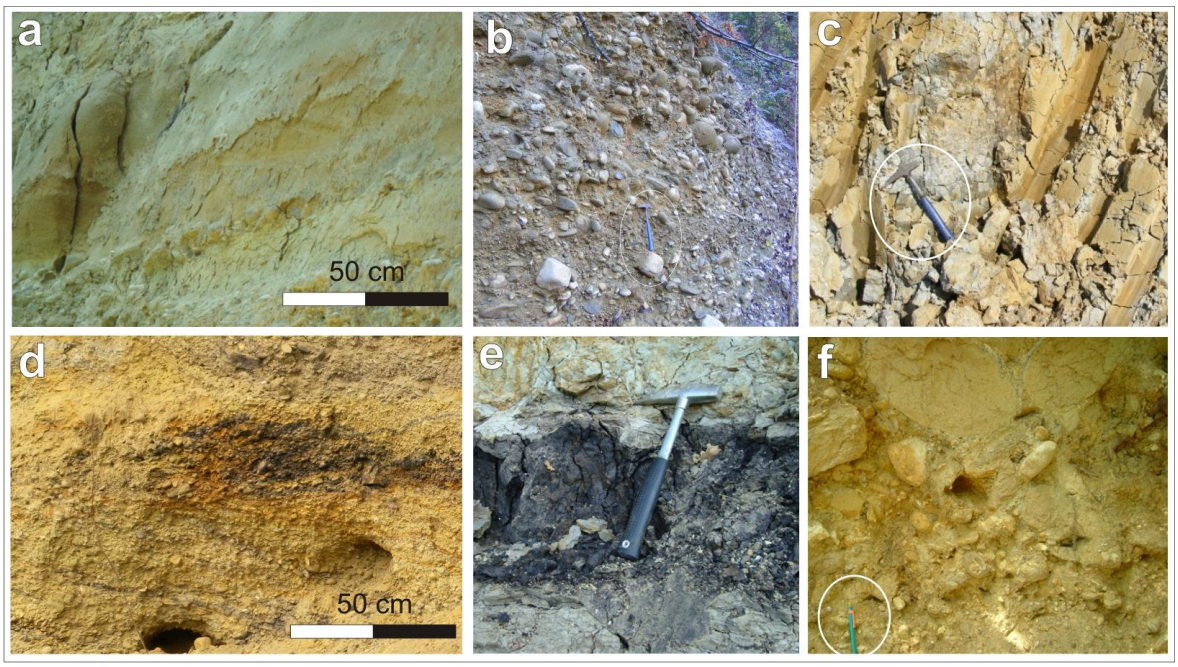

Figure 2.3: Sedimentary facies of the study deposits. A) fluvial sand with subordinate silt of V1; B) fluvial gravels with abundant sandy matrix (V1); C) muddy floodplain deposits of V2fla; C) fluvial, cross-stratified gravel of V2flb unit; E) organic-rich deposits of V2pl palustrine deposits; F) alluvial-fan gravel of unit V2af.

Gravelly fan-shape deposits (V2af) occur along the flanks of the U-shape depression both in the northern and southern sector. These bodies (up to 50 m) mainly comprise channelized gravelly deposits (Fig. 2.3F) that pass downstream into poorly channelized gravelly sand and show a paleotransport direction transverse to the belt axis, as defined by V2 deposits. The V2af deposits are attributed to an alluvial fan setting (Nemec & Muszynski, 1982; Nemec & Steel, 1984; Sohn *et al.*, 1999).

To the North, the alluvial fan deposits are heteropic with V2fla fluvial deposits, whereas to the South they are heteropic both with V2flb fluvial deposits and palustrine deposits (V2pl). The Calabrian age of this unit is inferred from the occurrence of Aculean stonetools in distal alluvial fan facies (Magi, 1992).

According to their geometries and sedimentological features, units V1 and V2 are interpreted as the infill of two paleovalleys that were nested in the northern sector of the study area, and offset in the southern part. The paleovalley was drained toward SW (units V1 and V2fla-b) and it received sediments from alluvial fans developed along its flanks (V2af).

2.2.5.4 Ionian deposits (alluvial terraces)

Fluvial terraces of the Ambra and Ombrone Rivers are easily distinguished in the present-day topography. They are made of sandy bodies capped by pedogenized mud and occur along the flanks of the modern valley, showing erosional base and flat top. The Ambra and Ombrone drainages developed two and one order of terraces, respectively.

2.2.6 Structural features

Several tectonic lineaments have been recognized in the selected area, and ascribed both to thrusts and high-angle normal faults (Lazzarotto *et al.*, in press). Thrusts separate Ligurian from Tuscan units and show a NE vergence resulting from the Late Cretaceous-Late Eocene compressional phase (Martini & Sagri, 1993). High-angle normal faults have a dominant "Apenninic" NW–SE trend and are associated with the post-collisional, extensional tectonic phase (Plio-Quaternary, Brogi *et al.*, 2005).

The most significant tectonic lineament of the area occurs nearby Castello di Montalto (Fig. 2.4A), and shows a NW-SE trend (i.e. normal to valley axis). Structural stations, measured along this lineament, show a 120° N trend and 30° N dip, with an overall normal movement, lowering the northern area (i.e. upstream valley sector). Field and well-core data (Fig. 2.4C) show a differential bedrock displacement, measured on Macigno Fm. outcrops, which increases from 40 to 60 m moving eastward along the fault. This fault displaces V1 deposits, which bear evidence of tectonic deformations (i.e. striation; Fig. 2.4B). The variability of fluvial deposits of unit V2 (V2fla and flb) across the fault zone could testify a syn-depositional tectonic sedimentation.

The present-day intense CO2 emission (Fig. 2.4D) indicates active tectonics, or, at least, a hydrothermalism as last step of a very recent activity. Activity of this fault is consistent with the latest stage of Siena Basin evolution (Brogi, 2011a), characterized by activation of high-angle normal faults after a phase of crustal detachments.

A further normal fault is located in the Terre Rosse area, where it displaces the Pliocene marine deposits and develops the escarpment, which sourced alluvial fan deposits of unit V2af.

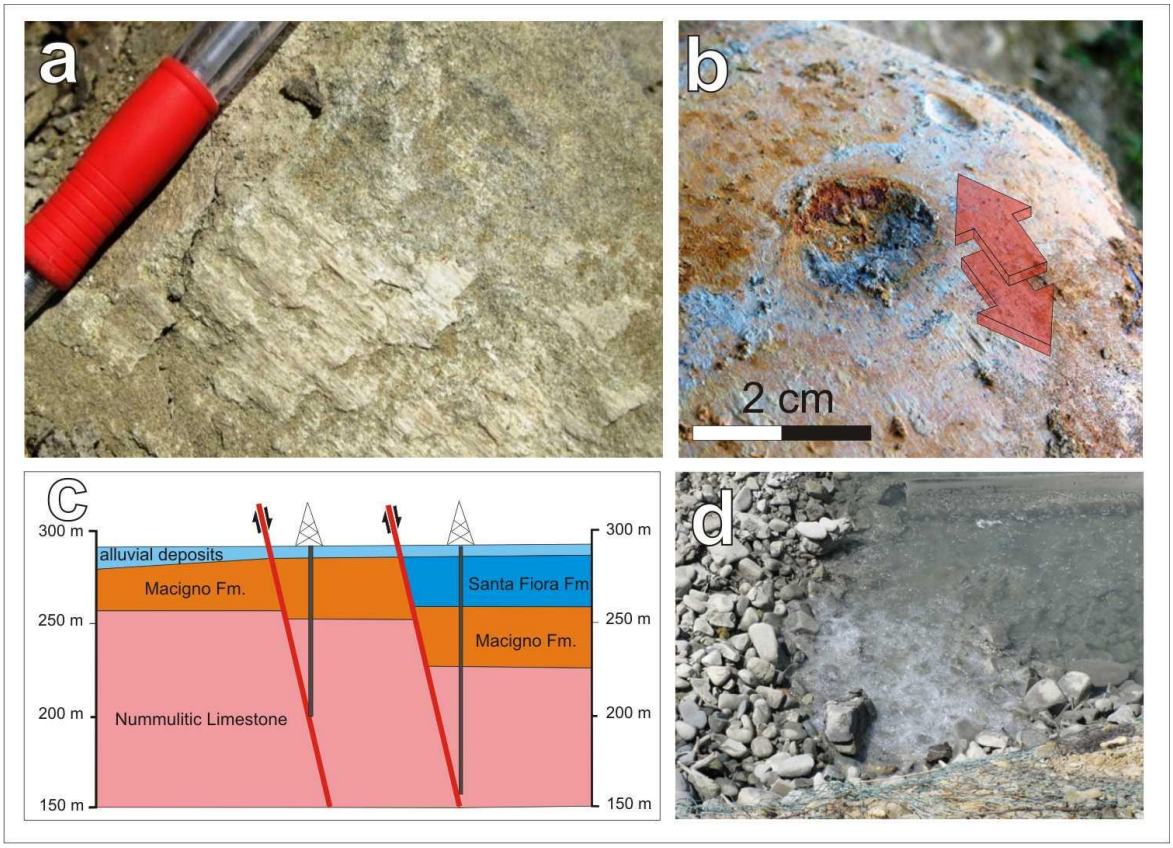

Figure 2.4: Structural features of the normal fault crossing the study paleovalley. A) Fault plane in sandstone (Macigno Fm.) and related kinematic indicators consisting of superposed generations of calcite fibers; B) Tectonic striations (red arrow) caused by intra-clast shearing induced by tectonic displacement; C) Well-core data showing bedrock displacement affected by the fault in the Castello di Montalto area; d) Natural CO^2emissions along the Ambra River.

2.2.7 Conclusions

This work provides a high-resolution geological map of the Pliocene and Pleistocene deposits exposed along northern margin of the Siena Basin through an allostratigraphic and sedimentological approach. The study deposits represent the infill of a SW-draining paleovalley, and consist of two main allounits, V1 and V2. These allounits are vertically stacked in the northern sector of the study area and offset in the southern sector. V1 mainly consists of gravelly fluvial deposits, whereas V2 deposits show a marked downvalley variability, manifested by poorly-drained floodplain deposits (V2fla) in the northern sector, and by gravel-bed river deposits (V2flb) in the southern one. Alluvial fan (V2af) and palustrine (V2pl) deposits are associated with V2 fluvial facies. A NW–SE

trending normal fault cuts transversally the paleovalley axis near Castello di Montalto. This fault displaces V2 deposits and is probably the cause of the along valley variability of V2fl deposits.

CHAPTER 3

TECTONICALLY-DRIVEN DEPOSITION AND LANDSCAPE EVOLUTION WITHIN UPLAND INCISED VALLEYS: THE AMBRA VALLEY FILL, PLIOCENE-PLEISTOCENE OF TUSCANY, ITALY.

3.1 OVERVIEW

This chapter is a journal paper submitted to Sedimentology (SED – 2014 – OM – 013). Facies and structural analysis, integrated with geophysical data from the Plio-Pleistocene Ambra palaeovalley were presented here in order to extricate the effects of tectonics of fluvial aggradation in an incised valley setting.

3.2 PAPER

VALERIA BIANCHI[1], MASSIMILIANO GHINASSI[1], MAURO ALDINUCCI[2], JACOPO BOAGA[1], ANDREA BROGI[3], RITA DEIANA[4]

[1] Dept. of Geoscience, University of Padova, Via Gradenigo 6, 35121 Padova, Italy

[2]Weatherford Petroleum Consultants A.S., 5147 Bergen, Norway

[3]Dept. of Earth and Geoenvironmental Sciences, University of Bari "Aldo Moro", Via Orabona 4, 70125 Bari, Italy

[4]Dept. of Cultural Heritages, University of Padova, Piazza Capitaniato, 7, 35121 Padova

3.2.1 Abstract

Sedimentation in the upstream reaches of incised valleys is predominantly fluvial and, in most cases, independent from relative sea level oscillations. The mechanisms of

facies distribution respond to a combination of factors such as tectonics, climate and landscape evolution. Tectonics can influence fluvial aggradation and degradation through local changes in gradient, both longitudinal and transverse to the valley slope. This paper deals with a Pliocene – Pleistocene fluvial valley fill developed in the northeastern shoulder of the Siena Basin (Northern Apennines, Italy). The valley lacked the control of sea level, and its morphological and depositional history resulted from the interaction of autogenic morphodynamics and extensional tectonics giving rise to normal and oblique-slip faults orthogonal and parallel to the valley axis. This research integrated field and geophysical data, with the main scope of introducing a comprehensive, tectono-sedimentary model of coeval longitudinal and lateral alluvial plain tilting.

Longitudinal tilting was generated by a transverse, upstream-dipping normal fault that mainly controlled the aggradation of fining-upward strata-sets. Upstream of the fault zone, valley backfilling generated an architecture similar to that of classic, sea-level-controlled, coastal incised valleys. Downstream of the fault zone, valley downfilling was related to an overwhelming sediment supply sourced and routed from the faulted zone itself. Lateral tilting was promoted by the activity of a fault parallel to the valley axis, as well as by different offsets along near orthogonal faults. As a result, the valley trunk system experienced complex lateral shifts, which were governed by interacting fault-generated subsidence and by the topographic confinement of progradational, flank-sourced alluvial fans.

Keywords: alluvial-valley fill; incised valley; fluvial sedimentation; extensional tectonics; valley avulsion

3.2.2 Introduction

The rise of seismic exploration as a key tool in exploration of hydrocarbon reservoirs over the last four decades (Posamentier & Vail, 1988; Posamentier *et al*., 1988), was followed by a dramatically-increasing interest on the dynamics of ancient valley fills, given their high potentials as oil- and gas-prone lithosomes (Van Wagoner *et al*., 1990; Dalrymple *et al*., 1994;). Different models of valley fill architecture and classification have been proposed in the past (Aslan & Blum, 1999; Blum & Tornqvist, 2000; Dalrymple, 2006; Simms *et al*., 2006; Gibling *et al*., 2011), most of them sharing the notion of palaeo-coastline as key control on facies distribution. As downstream valley reaches are closer to their coastal outlet, they show common evidence of marine influence and were widely described in the classical estuarine models (Dalrymple *et al*., 1994; Boyd *et al*. 2006; Gibling, 2006; Simms *et al*., 2006; Blum & Womack, 2009; Blum *et al*., 2013). On the opposite, upstream and fluvial-dominated valley reaches received much less attention (Gibling *et al*., 2011). Most downstream valley reaches are arguably cut and filled in response to relative sea-level changes (Allen & Posamentier, 1993; Dalrymple *et al*., 1994; Li *et al*., 2006; Simms *et al*., 2006; Breda *et al*., 2009), with inland expressions of tens to few hundreds of km upstream (Blum & Tornqvist 2000; Gibling *et al*., 2011). Upstream valley reaches have sedimentation solely controlled by fluvial processes (Dalrymple *et al*., 1994; Zaitlin *et al*., 1994; Vincent, 2001; Fielding *et al*., 2007), which in most cases do not betray the direct influence of relative-sea level oscillations (Currie, 1997; Legarreta & Uliana, 1998; Martinsen *et al*., 1999). In these cases, the mechanisms of facies distribution comprise complex interactions between tectonics, climate and drainage evolution (Shanley & McCabe, 1991, 1994; Blum & Tornqvist, 2000; Holbrook, 2001; Gibling *et al*., 2011). Inland valley systems are poorly documented because of the difficult

preservation of upstream portions, which in most cases are deeply affected by subsequent erosion, and because of their difficult discrimination from similar, extra-valley deposits (Gibling *et al*., 2011). Nonetheless, infill of Pleistocene upstream valleys (Gibling *et al*., 2011; Blum *et al*., 2013) proved to represent a precious, yet poorly explored archive of recent tectono-climatic evolution for inland areas. The effects of tectonics on fluvial sedimentation are known from modern rivers (Schumm, 1986; Holbrook & Schumm, 1999) and have been modelled in laboratory experiments (Ouchi, 1985; Lague *et al*., 2003; Hickson *et al*., 2005; Turowski *et al*., 2006). Results substantially demonstrate how tectonic activity involves significant modifications in terms of: i) geomorphic features and fluvial styles (Twidale, 1971; Ouchi, 1985; Blum & Tornqvist, 2000; Gibling, 2011); ii) modification of the equilibrium profile (Dalrymple, 2006); iii) alternation between phases of aggradation and degradation (Shanley & McCabe, 1991; Holbrook & Schumm, 1999); iv) and channel avulsive patterns (Bryant *et al*., 1995). Nevertheless, the tectonic forcing on valley fill aggradation is poorly known (Shanley & McCabe, 1991; Boyd *et al*., 2006), a gap particularly relevant considering difficult to disentangle signature of tectonics, climate and other forcings where reserved (Guiseppe & Heller, 1998; Holbrook & White, 1998; Vincent, 2001). Having said this, the specific questions that this paper is intended to address are: how do tectonics activity controls fluvial aggradation within upstream valley reaches? And how do tectonically-controlled fluvial valley fills differ from those controlled by relative sea-level?

This paper contributes to these topics via a multidisciplinary approach on a Plio-Pleistocene, fluvial valley fill currently exposed along the Ambra River Valley, southern Chianti (Northern Apennines, central Italy; Fig. 3.1). The study succession accumulated both on Pliocene marine sediments and on pre-Neogene bedrock (Aldinucci *et al*., 2007),

in response to the activity of normal faults (Baldi *et al*., 2006; Bianchi *et al*., 2013). The specific goals of this study are to: i) analyze the effects of tectonic on the spatial distribution of facies, and aggradation and degradation processes within the valley; ii) explore the role of tectonics on fluvial sedimentation within a spatially-confined setting; iii) investigate the relationship between tectonics and valley avulsion.

3.2.3 Geological Setting

3.2.3.1 Neogene – Quaternary basins of Northern Apennines

The Northern Apennines is an orogenic belt developed after the Late Cretaceous - Early Miocene convergence of Africa and Eurasia (Carmignani *et al*., 1994, 1995, 2001; Brogi, 2008; Barchi, 2010). After the collisional event (Oligocene-Early Miocene), Neogene-Quaternary basins (Fig. 3.1A) developed as the superficial response of a lithosphere-scale (Nicolich, 2001) extensional process (Carmignani *et al.,* 1994; Brogi *et al.*, 2005). These basins are mostly NW- and NNW-trending, up to 200 km long, and up to 25 km wide, showing articulated and mutually superimposed extensional structures (Brogi & Liotta, 2008), and are segmented into minor sub-depocentres by transversal, NNW-SSE-oriented lineaments (such as the Arbia-Val Marecchia line; Liotta, 1991), which often highlight to bedrock highs (Fig. 3.1A; Sacco, 1935; Signorini, 1935). Neogene-Quaternary basins show a wide spectrum of infill successions. Basins occurring west of the Chianti Ridge (Fig. 3.1A) are characterized by late Miocene – Pliocene fluvio-lacustrine and shallow-marine sedimentation (“central” basins *sensu* Martini & Sagri, 1993; such as the Siena Basin, Fig. 3.1A). Basins located east of the Chianti Ridge (Fig. 3.1) are filled with late Pliocene - Pleistocene continental deposits (“peripheral” basins, *sensu* Martini & Sagri, 1993; such as the Upper Valdarno Basin, Fig. 3.1A).

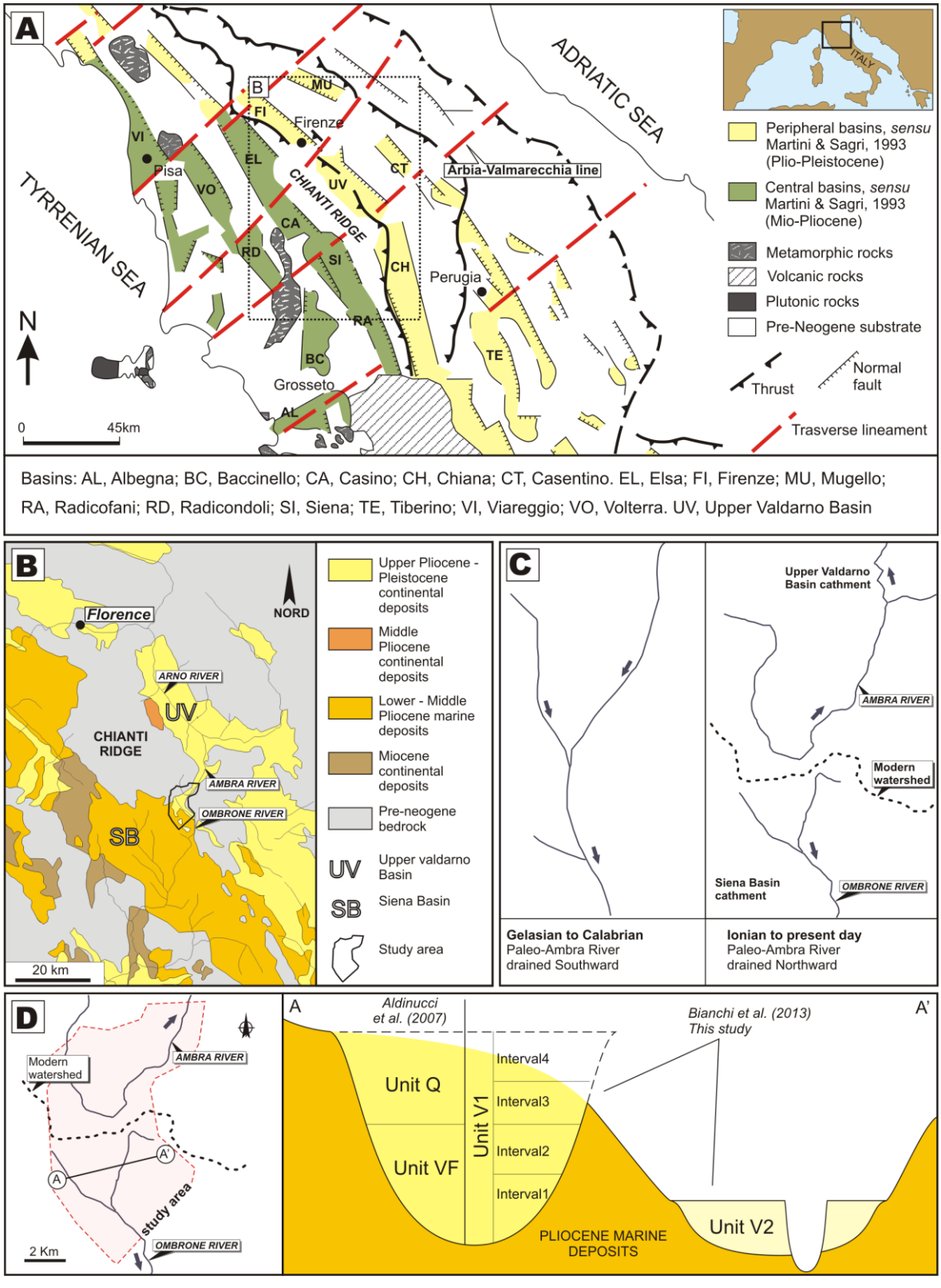

Figure 3.1: A) Simplified geological sketch of the Northern Apennines showing the Neogene-Quaternary basins with intervening bedrock ridges and main tectonic features; B) Schematic geological map of the area affected by the drainage changes discussed in this paper with the study area shown as inset; C) Sketch of the drainage modifications occurred in the studied area in the Gelasian-Recent time interval; D) Outline of the studied area with location of the Ambra and Ombrone rivers and present-day watershed; a schematic geometry of the sedimentary succession with the studied stratigraphic units along the cross-section A-A` is also shown.

3.2.3.2 The study area and previous works

The study area is located along the Chianti Ridge, and corresponds to a linking zone between the Upper Valdarno (Fidolini *et al*., 2013a; Ghinassi *et al*., 2013) and Siena basins (Brogi, 2011a; Martini *et al*., 2011). The Chianti Ridge is characterised by a pre-Neogene bedrock comprising uprooted and deformed tectonic units (Ligurian, Subligurian and Tuscan units; Abbate & Sagri, 1982; Lazzarotto *et al*., in press). The Ligurian, are only represented by the Cretaceous-Paleocene deposits (Lazzarotto *et al*., in press), composed of turbiditic, fine-grained siliciclastics and marly limestone (Santa Fiora and Monte Morello formations). Subligurian Unit consists of Palaeocene-Oligocene calcarenite, limestone, shale and minor sandstone (Canetolo group). The Tuscan Unit (Tuscan Nappe) consists of the Late Oligocene-Early Miocene siliciclastic turbidites (Macigno Fm.). The Pliocene Siena Basin infill (Martini *et al*., 2011; 2013; Arragoni *et al*., 2012) consists of Zanclean fluvio-deltaic gravels grading upward into marine sand and mud. Micropalaeontological analyses ascribe the uppermost part of the marine succession to the latest Piacentian (Bambini *et al*., 2010; Martini *et al*., 2011; Arragoni *et al*., 2012; Martini *et al*., 2013), when a regional tectonic doming caused a forced regression (Martini & Sagri, 1993). A 60-70 m thick fluvial valley fill succession overlies both the pre-Neogene Units and the marine deposits of the Siena Basin (Aldinucci *et al*., 2007; Bianchi *et al*., 2013). The valley was fed from the north (Fig. 3.1C), and successively terraced by the Ambra and Ombrone Rivers, which flows north- (i.e. Upper Valdarno Basin catchment) and southward (i.e. Siena Basin catchment), respectively (Fig. 3.1C). This drainage pattern is the result of the latest Calabrian – early Ionian piracy of the Ambra River, which was incorporated in the northward-flowing Arno River catchment (Fig. 3.1B) (Bartolini &

Pranzini, 1981; Fidolini *et al*., 2013a, 2013b).

Aldinucci *et al*. (2007) focused on the southern part of the study area (Fig. 3.1D), concluding that the valley fill lacks any evidence of marine-paralic influence since the latest Piacentian regional tectonic doming uplifted the paleo-coastline up to 700 m above the modern sea level, isolating the area from any marine influence. More recently, Bianchi *et al*. (2013) identified two distinct valley fill units (Fig. 3.1D). The lower gravel-dominated unit (henceforth referred to as unit V1) includes the Q and VF units of Aldinucci *et al*. (2007) (Fig. 3.1D). The upper unit (henceforth referred to as unit V2) is markedly heterogeneous, with both mud- and gravel-dominated deposits.

The study area is centered along a WSW-ENE-trending, regional tectonic lineament known as Arbia-Val Marecchia lineament (Liotta, 1991; Pascucci *et al*., 2007). The main local structural elements are the Ambra River and Terre Rosse normal faults (Bianchi *et al*., 2013). The Ambra River Fault dips towards NE, displacing unit V1 (Bianchi *et al*., 2013) and being characterized by intense CO_2 leakage (Minissale, 2004; Baldi *et al*., 2006). The Terre Rosse Fault dips toward SW and displaces Pliocene marine deposits (Bianchi *et al*., 2013).

3.2.4 Methods

3.2.4.1 Field investigations and borehole data

This work is based on field investigations, aimed at collecting sedimentological and structural data. The bulk of sedimentological and structural data were integrated with borehole and geophysical information. The geology of the study deposits was initially defined through mapping on 1:10.000 scale supports over an area of some 25 km^2 (Fig. 3.2A). Sedimentary units were detailed via bed-by-bed logging and outcrop line-drawing,

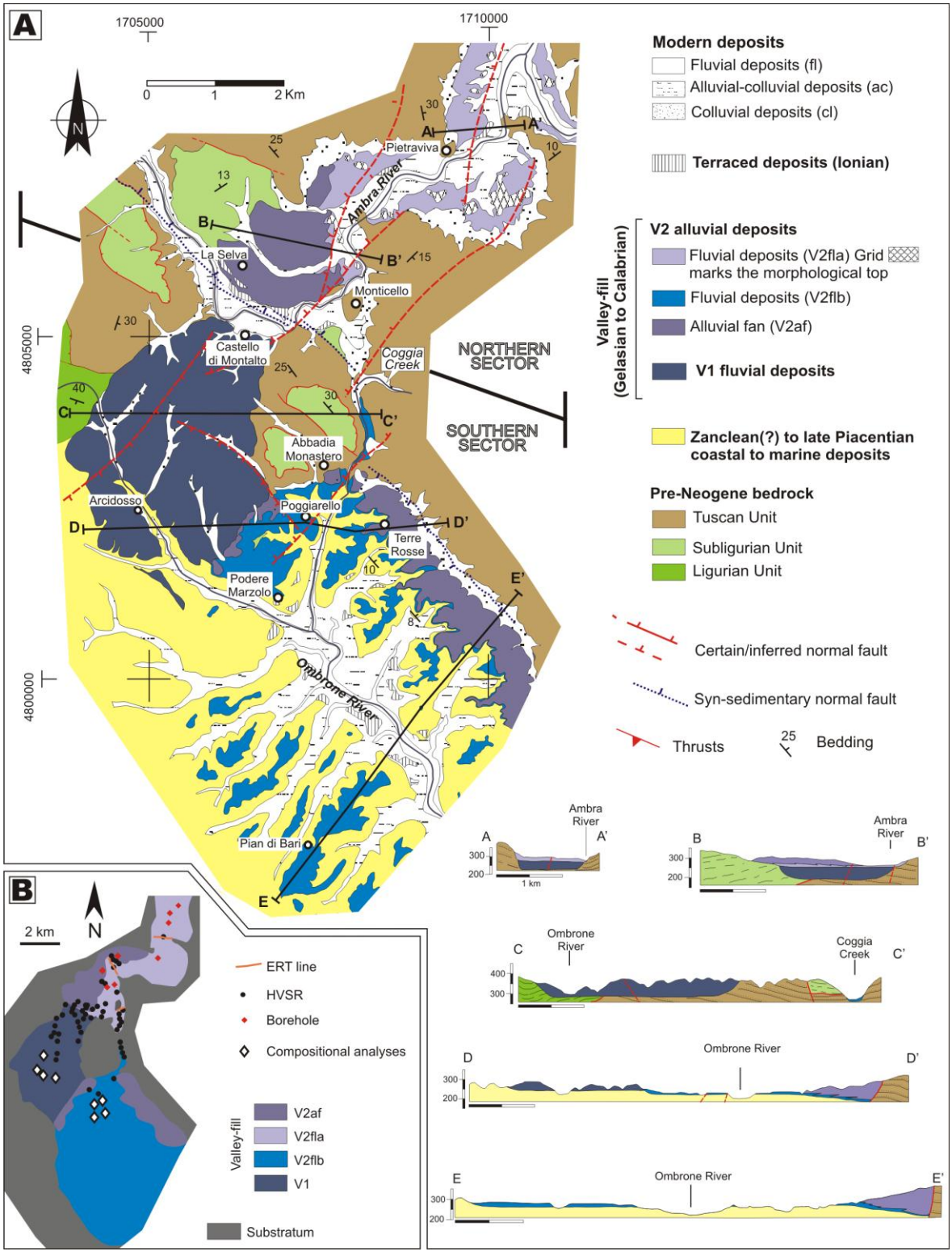

Figure 3.2: A) Detailed geological map of the studied area and geological cross sections with main localities mentioned in the text; B) Areal distribution of the recognized stratigraphic units showing the trace of ERT line and sites of boreholes, HVSR and compositional analyses.

with the aim of individuating groups of spatially and genetically related facies (i.e. facies associations). Facies associations were in turn interpreted as originated from distinct depositional environments. The main vectors of palaeo-drainage were inferred through the measurement of ca. 200 indicators of palaeoflow, using both *a*(t)*b*(i) clast imbrications and directions of cross-bedding progradation. Palaeocurrent data were accompanied by compositional analysis of gravelly deposits. Eight samples were collected (Fig. 3.2B), each one reporting 100 identifications performed on un-weathered surfaces of clasts having *b*-axis > 3 cm and sampled on horizontal lines.Structural analyses were focused on high-angle normal faults which are thought to represent the youngest regional structures affecting both unconsolidated Pliocene-Pleistocene deposits and pre-Neogene bedrock (Brogi *et al*., 2010; Brogi, 2011b; Cornamusini *et al*., 2012, Brogi *et al*., 2013). Structural and kinematic data represent discrete clusters (structural stations), along exposed meso-fault surfaces. The borehole dataset consists of 8 well logs located in the northern sector of the study area (Fig. 3.2B), and was coupled in places with Cone Penetration tests (CPT) (Fig. 3.3D). Borehole data proved to be useful in: i) defining the depth of the valley floor; 2) tracing the boundary between unit V1 and V2; and 3) calibrating the geophysical dataset.

3.2.4.1 Geophysical measurements

3.2.4.1.1 Electrical resistivity tomography (ERT)

Three ERT lines were collected in the Northern sector of the study area (Fig. 3.2B) using an IRIS Syscal Pro 72 instrument. The data acquisition was performed, for two of these lines (ERT1 and ERT 2) using 72 electrodes, while for the third line (ERT 3) were used 48 electrodes. All lines were collected using 5 m electrode spacing and the dipole-

dipole skip zero scheme, to ensure the best signal to noise ratio and optimal spatial resolution. In order to assess a data quality control, a full reciprocal acquisition was applied, swapping potential with current electrodes, in order to estimate data errors and reject the data exceeding a 5% difference between direct and reciprocal values, before the inversion processing (Daily *et al*., 2004, Cassiani *et al*., 2006; Deiana *et al*., 2008). The ERT tomographic inversion was performed using the ProfileR version 2.5 code (Binley, 2008), based on the Occam's inversion approach (LaBrecque *et al*., 1996), fitting the observation at a 5% error level.

3.2.4.1.2 Horizontal to Vertical Spectral Ratio (HVSR) single station measurements

Horizontal to Vertical Spectral Ratio technique (HVSR, Nogoshi & Igarashi, 1970 or "Nakamura's technique", Nakamura & Samizo*,* 1989) consists of passive recording of natural micro-tremors (seismic noise) through the use of 3 component receivers, and is used in order to identify the subsoil resonance frequency F_0 (Field & Jacob, 1993) which is related to material properties and to the depth of the main impedance contrast (Galgaro *et al.*, 2013). Single stations were performed in 42 sites located in the Monticello – La Selva – Abbadia di Monastero area (Fig. 3.2). We adopted digital 24bit seismometers equipped with 3 orthogonal velocimeters with noise threshold < 0.5 μV r.m.s. at 128 Hz sampling and a frequency response rate between 0.1Hz and 256 Hz. The instruments were installed with a spirit level with horizontal high precision of sensitivity of 5' arc (0.083°). Each acquisition lasted 30 minutes with 128 Hz sampling rate. The horizontal to vertical spectral ratio was computed for windows of 20 s length, with a smoothing of 10%. Each window was de-trended, tapered, padded, FF-transformed and smoothed with Konno & Omachi smoothing type windows, with a width equal to 20% of the central

frequency (Konno & Omachi, 1998). The euclidean average was used to combine EW and NS components in the single horizontal (H) spectrum, following the indications of the Sesame Project (SESAME, 2004; Chatelain *et al*., 2007).

3.2.5 Results

The study deposits show a marked variability in terms of geometry, thickness and facies distribution (Fig. 3.2A), and the sedimentological and stratigraphic features of the northern and southern sector of the study area will be described separately. The boundary between these two sectors is located in the Castello di Montalto area (Fig. 3.2A). In plan-view, units V1 and V2 appear as elongated bodies sharing a NNE-SSW to NNW-SSE orientation (Fig. 3.2A). Unit V1 is exposed only in the southern sector, between Castello di Montalto and Arcidosso (Fig. 3.2A), although subsurface data indicate that it sub-crops in the northern sector as well.

3.2.5.1 Sedimentary succession

3.2.5.1.1 Northern sector

3.2.5.1.1.1 Field and borehole data

Most of the northern sector is characterized by extensive covers of Holocene deposits, even if the upper portion of unit V2 is locally exposed (e.g. Pietraviva area, Fig. 3.2A). Unit V2 appears embanked in bedrock over a width of 0.8 to 1.5 km, following a wandering NNE-SSW trend. Unit V2 deposits consists of massive, horizontally-bedded mud with subordinate sand (V2fla), locally interbedded with pebble- to cobble-sized gravel (V2af; i.e. La Selva area). Mud of unit V2fla is commonly root-bioturbated (Fig. 3.3A), or significantly enriched in undecomposed organic matter and plant debris (Fig.

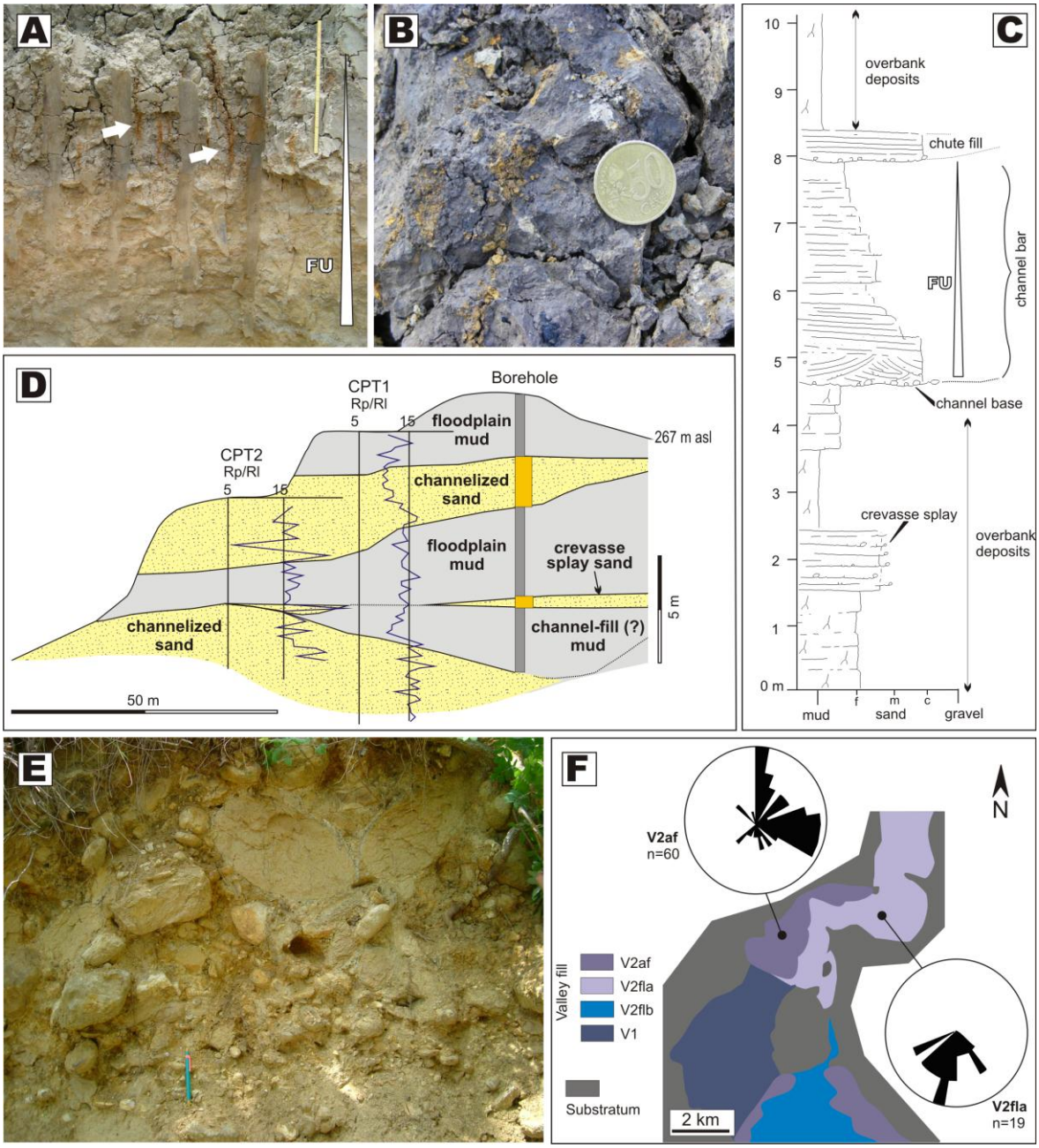

Figure 3.3: A) Detailed geological map of the studied area and geological cross sections with main localities mentioned in the text; B) Areal distribution of the recognized stratigraphic units showing the trace of ERT line and sites of boreholes, HVSR and compositional analyses.

3.3B). Sandy deposits consist of both sheets and lensoid bodies. Sheets are up to 1.5 m thick and composed of massive to plane parallel-stratified, medium- to fine-grained sand. Lensoid bodies are up to 4-5 m thick and at least 50-60 m wide along-strike (Fig. 3.3D), and composed of fining-upward bedsets of pebbly, coarse-grained sand (Fig. 3.3C)

grading into pedogenized mud (Fig. 3.3A and C). Their internal architecture is featured by large-scale inclined beds (Fig. 3.3C) dipping at 5° to 10°. Single inclined beds display plane parallel-, trough cross-stratification and ripple cross-lamination. Palaeoflow is oriented towards the south (Fig. 3.3F). In the La Selva area (Fig. 3.2A), unit V2fla deposits are also interbedded with poorly organized gravels (Fig. 3.3E) onlapping the bedrock along the hydrographic right flank of the modern Ambra valley (Fig. 3.2A). Unit V2af deposits are poorly exposed and consist of clast-supported, moderately- to well-rounded, pebble- to boulder-sized gravels with subordinate sandy intercalations (Fig. 3.3E). Gravels form 1- 2 m thick units, which show a basal concave surface floored by imbricated a(t)b(i) boulders. Lensoid units show an overall fining-upward trend and range from bottom massive to top, crudely plane-parallel stratified. When in proximity to bedrock, disorganized to inversely-graded, unsorted pebble- to boulder-sized gravel occurs in tabular beds. The latter are up to 1m thick, and show an a(p)/a(p)a(i) fabric. For the latter, imbrication indicates palaeoflow towards east (Fig. 3.3F).

Borehole data show that unit V2fla is covered by up to 7 m of Holocene alluvium, and the integration with field observations indicate a thickness for the units V2fla and V2af of ca. 25 – 30 m, and 35 – 40 m, respectively. In the Monticello – La Selva area, the Ambra 01 borehole (Fig. 3.4A and B) encountered 60 – 70 m of gravel below unit V2fla, topping at a quote of 255 m asl. Boreholes Ambra 08 and Ambra 02 encountered the same boundary at a similar quote.

3.2.5.1.1.2 Geophysical data

The ERT results (Fig. 3.4A and C), highlight the presence of three different resistivity zones. In particular, a lower part with resistivity higher than 140 Ohm m

appears separated from an upper part, that shows resistivity values lower than 80 Ohm m, with an intermediate zone with 80 to 140 Ohm m. The unit with a resistivity higher than 140 Ohm m appears in ERT 2 and ERT 3 results, and shows an irregular top surface at an elevation of 200 to 240 m a.s.l. (Fig. 3.4C). Similar values are also highlighted in the eastern side of ERT1 section at about 200 m a.s.l. (Fig. 3.4 C). The unit with a resistivity comprised between 80 and 140 Ohm m occurs in ERT 1 and ERT 2 sections (Fig. 3.4 C). This unit shows a convex-upward basal surface and irregular top (well expressed in the ERT 2 result) and a maximum thickness of some 60 m (Fig. 3.4 C). The uppermost unit (i.e. resistivity lower than 80 Ohm m) occurs above 240-260 m a.s.l. in all ERT sections (Fig. 3.4 C). ERT 1 shows spots of higher resistivity (120-140 Ohm m), which are several m-thick and laterally extensive for 150-200 m (Fig. 3.4 C). In the uppermost part of the same ERT section, 3-5 m-thick deposits with a resistivity close to 200 Ohm m also occur locally.

HVSR analyses (Fig. 3.5A) identified three resonance frequency ranges, corresponding to three different depths of acoustic impedance contrast between layers. Narrow peaks were referred to intense contrasts of acoustic impedance, whereas broad peaks were identified as weak contrasts (Fig. 3.5B). Two main NW-SE trending sections (A-A' and B-B'), derived from interpolated HVSR data (Fig. 3.5A and C), allowed to characterize the geometry of the most distinctive surfaces of acoustic impedance contrast. Section A-A' is underlain by units V2af and V2fla, highlighting a different amplitudes of HVSR peaks, which are greater in the eastern sector of the section (Fig. 3.5B). Section B-B' is located in the southernmost part of the northern sector and, similarly to section A-A', is underlain by both V2af and V2fla deposits.

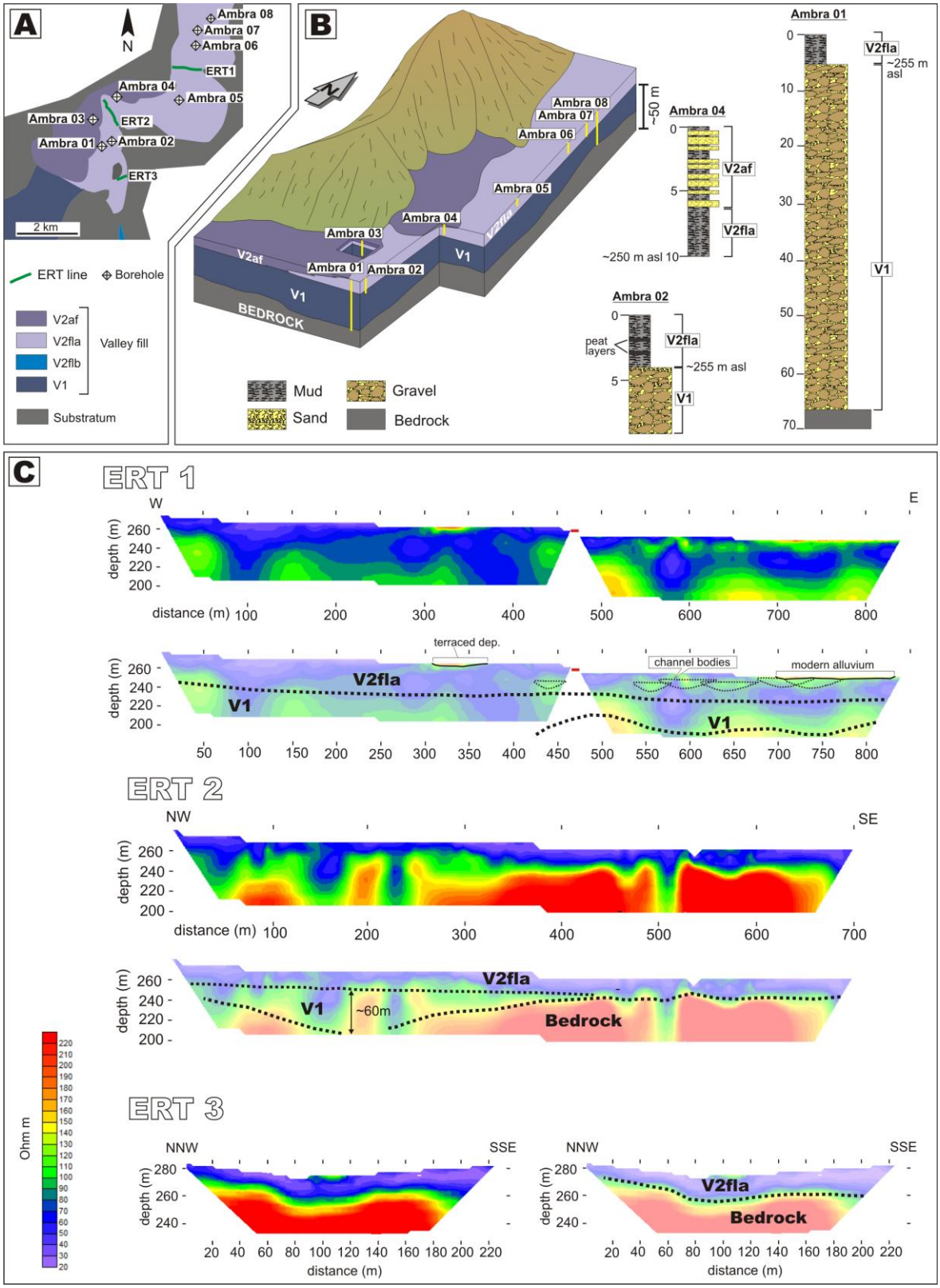

Figure 3.4: A) Areal distribution of boreholes plotted on a schematic geological map of the northern part of the studied area with indication of ERT lines; Note that boreholes are only located upvalley of the Ambra River Fault; B) 3D geological sketch of the inset area in Fig 4A with the reconstructed stratigraphy of the sediments penetrated by the Ambra 01, 02 and 04 boreholes; C) Interpreted (and uninterpreted) ERT profiles showing the subsurface architecture of units V1 and V2fla along with bedrock palaeomorphology.

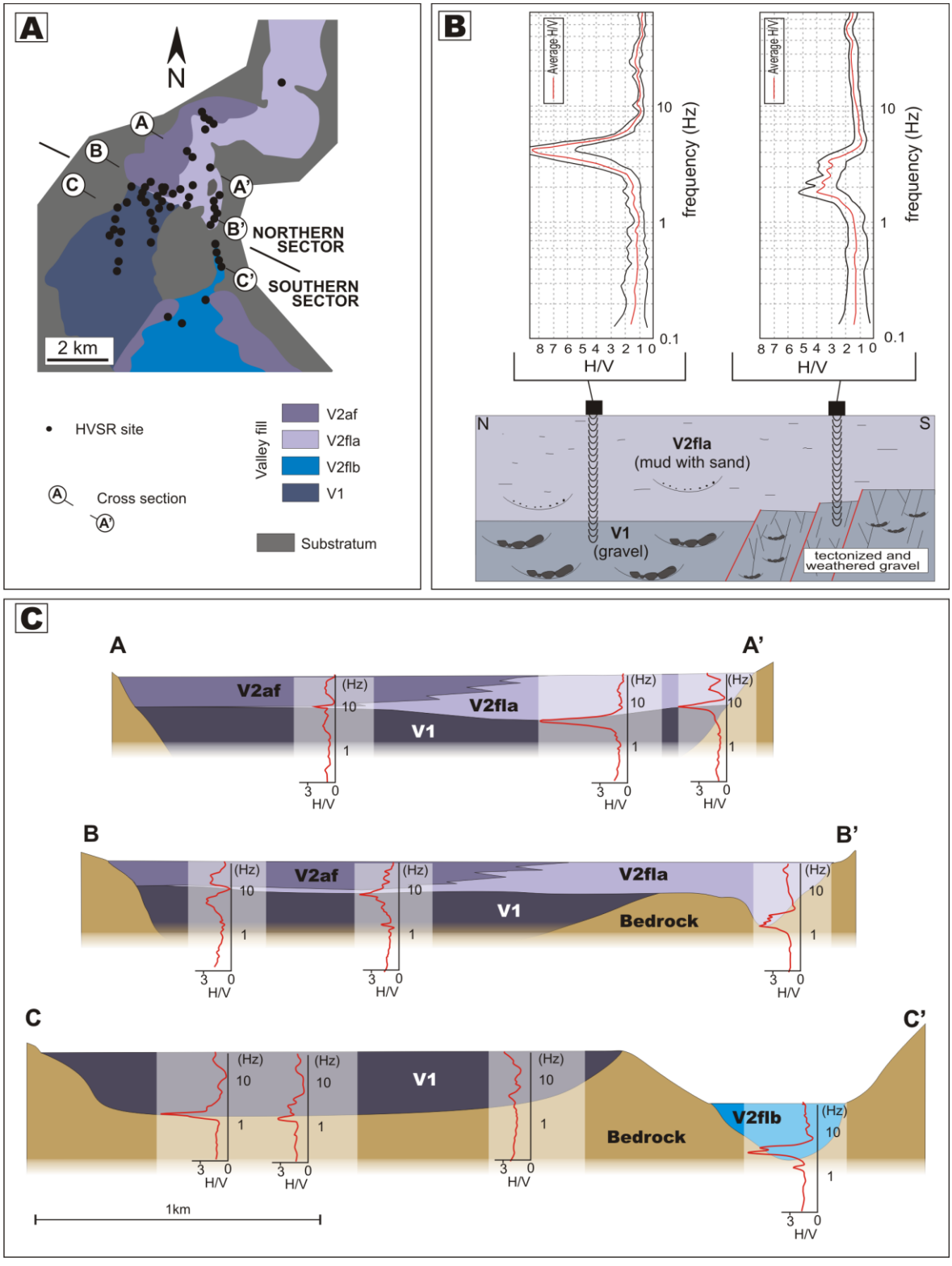

Figure 3.5: A) Areal distribution of HVSR sites plotted on a schematic geological map of the central-northern part of the studied area with traces of interpreted geological cross-sections; B) Frequency ranges of acoustic impedance contrasts between V2fla unit and underlying V1 gravels, both weathered and unweathered; C) Geological cross-sections derived from the interpolation of HVSR data with constraints from the geological map.

3.2.5.1.1.3 Interpretation

V2fla were interpreted as accumulated in an alluvial plain (Bridge, 2003), with tabular mud and sands representing floodbasin and crevasse splay deposits, respectively (Ethridge *et al.,* 1981). Floodbasin deposits probably accumulated from sediment fallout in ephemeral, flood-generated ponds (Bridge, 2003), which occasionally persisted long enough to develop swamps (Basilici, 1997; Miola *et al.*, 2006). Lens-shaped bodies are interpreted as the fill of 4-5 m-deep channels that wandered across the floodbasin. The isolated and scattered occurrence of channel bodies engulfed within overbank deposits suggests their pertinence to single-channeled, through-going systems (Ielpi, 2013), transecting high-accommodation plains (Martinsen *et al*., 1999). V2af gravels are interpreted as flanking alluvial-fan deposits (Blair & McPherson, 1994a, 1994b) that possibly accumulated at the entrance of tributaries into the valley; this interpretation is supported by their palaeoflow, which is orthogonal to that of the trunk systems. Lensoid conglomerates represent channel fill deposits, with their flooring boulders representing channel lags (Miall, 1985). Massive, ungraded to inversely graded conglomerates indicate that non-selective, mass-transport processes dominated by buoyancy (i.e. debris flows; Nemec & Steel, 1984) occurred in the most proximal areas of the fans. Borehole data also supports the interpretation of a southward-draining axial fluvial system (represented by unit V2fla), locally interfingered with flanking alluvial fans (unit V2af). The gravelly deposits underlying the unit V2 probably represent the sub-cropping unit V1.

The calibration of ERT lines with field and borehole data allows to interpret the high, intermediate and low domains of resistivity as bedrock, and units V1 and V2fla, respectively. ERT data substantially confirm the ubiquitous distribution of unit V2fla deposits along the valley axis, with a progressive increase in thickness downstream. Unit

V1 and V2fla fills a 80 – 90 m-deep, 800 m-wide depression cut onto the bedrock. The uneven surface interposed between units V1 and V2 and visible on lines ERT1 and ERT2 is interpreted as a scour featured by 10 to 15 m of erosional relief. In the ERT 1 profile (Fig. 3.4C), the high resistivity spots embedded within unit V2fla possibly represent sandy channel bodies, whereas the 3 – 5 m thick unit with resistivity approximating 200 Ohm m could represent sub-modern alluvial, terraced sand and gravel.

Further constraints on the spatial distribution of the study deposits come from the HVSR dataset. The contrasts of acoustic impedance in the A-A' section is interpreted as the unit V1 top (Fig. 3.5B). Accordingly, the peaks in the eastern side of the section mark the boundary between units V2fla and V1. The peak in the western side of the section marks the boundary between units V1 and V2af, here both dominated by coarse-grained deposits, and thus characterized by a lower contrast of acoustic impedance; a similar low contrast of acoustic impedance also marks the boundary between unit V1 and V2af gravels in the western part of section B-B'. On the opposite, the sharp peak in the eastern portion records indicates again a high impedance contrast between the mud-dominated unit V2fla deposits and the underlying bedrock (Fig. 3.4B).

3.2.5.1.2 Southern sector

3.2.5.1.2.1 Field data

The southern sector is characterized by both units V1 and V2 exposures (Fig. 3.2A). In the Castello di Montalto area, unit V1 is cut onto bedrock and composes a body ca. 1.2 km-wide and 60 – 70 m-thick. In the Arcidosso area, it is cut onto Pliocene marine deposits, it shows a similar thickness, and occupies a ca. 2.5 km-wide outcrop belt. Unit V2 occurs eastward of unit V1, showing in plan-view a fan shape (Fig. 3.2A), with the apex

located in the nearby of Abbadia Monastero (Fig. 3.2A). The fan body trends NNW-SSE and is cut both onto unit V1 and Pliocene marine deposits (see section D – D' in Fig. 3.2A). The fan body is up to 5 km wide and 15-20 m thick (Pian di Bari area; Fig. 3.2A).

Deposits of unit V1 are well exposed in the Arcidosso area (Fig. 3.2A), where they display four vertically-stacked intervals of channelized gravel and gravelly sand grading upward into sheets of sand to mud (Fig. 3.6A, B and E). Gravels and gravelly sand are composed of multilater, 4-5 m-thick bodies internally structured in sets of large-scale inclined beds dipping transversely to the main paleo-transport direction (Fig. 3.6D and E); inclined beds overlie a pavement of pebbles and cobbles. Gravelly beds are made of moderately-sorted, clast-supported pebbles with plane parallel- and planar cross-stratification. Sandier bedsets vary from plane parallel- to trough cross-stratified (Fig. 3.6I), are bounded by erosional surfaces, and commonly floored by clast-supported, pebble-sized mud-clasts (Fig. 3.6G). Large-scale inclined beds are in places overlain by wedge-shaped, fine-grained sand and mud (Fig. 3.6D). Sheet-bedded deposits are up to 6-7 m thick and vary from mud- (e.g. top of first interval; Fig. 3.6D and F) to sand-dominated (e.g. top of third interval; Fig. 3.6A). Mud-dominated beds are massive, and contain root bioturbation and pedogenic carbonate concretions. Organic-rich portion (Fig. 3.6H) have limited evidence of pedogenesis and bear gastropods shells (i.e. *Pomatia elegans* and *Retinella sp.*; Aldinucci *et al*., 2007). Sand-dominated beds are normally-graded, erosively-based and display plane parallel-stratification and ripple cross-lamination. The overall palaeoflow of unit V1 deposits is southward (i.e. towards the Siena Basin). The sand- to mud-dominated deposits capping the four fining-upward intervals detected in the Arcidosso area tends to less traceability northward, and toward the Castello di Montalto

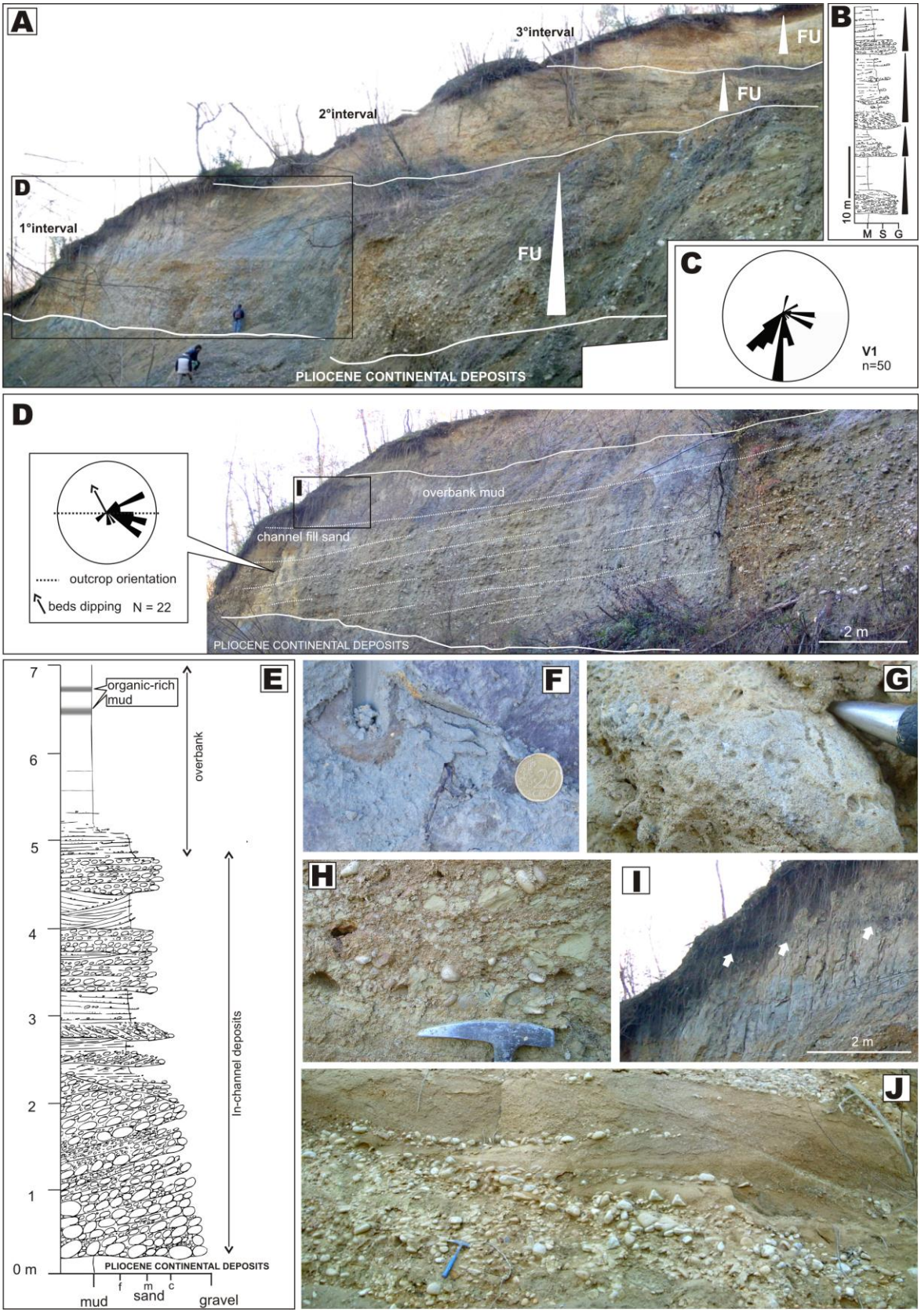

Figure 3.6: A) Panoramic view of unit V1 unconformably resting on Pliocene continental deposits and showing three of the four component FU successions; B) Sedimentary log showing depositional features of unit V1. Note the four FU constituent successions each formed by basal channelized gravel rapidly grading to overlying floodplain mud; C) Rose diagram showing an overall southward transport direction; D) Close-up view of the inset in Fig. 6A. Note the internal organization of the lowermost FU succession

characterized by inclined gravel beds locally overlain by channel-fill sand manifesting the channel-abandonment stage. Inclined gravel beds dip transverse to the main palaeotransport direction as detected from imbricated gravel-floor pebbles. Channel gravel and sand are finally overlain by overbank mud; E) Sedimentary log showing depositional features of the lowermost FU succession of unit V1; F) Mottled mud with pedogenic carbonatic concretions at the top of the lowermost FU succession (unit V1); G) Pebble showing abraded lithopaga traces; H) Erosive-based, clast-supported gravel formed by dominant mud clasts and representing the basal interval of a sand bed; I) Organic-rich mud layers at the top of the lowermost FU succession (unit V1); J) Through-cross stratified sand overlying a plane-parallel stratified basal gravel locally rich in mud clasts.

area (Fig. 3.2B) unit V1 transitions into amalgamated gravelly deposits, with features similar to those encountered in Ambra 01 borehole (Fig. 3.4B).

Unit V2 consists of V2flb and V2af deposits, located in the axial part and along the flanks of the palaeovalley, respectively (Fig. 3.2A). In the Poggiarello area (Fig. 3.2A), V2flb deposits are about 15 m thick and consist of gravel grading upward into pedogenized sand and mud (Fig. 3.7A, E and B). Gravel occurs in 1 – 2 m-thick, multistorey channel bodies (Fig. 3.7F), commonly floored by a(t)b(i)-imbricated pebbles and scattered, angular boulder-sized clasts (Fig. 3.7A and D). In some channelized bodies, sub-horizontal, plane parallel-stratified gravelly beds are vertically stacked and form coarsening-upward packages up to 1 m-thick. Elsewhere, plane parallel-stratified gravelly beds dip at 5°-10° (Fig. 3.7C) towards the basal channel surface. Locally, 1 – 1.5 m-thick sets of planar cross-stratified gravels display evidence of downstream-accretion and -migration. These gravels record southward palaeoflow (Fig. 3.7G), and tend to fine in the downstream direction (i.e. Pian di Bari area; Fig. 3.2A), where they grade into fining-upward, sand- to mud-dominated bedsets (Fig. 3.8D). The latter bedsets have a basal, up to 5 m-thick, medium-grained sand floored by fine pebbles (Fig. 3.8F and C) and fine upward into pedogenized fine-grained sand and mud. The sandy interval is structured into sets of large-scale inclined beds dipping at 5° to 20° (Fig. 3.8E and C). Inclined beds display internally a compound, plane parallel- / trough cross-stratification and ripple cross-lamination.

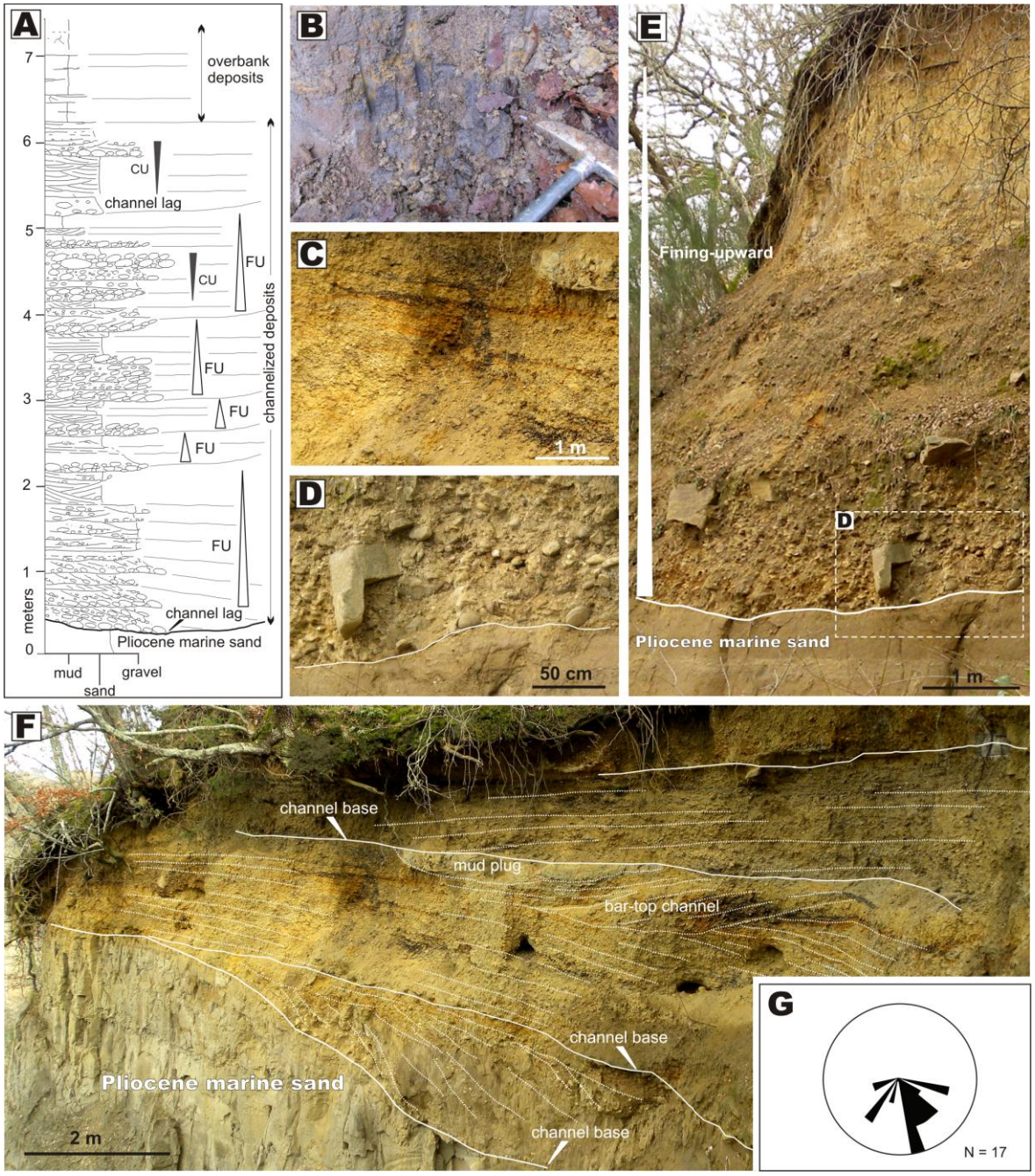

Figure 3.7: A) Sedimentary log showing depositional features of unit V2flb; B) Pedogenized sand and mud at the top of unit V2flb; C) Slightly inclined, plane-parallel stratified gravel (Unit V2flb); D) Close-up of insect in Fig. 7E showing outsized (boulder) clasts in channel-base gravels; E) Large-scale view of a FU succession of unit V2flb; F) Multi-storey, gravel-dominated channel fill resting unconformably on Pliocene marine sand; G) Rose diagram showing an overall southward transport direction.

Palaeotransport direction was assessed on the basal pebbles, being transverse to the dip of inclined beds. The overlying mud-dominated deposits display evidence of pedogenesis and are toppped by organic-, freshwater shells-rich beds (Fig. 3.8A, B and C; Bianchi *et al*., 2013).

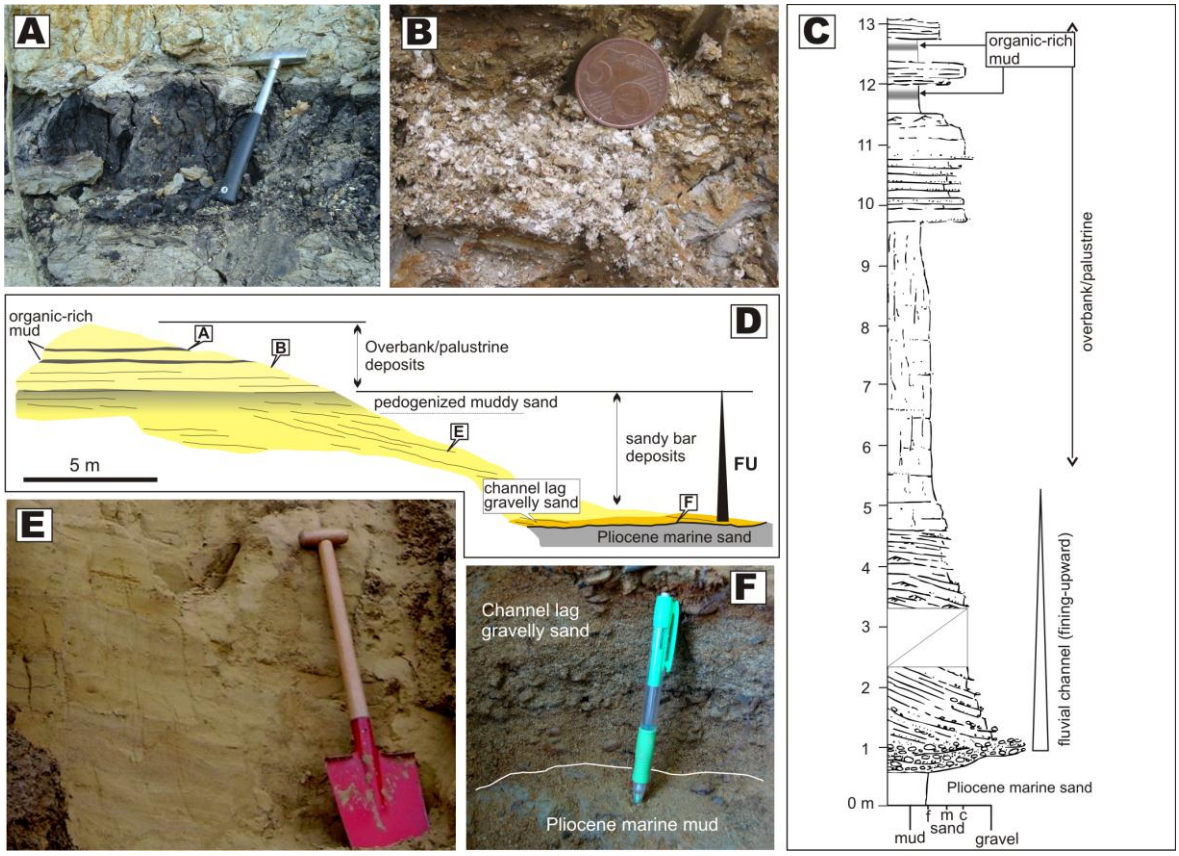

Figure 3.8: A) Pedogenized to organic-rich mud at the top of the distal V2flb unit; B) Freshwater shell-rich sand at the top of the distal V2flb unit; C) Sedimentary log showing depositional features of the distal expression of unit V2flb; D) Outcrop-based line drawing of a complete section of the distal portion of V2flb. Note the FU sandy channel-fill with evidence of inclined bedding overlying a basal lag gravelly sand and in turn overlain by overbank fines; E) Large-scale inclined sandy beds dipping transverse to the main palaeocurrent direction as inferred from imbricated basal pebbles; F) Lag deposit at the base of the distal V2flb unit.

Unit V2af is well developed in the Terre Rosse area (Fig. 3.2A), where it reaches up to 50 m in thickness. Unit V2af is mostly composed of pedogenized sand that passes upward into channelized gravels (Fig. 3.9A and B). Sand-grained deposits consists of vertically-stacked, tabular beds with dispersed lenses of pebbles. Beds are up to 1 m-thick and are both massive or faintly plane parallel-stratified, with bedding overprinted by pedogenesis (Fig. 3.9D). The architecture of the channelized gravels is similar to that of unit V2flb, showing inclined beds dipping at up to 10° - 20° (Fig. 3.9C), and coarsening-upward sets of sub-horizontal beds up to 50 cm thick. In the nearby of the valley flanks,

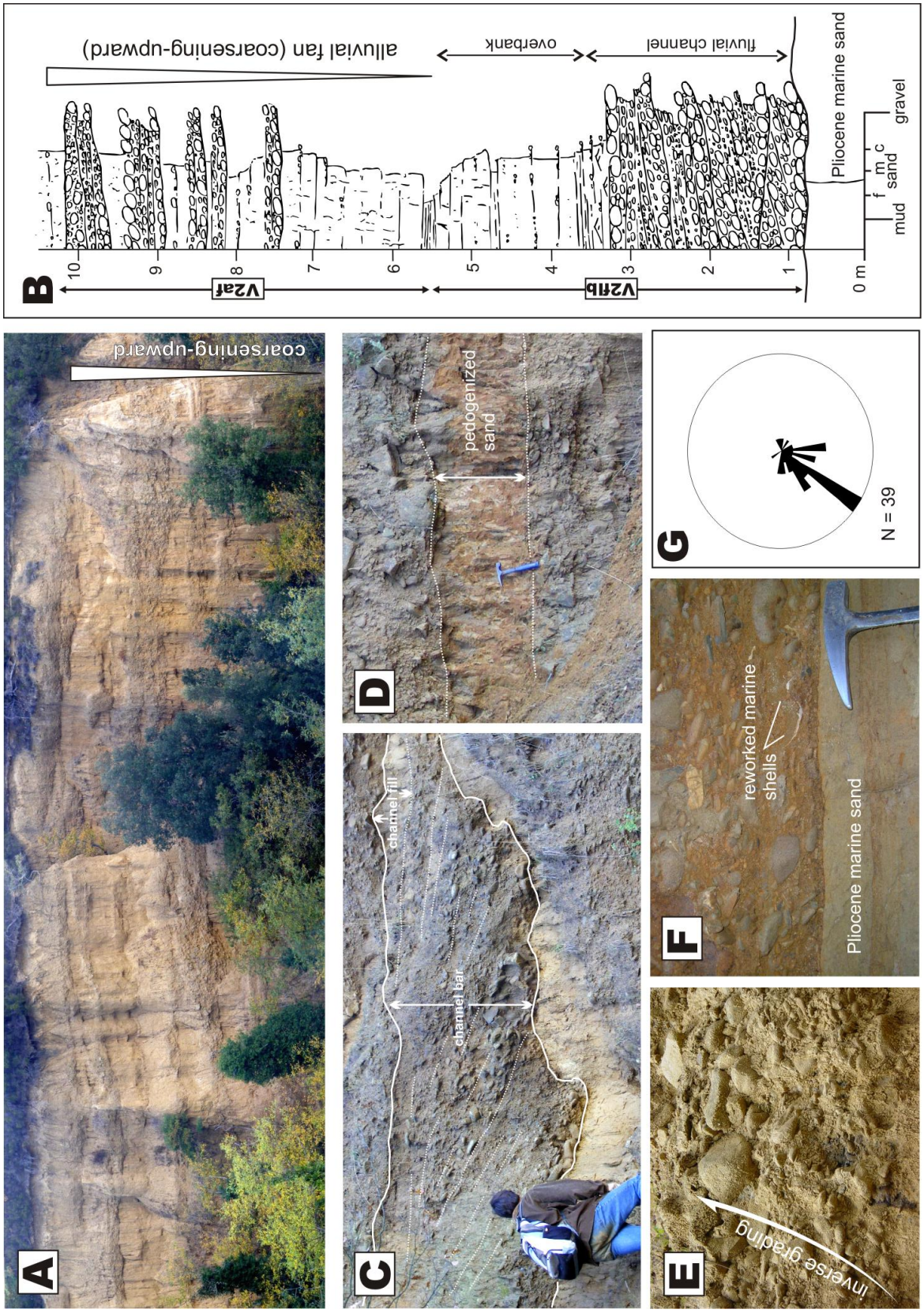

Figure 3.9: A) Panoramic view of unit V2af showing an overall CU trend; B) Sedimentary log showing depositional features of units V2flb and V2fa at Terre Rosse; C) Channelized gravel of unit V2af consisting of inclined gravel beds overlain by channel-fill sand. Gravel beds dip transverse to the main paleocurrent as inferred by basal embricated pebbles; D) Pedogenized sand interval between gravels of unit V2af; E) Close-up of inverse-graded gravel of unit V2af occurring close to the valley flank; F) Fragmented marine shells within gravel overlying the unconformity between marine Pliocene sand and unit V2flb; G) Rose diagram indicating an overall southward transport direction.

beds of disorganized and poorly-sorted, inversely-graded gravel occur as well (Fig. 3.9C). The overall palaeoflow of unit V2af is southwest-ward (Fig. 3.9E).

In the southern sector, V2flb deposits represent most of the unit V2. They cap Pliocene marine deposits (Fig. 3.7A, 3.8C and 3.9B) and bear abundant fragments of reworked marine shells (Fig. 3.9D) and gravel with abraded lithophaga borings (Fig. 3.6F). In the Terre Rosse area, they are also interbedded with, and covered by gravelly sands of unit V2af (section D – D' in Fig. 3.2A; Fig. 3.9B).

3.2.5.1.2.2 Gravel composition

Four samples of 100 clasts each were collected in the Arcidosso (unit V1) and Poggiarello (unit V2flb) areas, respectively (Fig. 3.2B). Gravels are composed by clasts of sandstone, calcareous micrite, calcarenite, flint and shale (Fig. 3.10) and derive from the erosion of rocks belonging to the Ligurian, Subligurian and Tuscan tectonic units exposed in the surrounding bedrock. Compositional analyses shows that unit V1 gravels are composed of ca. 40% of sandstone clasts, commonly deeply weathered, and 45% of calcarenite clasts relatively unaffected by weathering. Differently, unit V2flb gravels are composed of 85% of sandstone clasts, which are relatively unaffected by weathering, and just 4.6% of calcarenites.

3.2.5.1.2.3 Geophysical data

HVSR measurements were performed in the northernmost portion of the southern sector, in order to assess the sub-cropping depth of units V1 and V2flb in the Castello di Montalto and Abbadia di Monastero areas (i.e. section C – C' in Fig. 3.5B). Results display how, in these areas, units V1 and V2flb are mainly composed of gravelly deposits

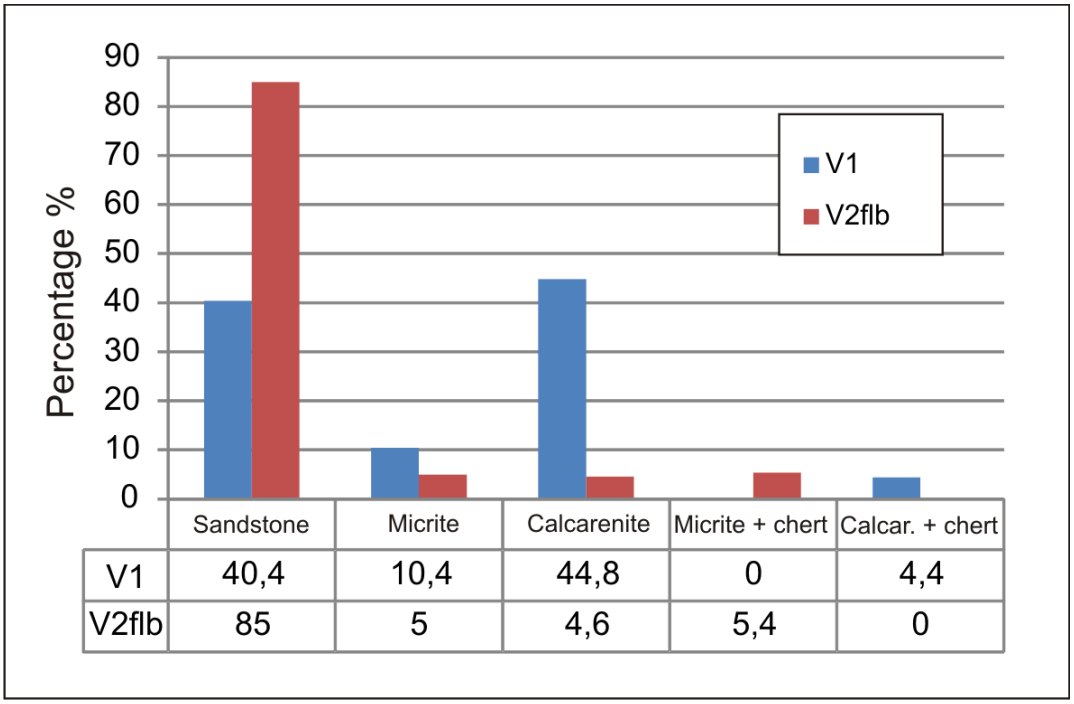

	Sandstone	Micrite	Calcarenite	Micrite + chert	Calcar. + chert
V1	40,4	10,4	44,8	0	4,4
V2flb	85	5	4,6	5,4	0

Figure 3.10: Compositional analysis of gravel from units V1 and V2flb (see text for methodology) showing two distinct populations.

overlying the bedrock (Fig. 3.2A). Measurements performed on units V1 and V2flb deposits showed weak peaks of HVSR, which means relatively low contrast of acoustic impedance.

3.2.5.1.2.4 Interpretation

Channelized gravels and gravelly sands of unit V1 are interpreted as lateral channel bars (Bartholdy & Billi, 2002; Rice *et al.*, 2009; Rice & Churchs, 2010) of relatively sinuous, 4-5 m-deep rivers, where clasts were transported over the bars as dunes or bedload sheets (Bridge, 2003). The coarser pavement flooring the channel probably represents a thalweg lag (Collinson, 1986), whereas the top wedge-shaped sands and muds represent accordingly abandonment fills (Bluck, 1980). Tabular sand and mud were accumulated as overbank deposits (Bridge, 2003) in response to major floods that induced channel over-spilling. Sandy beds probably represent crevasse splays (Ethridge *et*

al., 1981), and organic-rich muds represent fallout deposition in ephemeral, vegetated ponds (Bridge, 2003).

Gravelly deposits of unit V2flb in the Poggiarello area were interpreted as belonging to a variety of fluvial bars; downstream-progradational, longitudinal bars are indicated by coarsening-upward packages of horizontally-stratified gravel (Nemec & Postma, 1993); lateral bars are instead represented by inclined beds dipping towards the channel axis (Lewin, 1976; Bridge, 1993). Subordinate transverse bars (Smith, 1971; Miall, 1977) can be linked with downstream-migrating, cross-stratified deposits. The coexistence of these fluvial forms point out to a multi-channeled system, possibly braided, characterized by relatively shallow, 1-2 m-deep channels. The angular, cobble- to boulder-sized clasts occurring in the lowermost part of channelized bodies indicates the vicinity to source areas, and the limited routing capacity of a proximal, supply-dominated fluvial system. Pedogenized sand and mud are interpreted as overbank deposits accumulated in tractional-plus-fallout conditions during high flood-stages. Sand-grained, unit V2flb deposits in the nearby of Pian di Bari are interpreted as accumulated in 5 m-deep channels floored by pebbly lags. Facies and palaeoflow indicates together their pertinence to lateral bars of poorly to moderately sinuous streams (Jackson, 1976; Nanson, 1980; Brierley, 1991a, 1991b; Bartholdy & Billi, 2002; Ghinassi, 2011). The top mud and sand deposits are interpreted as overbank beds accumulated in poorly drained floodbasins, and record accordingly waning flood-stages.

Unit V2af deposits along Terre Rosse were interpreted as accumulated by progradational alluvial fans (Blair & McPherson, 1994a, 1994b), which were sourced from the north-eastern (hydrographic left) flank of the palaeovalley. Sands accumulated in intermediate to distal fan portions record a scarce flows confinement (Blair & McPherson,

1994a), and were most probably transported and reworked by tractional flows; even so, the subsequent pedogenic imprint masked most of their primary sedimentary signature. Their sedimentological features are similar to those of channelized unit V2flb gravels, suggesting that they were formed in a shallow multi-channeled system. In the proximity of the valley flanks, disorganized and inversely-graded deposits record mass-transport, buoyancy-dominated processes typical of plastic debris flows (Nemec & Steel, 1984).

The abundance in unit V1 of clasts derived from Ligurian and Sub-Ligurian units suggests how, during the early phases of in-valley deposition, Tuscan units (i.e. Macigno Fm. sandstone) were not experiencing dismantling in the local drainage basin of the study area. The dramatic increase in sandstone clasts observed in unit V2flb indicates instead a progression in the un-roofing and denudation of lower tectonic units, with dismantling of Tuscan units, as attested by the dominance of fresh sandstone clasts along with angular sandstone blocks. In this later phase however, Ligurian rocks were still eroded, and provided an ongoing contribution to the processes of sediment sourcing and routing (Fig. 3.2A) although activation of a localized source also occurred, as attested by the dominance of fresh sandstone clasts along with angular sandstone blocks. The further presence of calcareous clasts with abraded lithophaga borings in both units V1 and V2flb deposits also indicates undercutting and routing of the underlying Pliocene marine deposits.

Once calibrated with field data, HVSR suggests that the peaks measured along the C - C’ transect (Fig. 3.5C) can be ascribed to an impedance contrast at the depth of about 65 and 20 m, respectively. These depths are overall consistent with the thickness of units V1 and V2flb.

3.2.5.2 Structural data

3.2.5.2.1 Pliocene-Pleistocene tectonic structures

Pliocene-Pleistocene tectonic structures mainly developed in response to brittle deformation. Two main northeast- and northwest-trending faults systems control (and controlled) hydrothermal fluids circulation and CO_2 discharge (Fig. 3.11). CO_2 leakage mainly occurs along the trace of a northwest-trending fault (Ambra River Fault). A set of northeast-trending faults defines a shear zone, up to 1 km-wide, formed by anastomosed segments that locally dissect and displace the Ambra River Fault (Fig. 3.11).

Bedrock is affected by meso-faults characterized by cm-thick core zones and damage zones up to 3 m-wide; meso-faults display well-developed sets of fractures, often with en-échelon geometry and concentrated near the slip surface (Fig. 3.12A). A number of kinematic indicators comprise: mechanical striation and subordinate calcite fibres (Fig. 3.12B-C); arrays of extensional jogs; and T-fractures in damaged rock masses. Meso-faults affecting Quaternary deposits are defined by sharp surfaces, rarely striated (Fig. 3.12D). Their offset does not exceed few m and is characterized by a dominantly normal displacement; these are associated to minor drag folds, as well as to conjugated minor faults and fractures. Faults affecting gravel display m-thick shear zones characterized by cataclastic flow, which is indicated by striation, fracturing and fragmentation of pebbles that underwent mutual friction along the fault slip surface (Fig. 3.12E-H). Diffuse hydrothermal alteration is related to CO_2 venting along the most permeable fault sectors, and is expressed by a deep argillification and/or decarbonation of the deposits (Fig. 3.12I). In places, mm-thick iron hydroxide-rich patinae and diffuse encrustation developed around pebbles (Fig. 3.12J) indicating again hydrothermal flowing associated to the CO_2 leakage.

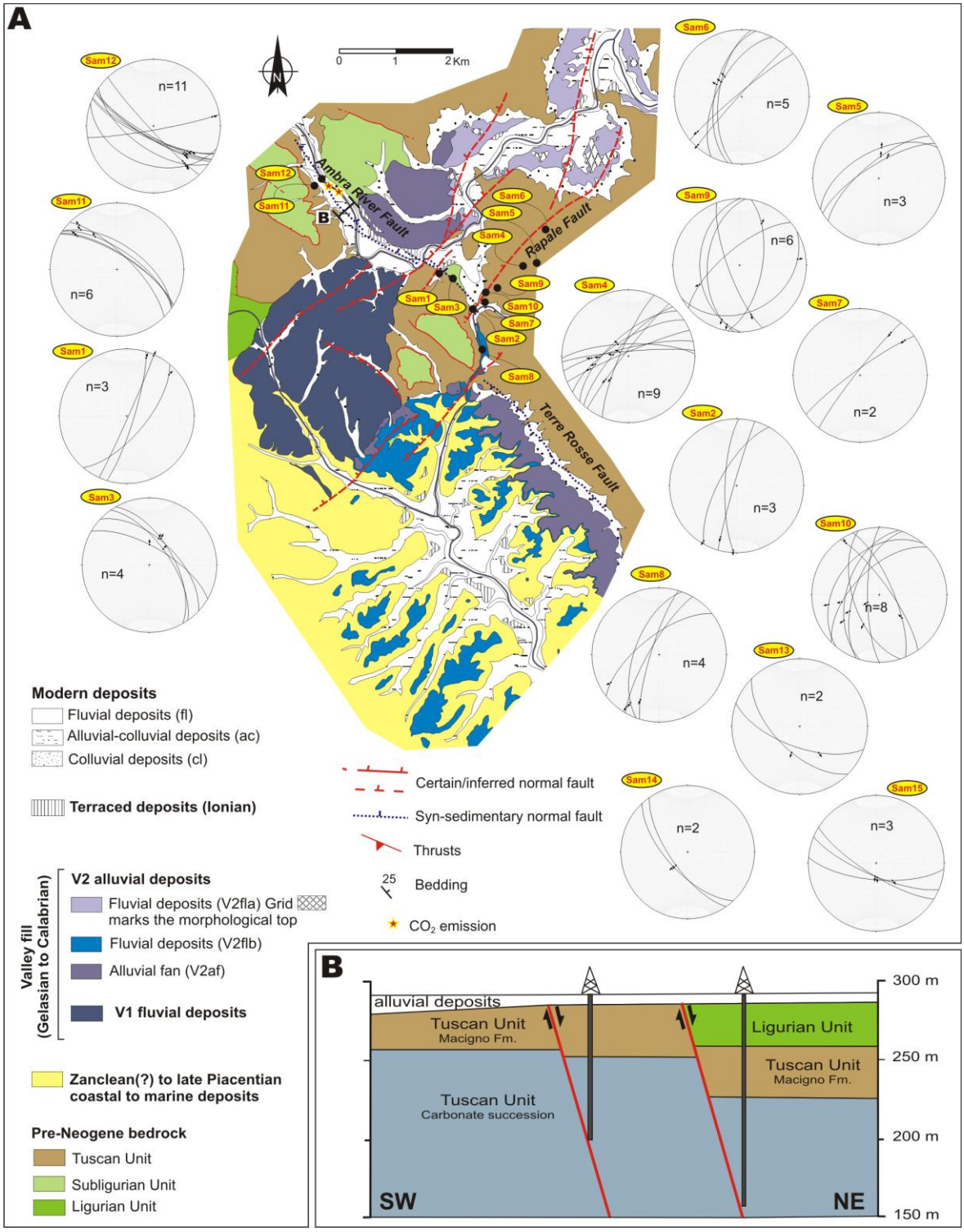

Figure 3.11: A) tectonic sketch-map of the study area and location of the structural stations; Stereonets (lower hemisphere, equal angle projection) illustrate the collected meso-fault dataset; B) Geological cross-sections through the Ambra River Fault. The trace is indicated in A.

Although northeast- and northwest-trending faults are featured by overall similar architecture, they developed under different kinematic regimes: i) northeast-trending faults are characterised by a dominant left-lateral strike- to oblique-slip movements,

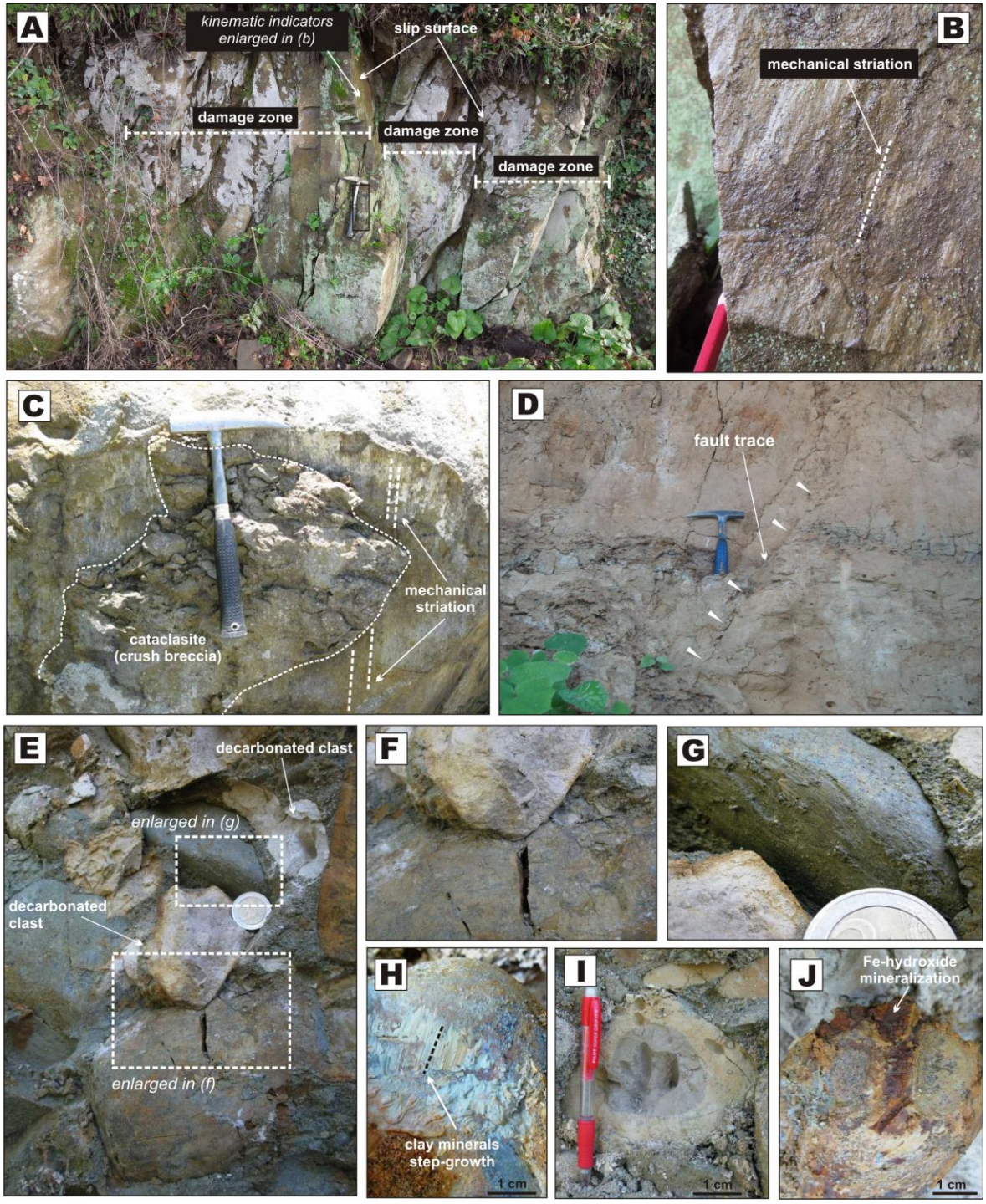

Figure 3.12: A) Meters wide fault zone affecting the bedrock (Macigno Fm) composed by discrete fracture sets and slip-surfaces. B) The kinematic indicators consist of mechanical striations supporting for a brittle deformation occurred at very shallow depth. C) Particular of a cataclasite lens on a slip surface affecting the Macigno Fm, with mechanical striation covered by calcite-sulphide mineralization. D) Fault with decimetre offset affecting unconsolidated sediments. E) Deformational features of gravels involved in a shear zone dominated by cataclastic flow. F-J) particulars of the deformed gravels: localised pressure-induced cracks (F); mechanical striation on gravel surfaces (G-H); localised hydrothermal alteration and mineralization due to the CO2 and hydrothermal fluids circulation (I-J).

occasionally overlapped by normal slip; ii) the northwest-trending faults are instead characterised by dominant normal kinematics. A synthesis of the collected data is reported in Figure 3.11, and shows similarities with the tectonic frame described for the Upper Valdarno Basin by Brogi *et al*., (2013) (Fig. 3.1A and B). The most prominent tectonic lineament in the study area consists of the northwest-trending alignment of the Ambra River and Terre Rosse faults, which are detailed below.

3.2.5.2.2 The Ambra River - Terre Rosse Faults

The Ambra River Fault is exposed in the northern part of the study area. (Fig. 3.11). CO_2 leakage is economically exploited by a number of wells that penetrates the nearby of this fault for up to 150 m (Fig. 3.11B). The Ambra River fault zone comprises a set of minor synthetic faults that gave rise to a significant volume of damaged rock. A large tract of this tectonic structure is capped by modern alluvium, and the main exposures occur along its northwest bedrock wall (Fig. 3.11A). The main slip surface dips northeastward and is characterized by oblique-slip to normal kinematics. In its northern part, the fault offset is estimated in about 40 m, on the basis of borehole data (Fig. 3.11B), whereas an offset of about 60 – 70m can be estimated, through geophysical data, for its southeast side, where the Fault is interrupted and transferred by the northeast-trending Rapale Fault (Fig. 3.11). This implies differentiated displacements along the whole fault tract, with the maximum value in its southeastern side, where the Ambra River fault intersects the Rapale Fault system.

The Terre Rosse Fault dips southwestward and delimits, for at least 3km, the easternmost Pliocene sediments filling the Siena Basin from the bedrock composed of the Macigno Fm. The fault trace is buried by Quaternary deposits, therefore denying direct

observation and kinematic analyses. Its maximum offset can be estimated in several teens of meters. The Terre Rosse Fault is interrupted to the northwest by a southeast dipping fault segment belonging to the northwest trending Rapale Fault system, and therefore transferred toward west (Fig. 3.11). In the corner defined by the intersection of the two faults, the maximum offset is expected, as supported by a distributed tilting of the Pliocene sediments which result back-rotated about 5-10° toward the Terre Rosse Fault footwall. Kinematics analyses on its minor structures, consisting of synthetic minor faults developed in the footwall, support for a dominant normal kinematics (Fig 3.11).

3.2.6 Discussion

3.2.6.1 Tectono-depositional history of the valley

Even if the processes of valley incision probably acted as a consequence of the regional, late Piacentian forced regression (Martini & Sagri 1993; Martini *et al*., 2001), the depositional history of the study area responded to a combination of tectonics processes, autogenic depositional forcing, and local base levels. With mechanisms applicable to the study area as well, Aldinucci *et al*. (2007) discussed how the deposition of unit V1 (Stage 1 of Fig. 3.13) could be ascribed to an episode of valley down-filling (*sensu* Boyd *et al*., 2006) related to the uplift of the surrounding Chianti Ridge, well- documented in the adjoining Upper Valdarno Basin (Bonini *et al.*, 2013; Brogi *et al.*, 2013; Fidolini *et al.*, 2013a), possibly enhanced by renewed humid climate (Ghinassi *et al.*, 2004). These authors also interpreted the mud capping the first interval of unit V1 as accumulated in response to upstream gravel trapping, due to a tectonic-induced gradient decrease along the Ambra River Fault. After the deposition of unit V1, the activation of northwest-

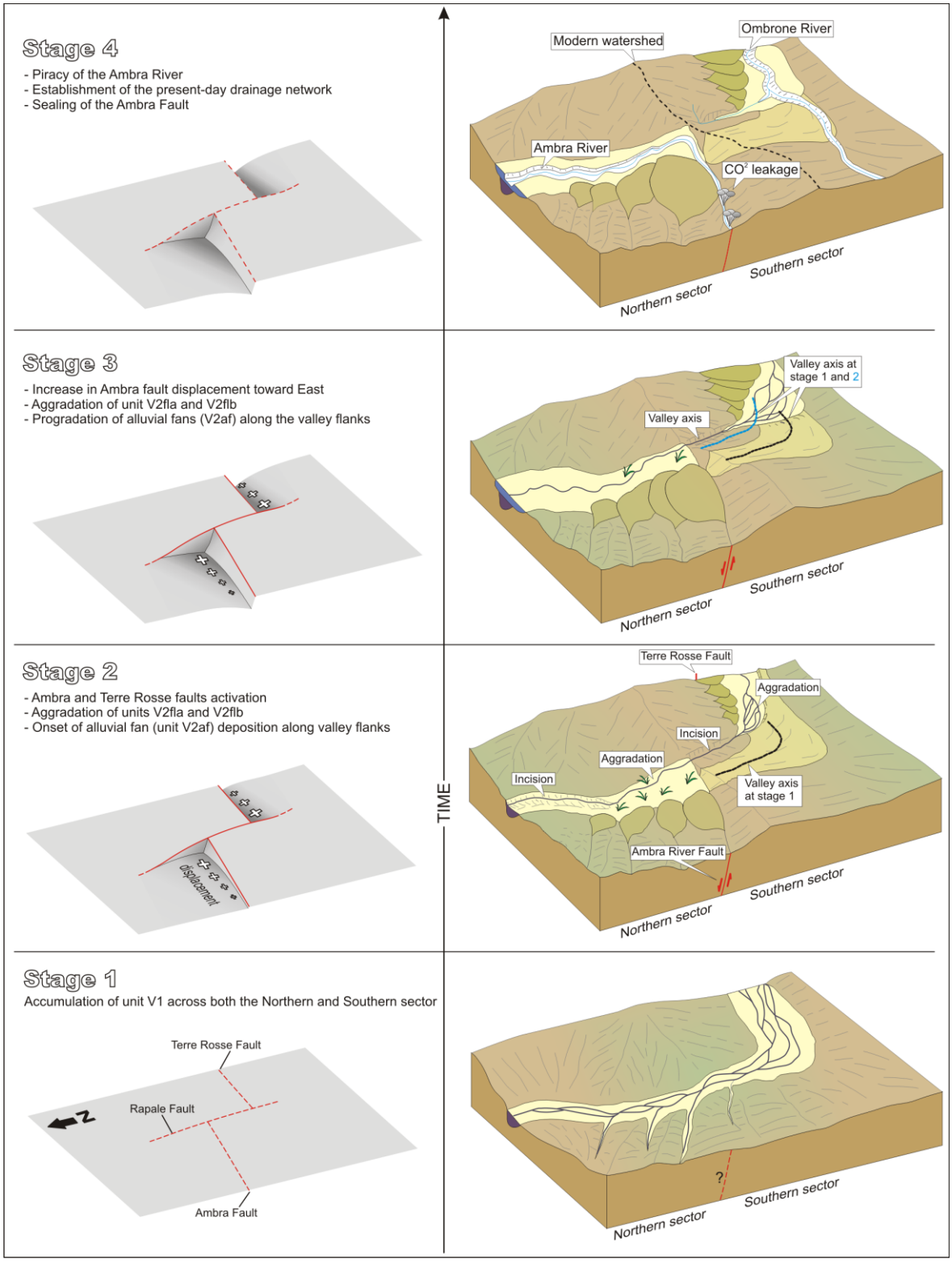

Figure 3.13: Tectono-sedimentary evolution of the studied area illustrated in a four-step 3D sketch. Note the relationships between tectonic movements and drainage evolution with resulting sedimentation patterns.

trending faults (Stage 2 of Fig. 3.13) caused a sudden drainage reorganization: the Ambra River Fault caused subsidence in the northern sector and most probably induced an overall decrease in transport capability of the valley trunk systems; the respective response of the depositional system involved the accumulation of unit V2fla muds, with gravel deposition (unit V2af) restricted to tributary inlets along the valley flanks. At this time, fluvial incision occurred at the boundary between the northern and southern sector of the valley, where both the Macigno Fm. and Pliocene marine deposits were eroded and routed downstream, sourcing in turn the unit V2flb deposits. Relatively un-weathered sandstone clasts, angular boulders and carbonate clasts with abraded lithophaga occur within V2flb gravels, supporting this hypothesis.

As the study area underwent uplift, the axis of fluvial incision within the valley progressively shifted towards the hydrographic left, a mechanism ascribable to the Ambra River Fault growth towards its south-eastern reaches. This process was possibly also favored by the enhanced erodibility of damaged bedrock along the northeast-trending shear zone of the Rapale Fault. In the southern sector instead, the Terre Rosse Fault activity caused deflection of the axial fluvial drainage toward southeast, and then triggered the development of alluvial fans along the left-hand valley flank. Even if dynamic, this morphological configuration was probably maintained stable by the persisting fault growth of the Ambra River and Terre Rosse structures (Stage 3 of Fig. 3.13), at least until the progradational alluvial fans flanking the valley induced an autogenic shift of the fluvial system. The latter autogenic forcing was probably more prominent in the southern sector of the study area. Finally, the piracy of the Ambra River into the Upper Valdarno Basin (Bartolini & Pranzini, 1981), occurred during the early

Ionian (Albianelli *et al*., 1995; Fidolini *et al*., 2013a, 2013b), marked the establishment of the present-day drainage configuration (Stage 4 of Fig. 3.13).

Summarizing, the palaeo-drainage of the study area appears as developed along a tectonically active zone where the slope of the incised valley was affected by differential tilting. Tilting appears to have had both a parallel and normal component to the valley axis, expression of the Terre Rosse and Ambra River Faults, respectively. Tilting further induced different styles of valley profile deformation, here defined as longitudinal and lateral, respectively (cf. nomenclature of Holbrook & Schumm (1999). Although these processes were most probably interacting, their effects on the valley infill dynamics are discussed separately.

3.2.6.2 Valley fill aggradation: the role of longitudinal tilting

Aggradational *vs*. degradational morphodynamics within incised valleys are controlled by the transport capacity of the fluvial trunk, which depends in turn on channel slope, sediment supply and runoff (Lane, 1955; Gibling *et al*., 2011). The interaction between tectonics (e.g. uplift of the source area), climate and drainage evolution (e.g. piracy) also contributes in varying the fluvial transport capability, particularly in upstream portion of alluvial valleys (Zaitlin *et al*., 1994; Blum & Tornqvist, 2000; Boyd *et al*., 2006; Blum *et al*., 2013). Although a climate influence on sedimentation cannot be completely ruled out, our results strongly support the hypothesis that the accumulation of unit V2 was mostly a result of localized uplift and associated alteration in valley profile (Holbrook & Schumm, 1999; Schumm *et al*., 2000).

Notably, the activation of the Ambra River Fault promoted coeval aggradation and degradation in adjacent valley segments. Ouchi (1985) and Holbrook & Schumm (1999)

recognized how upwarped incised valleys can be subdivided in three segments: i) a segment located upstream of the deformed area; ii) a central segment, corresponding to the deformed area; iii) and a segment located downstream of the deformed area. This model generally applies to study area, with the up- and downstream segments corresponding to the northern and southern sectors, respectively. The central segment is instead here represented by a narrow belt located along the boundary between the northern and southern study area. Modern examples such as the Rio Grande River crossing the Socorro magma body, New Mexico (Holbrook & Schumm, 1999), and laboratory experiments (Ouchi, 1985) show that aggradation occurs both upstream and downstream of the uplifted area, which is commonly affected by degradation.

In the northern sector, the high-accommodation unit V2fla deposits well fit with this model (cf. Martinsen *et al*., 1999). Here, the aggradation potential was probably linked by the relative elevation of the trunk thalweg crossing the footwall block. As this elevation moved vertically, a dynamic equilibrium balanced the fault-controlled uplift rate and the erosion capacity of river system. This dynamic equilibrium acted *de facto* as a local base level for this segment of the valley (Blum & Tornqvist, 2000). When the fault uplift rate outpaced that of the footwall incision, a resulting base level rise increased the accommodation potential in the northern sector, resulting in the engulfment of isolated channel bodies within poorly drained floodplain mud. In similar settings, if uplift rate outpaces significantly that of river incision, damming can also occur (Doornkamp & Temple, 1966; Rasanen *et al*., 1987; Dumont, 1992, 1993; Marple & Talwani, 1993). In our case, the reduction of river transport capability associated to slope decrease caused the development of flanking alluvial fans (Zaitlin *et al*., 1994). Even so, the erosionally-based unit V2fla (line ERT 1 in Fig. 3.4) indicates that entrenchment predated aggradation,

possibly in response to an early slope steepening when approaching the subsiding zone (Ouchi, 1985; Holbrook & Schumm, 1999). The sediment produced after entrenchment was in turn trapped in the subsiding zone, following the natural evolution of the river gradient profile (Lane, 1955; Schumm, 1993). The steepened areas (Fig. 3.14) favored an upstream migration of streambed degradation (Ethridge, 1985; Einsele, 1992; Posamentier & Allen, 1999), which caused erosion of unit V1, as well as storing of alluvium along the subsiding valley portions (Fidolini *et al*., 2013b) (Fig. 3.14). The sum of these processes involved an upstream propagation of mud-dominated accumulation, which lead in turn to the individuation of a fining-upward, upstream-thinning succession overlying the basal erosional surface (Fig. 3.14). This sedimentary motif strikingly resembles the fluvial infill of sea level-controlled, inner incised valleys (*sensu* Boyd *et al*., 2006), typically featured by a basal sub-aerial unconformity overlain by a fining-upward, upstream-thinning fill (Wright and Marriot, 1993; Boyd & Diessel, 1994; Shanley & McCabe, 1994; Boyd *et al*., 2006). Following this model, the deposition of unit V2fla can therefore be regarded as a valley backfilling (Zaitlin *et al*., 1994; Boyd *et al*., 2006), where an episode of base level rise originates an upstream-pinching wedge, and with a significant aggradational component favoured by sediment supply of lateral tributaries (Legarreta & Uliana, 1998).

Following classical models, at the boundary between the up- and downstream sectors, the central, uplifting sector should experience prevailing degradation, recorded by erosional unconformities and thinning trends within the valley fill (Schwartz, 1982; Pivnik & Johnson, 1995; Greb & Chesnut, 1996). These features are not expressed in the study area, as the footwall uplift was associated to an eastward shifting of the fluvial system. This process enhanced the preservation of unit V1 on the uplifted block; also,

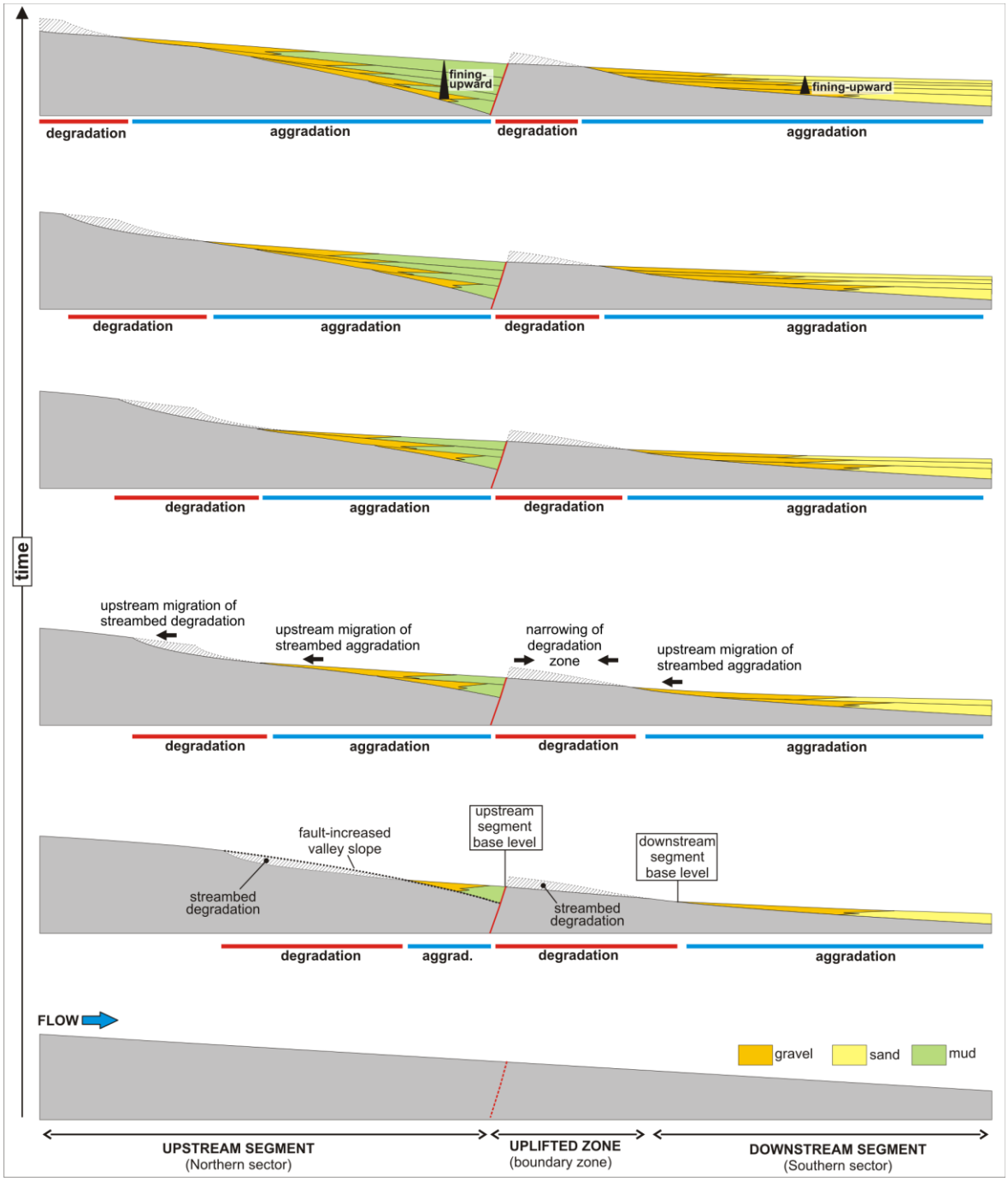

Figure 3.14: Along-valley cross-sections showing the impact of the Ambra Fault movements on the valley river equilibrium profile with resulting degradational vs aggradational patterns, sediments distribution and depositional trends.

since the fluvial system shifted over a resistant bedrock bank, its erosion capacity did not outpace the uplift rate induced by the fault slip, resulting in a bolstered base level rise in the northern sector (Fig. 3.14).

In the southern sector, the aggradation of low-accommodation unit V2fla deposits (Martinsen *et al*., 1999), well fits with the general notion of fluvial deposition downstream of the upwarped area (Ouchi, 1985; Holbrook & Schumm, 1999). However, the erosional surface flooring unit V2 indicates that the eastward-shifting trunk system had in this phase a maximum bedload transport rate exceeding the sediment supply (Blum & Tornqvist, 2000; Paola, 2000). This condition probably reflects the loss of a substantial bedload fraction in the northern sector (Lane, 1955). Once entered the Siena Basin, the trunk system probably had a relatively high incision potential, facilitated in turn by the unconsolidated nature of the Pliocene marine sediments. The following phase of fluvial aggradation was eventually favored by the progressive dismantling of uplifted block, a process that restored the maximum bedload capability of the trunk system (Paola, 2000). At this time, a substantial coarse sediment input interested the area downstream of the upwarped zone (Fig. 3.14), favouring the configuration of a supply-dominated braided configuration (cf. Ouchi, 1985). Storing of coarse sediment was probably limited in this sector of the valley, whereas finer deposition persisted in the downstream Pian di Bari area. As the footwall uplift rate of the Ambra River Fault decreased, the trunk system re-established its ideal equilibrium profile, favouring fining-upward aggradation (unit V2flb) (Posamentier & Allen, 1999; Fidolini *et al*., 2013b). With a pattern similar to that already described for unit V2fla, the fining-upward, upstream-thinning stratal stacking resembles that of incised valleys controlled by relative sea level (Boyd *et al*., 2006). However, we postulate that our result rather point out to processes of

downfilling (Schumm; 1993; Zaitlin *et al*., 1994), originated by an overwhelming sediment supply from upstream point sources (i.e. uplifted zone) that caused rising of the equilibrium profile above the valley floor (Blum & Tornqvist, 2000).

3.2.6.3 Avulsion of the valley: the role of lateral tilting

Lateral thalweg shifting towards down-tilted sides of the alluvial plain is a typical evidence of cross-valley tilting (Alexander & Leeder, 1987). This process has been commonly considered as active at the scale of the channel belt (Bridge & Leeder, 1979; Alexander & Leeder, 1987; Bridge & Mackey, 1993; Dumont & Hanagarth, 1993; Mack & James, 1993), although a marked channel belt mobility can lead in turn to valley axis relocation over time (Blum & Price, 1998; Blum & Aslan, 2006; Blum *et al*., 2013), especially if coupled with the control of inherited morphologies and contrasts in erodibility within the valley. In the study area, the earliest evidence of lateral shift would link the eastward deflection of unit V1 trunk drainage with the displacement associated to the Terre Rosse Fault (Fig. 3.15A). This process was followed by valley avulsion, controlled in turn: by the differential, eastwardly-increasing displacement of the Ambra River Fault, which forced the trunk system into eroding preferentially the hydrographic left the valley (Fig. 3.15B); by the enhanced subsidence generated by the Terre Rosse Fault (Fig. 3.15B). During the deposition of unit V2, the southern valley sector experienced a westward shift of its trunk system, probably assisted by the progradation of alluvial fans sourced from the Terre Rosse area (Fig. 3.15C). In a nutshell, this morphodynamic evolution highlights how valley avulsion can respond directly to tectonic tilting (Leeder & Gawthorpe, 1987), as well as to inherited morphologies and contrasts in erodibility.

The drainage evolution related to the activity of the Ambra River Fault substantially differs from the classical models of lateral tilting (Bridge & Leeder, 1979; Alexander & Leeder, 1987; Dumont & Hanagarth, 1993), which predict shifts in response to faulting with strike parallel to that of the channel belt axis. Although the Ambra River Fault trends normal to the valley axis, its along-strike differential displacement favors an eastward cross-valley tilting (Fig. 3.15D). Once the trunk system adapted to the cross-valley gradient, the activation of alluvial fans in the La Selva area provided a further impulse towards the hydrographic left flank (Blair, 1987). Cross-valley tilting associated to the Ambra River Fault activity is also consistent with "combing" of the channel bodies in the ERT 1 line (*sensu* Todd & Went, 1991) (Fig. 3.4), which progressively migrated in the down-tilt direction without producing an immediate avulsion (Peakall, 1995).

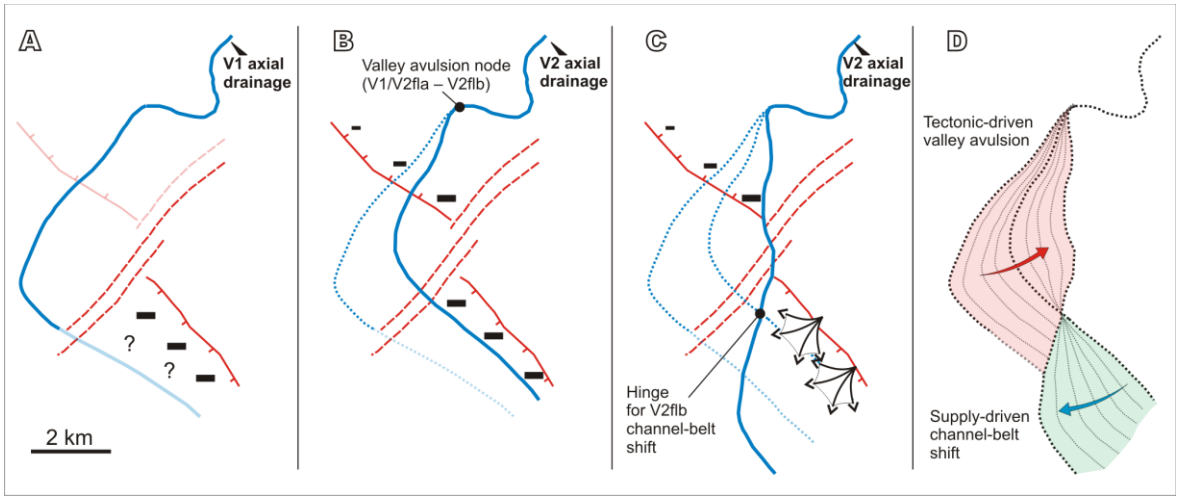

Figure 3.15: Plan-view evolution of drainage patterns in relation to faults activity.

The Terre Rosse Fault had instead a strike parallel to that of the channel belt axis, and the mechanisms of induced channel belt shifting followed those previously described by Bridge & Leeder (1979), Alexander & Leeder (1987) and Dumont & Hanagarth (1993). The occurrence of unit V2flb fluvial deposit in the Terre Rosse Fault zone indicates that

the rate of subsidence was sufficient to diverge the trunk system towards the fault escarpment (Leeder & Gawthorpe, 1987; Peakall, 1995), even if not high enough to preserve unit V1 deposits from the erosion acted by the unit V2flb trunk system. Although mechanisms of trunk shift induced by alluvial fan growth have been previously described (Blair, 1987), our case study also underlines the pivotal role of flank faulting in controlling the ratio between subsidence rate and sediment supply. High subsidence rate: sediment supply ratios will force the trunk system to diverge towards the fault escarpment; Rejuvenated topography will however increase the sediment supply, inducing a subsequent progradation of fault-sourced alluvial fans and related shift of the trunk system towards the opposite valley flank (Fig. 3.15D). In both cases, the rate of lateral trunk shifting will be however also controlled by the erodibility of the valley flanks, especially in strongly incised and confined systems. In alluvial valleys superimposed onto unconsolidated sediments, lateral trunk shifting will be capable of altering significantly the valley aspect over short times, allowing sudden widening yet without a significant deepening (Gibling, 2006).

3.2.7 Conclusions

The present study illustrated a comprehensive model of tectono-sedimentary evolution for a nonmarine incised palaeo-valley draining the northeastern margin of the Siena Basin (Northern Apennines, Italy). The major drivers of facies distribution within the study area consisted of a set of extensional/transtensional, NW- and NE- trending faults active during the Gelasian – Calabrian time span. Syn-sedimentary faulting appears to have controlled most of the alluvial depositional dynamics in the upland sector of the

incised valley, involving coeval tilting of the fluvial drainage along both its major (valley-longitudinal) and minor (valley-parallel) axis.

Longitudinal tilting was forced by a major normal lineament that had striking transverse to the valley axis and upstream-dip. This peculiar geometry involved fluvial aggradation both upstream and downstream of a central uplifted area, which experienced instead landscape degradation. The onset of faulting within the valley resulted in the individuation of two separate knickpoints (upstream and downstream of the faulted zone), the upstream one responding to local increase of valley slope, the downstream one responding to increased stream power due to upstream bedload trapping. Fluvial aggradation produced fining-upward successions both upstream and downstream of the upwarped, faulted area. In the upstream zone, a progressive valley backfilling generated an architecture similar to that of sea-level-controlled, coastal incised valleys. Downstream of the faulted area, aggradation occurred as a downfilling related to an overwhelming sediment supply, which caused the fluvial equilibrium profile to rise above the valley floor.

Lateral tilting affected the fluvial morphodynamics in distinct ways: the activity of a normal fault striking parallel to the valley axis was associated with a down-dip shift of the trunk system; lateral increase in displacement along faults striking transverse to the valley axis also involved a shift of the trunk system towards the faulted valley flank. The latter process was counter-balanced by the activation of fault-sourced, supply-dominated alluvial fans that generated positive topography and shifted back the trunk system towards the valley axis.

The present study sheds light on the effects of tectonics as an active control fluvial aggradational *vs*. degradational dynamics, with a particular focus on upstream, sea-level-

independent reaches. It is finally demonstrated how differential, complex faulting can deeply influence the facies distribution of alluvial valleys, and is capable of promoting significant trunk system shifts, once its effects are coupled with those of inherited morphologies and contrasts in bedrock erodibility.

CHAPTER 4

TECTONICALLY-DRIVEN DEPOSITION AND LANDSCAPE EVOLUTION OF UPLAND INCISED VALLEYS: NUMERICAL MODELLING OF THE PLIOCENE-PLEISTOCENE AMBRA VALLEY (TUSCANY, ITALY)

4.1 OVERVIEW

This chapter is a journal paper in preparation (to be submitted to Earth Surface Processes and Landforms). In this chapter, numerical modelling allowed to assess and quantify the tectonic control on sedimentation of the Ambra palaeovalley fill succession, through a numerical reconstruction. Furthermore the effects of the interaction between fluvial discharge and fault uplift are discussed.

4.2 PAPER

VALERIA BIANCHI[1], TRISTAN SALLES[2], MASSIMILIANO GHINASSI[1], PAOLO BILLI[3], EDOARDO DALLANAVE[4], GUILLAUME DUCLAUX[2]

[1]Dept. of Geoscience, Padova, Italy

[2]CSIRO Earth Science & Resource Engineering, North Ryde, Sydney, Australia

[3]Dept. of Physics and Earth Sciences, Ferrara, Italy

[4]Department of Earth and Environmental Science, Munich, Germany

4.2.1 Abstract

Fluvial sedimentation is predominant within upstream reaches of incised valleys, where it is controlled by interaction between climate and tectonics. Tectonic control on

fluvial sedimentation was the main theme in modelling context for several years, focusing on variation of architectures at the mesoscale. Within tectonically driven uplift context, fluvial response induces rapid and dangerous phenomena such as flooding and avulsion. This study focuses on a Plio-Pleistocene fluvial valley fill in the northeastern margin of Siena Basin (Northern Apennines, Italy), which sedimentation was controlled by the interaction between two opposite-dipping normal faults orthogonal to the valley axis generating a local uplift relative to the fluvial initial base level. The work aims to assess and quantify the tectonic control on fluvial aggradation, through a numerical reconstruction of the valley evolution. Calibration was performed integrating previous field study with palaeo-hydraulic and palaeo-magnetic data. In a broader context, a set of generic models is produced to quantify and generalise the interplay existing between fluvial discharge and uplift rate. The numerical reconstruction highlighted the pre-tectonic system steady state and differential syn-tectonic aggradation, then a system relaxation for the post-tectonic phase. The aggradation is manifested by fine-sediment backfilling aggradation upstream and coarse-sediment downfilling aggradation downstream of the uplifted area. The two aggradations formed diachronous deposits, firstly upstream and secondly downstream, as a rapid consequence to uplift movement. Aggradation phases are spaced out by the time required for the system avulsion and the uplift degradation. Generic models emphasised the speed and intensity of fluvial response to uplift movement, highlighting valley sedimentation and deposit heterogeneity sensibility to several types of uplift movements and fluvial discharge settings.

Keywords: alluvial-valley fill; extensional tectonics; numerical modelling.

4.2.2 Introduction

Understanding the evolution of the Earth's surface has been the challenging objective of geomorphologists and sedimentologists for over a century (Gilbert, 1895; Davis, 1899). The development of methods such as geochronological techniques, remote sensing and geographic information systems (GIS) have made it possible to gather quantitative data and better constrain the evolution of the Earth's surface in a variety of environments. Modelling surface processes has allowed the geoscience community to test and develop new conceptual models and to quantify the drivers and feedback mechanisms responsible for shaping the Earth's surface (e.g., England & Molnar, 1990; Hasbargen & Paola, 2000; Bonnet & Crave, 2003; Paola *et al.*, 2009). Over the past three decades, new numerical modelling methods have been developed to address medium- to large- scale landscape evolution and stratigraphy reconstruction over spatial dimensions of a catchment to an orogen and temporal dimensions of 10^4 to 10^6 years (e.g., Koons, 1989; 1994; Kooi & Beaumont, 1994, 1996; Dietrich *et al.*, 2003; Braun & van der Beek, 2004; Willgoose, 2005; Paola *et al.*, 2009; Tucker & Hancock, 2010).

The tectonic control on fluvial sedimentation was the main theme in the modelling context for several years since the revealing papers involving the LAB models, so-called by Bryant *et al.* (1995) including Leeder's paper (1978) and coworkers (e.g. Alexander & Leeder, 1987; Allen, 1978; Bridge & Leeder, 1979; Mackey & Bridge, 1995). These studies focused on the influence of external and internal forcing on alluvial architecture, with emphasis on channel-belt deposits (mesoscale), their connectivity and their implications for petroleum and aquifer research (Leeder, 1993; Dalrymple, 2006; Bersezio *et al.*, 2004). Numerical modelling in these types of research presents a unique and physically valid approach to quantify the interplay between mesoscale architectures and selected forcing

factors involved during sedimentation (Hickson *et al.*, 2005).

For incised-valley systems, tectonic and climate are considered to be the main controls of fluvial sedimentation in upstream reaches (Shanley & McCabe, 1991; Currie, 1997; Blum & Tornqvist, 2000; Holbrook, 2001), whereas relative sea-level fluctuations are mainly controlling the downstream evolution of valley fill (Zaitlin *et al.*, 1994; Boyd *et al.*, 2006). Recent studies from Blum *et al.* (2013) show that water, sediment supply, as well as the distribution of vertical displacements along incised-valley, are the primary upstream boundary conditions for any fluvial system.

Tectonic control, in the majority of fluvial valley studies refers to the effects of subsidence variations on fluvial aggradation (Leeder, 1978; Hickson *et al.*, 2005), and only few of them take into account the effects of uplift movements (Burnett & Schumm, 1983; Ouchi, 1985). However, uplift rate in fluvial setting leads to more rapid and concentrated facies variations than those produced by subsidence (Schumm, 1986; Guiseppe & Heller, 1998). Rapid uplift movements (>10 mm/yr) can produce sudden valley flooding (New Madrid earthquake, Russ, 1982; Schumm, 1986; Gibling *et al.*, 2006; Hengesh & Lettis, 2002) and avulsions (Indus Valley, Dales, 1966; Hole, 2011). The topographic steady state in a tectonically active setting could be referred as the achievement of the balance between the long-term erosion rate and the rock uplift rate; consequently, the topography is statistically invariant over the long term (Whipple, 2004). Tectonic forcing disturbs the equilibrium profile of the river and increases stratal heterogeneities, variation in grain-size distribution, avulsion and incision (Ouchi 1985; Holbrook & Schumm 1999; Blum & Tornqvist, 2000; Hickson *et al.*, 2005; Blum *et al.*, 2013).

The Plio-Pleistocene fluvial infill of the Ambra Valley (Northern Apennines, Italy) is an outstanding example of sedimentation in an upstream valley reaches, where

aggradation is primary driven by an upstream-dipping, normal fault trending transversally to valley axis. Recent studies (Aldinucci *et al.*, 2007; Bianchi *et al.*, 2013; Bianchi *et al.*, submitted) provided a detailed field-based dataset necessary to produce meaningful numerical results (Leeder, 1978, Mackey & Bridge, 1995; Whipple, 2004; Hickson *et al.*, 2005).

This chapter presents the physical equations and the calibration techniques used to develop a numerical model for the valley-fill accumulation. Results of this work will be compared with those stemmed out from field investigations. Finally generic models are developed to study the impact of fluvial discharge and uplift rate on recorded fluvial architectures. Using these numerical experiments relationships between fluvial valleys and uplift forcing are discussed.

4.2.3 Geological setting

The study valley-fill succession is located along the northern margin of the Siena Basin, one of the Neogene-Quaternary depressions (Fig. 4.1A) developed on the Northern Apennines (Italy) as superficial response to a lithospheric scale extensional process (Carmignani *et al.*, 1994, 1995, 2001; Barchi, 2010; Brogi, 2008). These basins, up to 200 km long and up to 25 km wide, are filled with continental to marine deposits (Martini & Sagri, 1993). The basins are NW- and NNW-trending and segmented into minor depressions by NNW-SSE-oriented tectonic lineaments (Liotta, 1991; Martini & Sagri, 1993; Bonini & Sani, 2002; Pascucci *et al.*, 2007), which control organization of the present-day fluvial drainage (Bartolini & Pranzini, 1981).

The study area (Fig. 4.1B) is located where the northern margin of the Siena Basin crosses one of these lineaments (i.e. Arbia Val - Marecchia line; Liotta, 1991). The margin

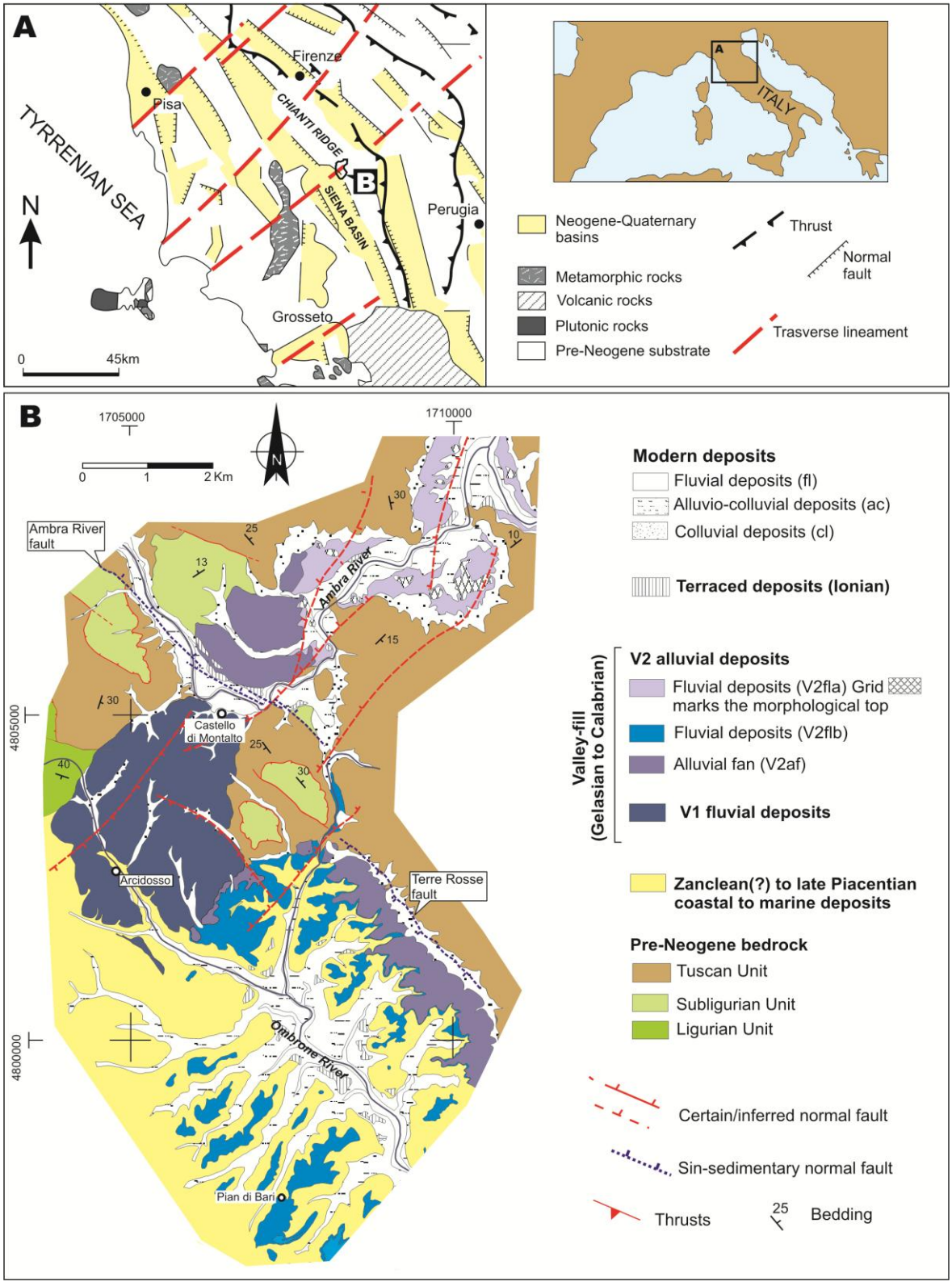

Figure 4.1: A) Simplified geological sketch of the Northern Apennines showing the Neogene-Quaternary basins bounded by bedrock ridges and main tectonic features; B) detailed geological map of the studied area with the main localities mentioned in the text.

of the Siena Basin is made of Cretaceous to Oligocene sedimentary rocks (Abbate & Sagri, 1982) mainly consisting of sandstone with subordinate marlstone and shale. Sedimentation in the Siena Basin started in the late Miocene in a fluvio-lacustrine setting, and followed into marine realm from the early Zanclean to late Piacentian (Bambini *et al.*, 2010; Martini *et al.*, 2011, 2013; Arragoni *et al.*, 2012), when a regional tectonic doming caused a widespread forced regression (Martini *et al.*, 2001). The studied palaeovalley was cut as a consequence of this regression both onto the rocky margin (Chianti Ridge; Fig. 4.1A) and marine sand and mud (Fig. 4.1B), and was successively filled with fluvial deposits (Aldinucci *et al.*, 2007; Bianchi *et al.*, submitted) sourced from North (i.e. Chianti Ridge). Drainage reorganization caused the valley to be abandoned and dissected by minor watercourses during the latest Calabrian/early Ionian (Bartolini & Pranzini, 1981; Fidolini *et al.*, 2013a, 2013b).

4.2.4 Depositional history

Regional evidence demonstrates that valley filling occurred beyond the influence of relative sea-level (Aldinucci *et al.*, 2007). Specifically, the upper part of this succession stemmed out from the interaction between the southward-draining fluvial system and two normal faults, named here Ambra River and Terre Rosse fault. The Ambra River fault (Minissale, 2004; Baldi *et al.*, 2006) cuts the pre-Neogene bedrock, dips toward NE (i.e. transverse to the valley axis) whereas the Terre Rosse fault dips toward SW (i.e parallel to the valley axis) and displaces Pliocene marine deposits (Bianchi *et al.*, 2013).

Bianchi *et al.* (2013) and Bianchi *et al.* (submitted) divided the valley-fill succession into two main sedimentary units (V1 and V2) and summarized their tectono-sedimentary evolution as follow (Fig. 4.2A):

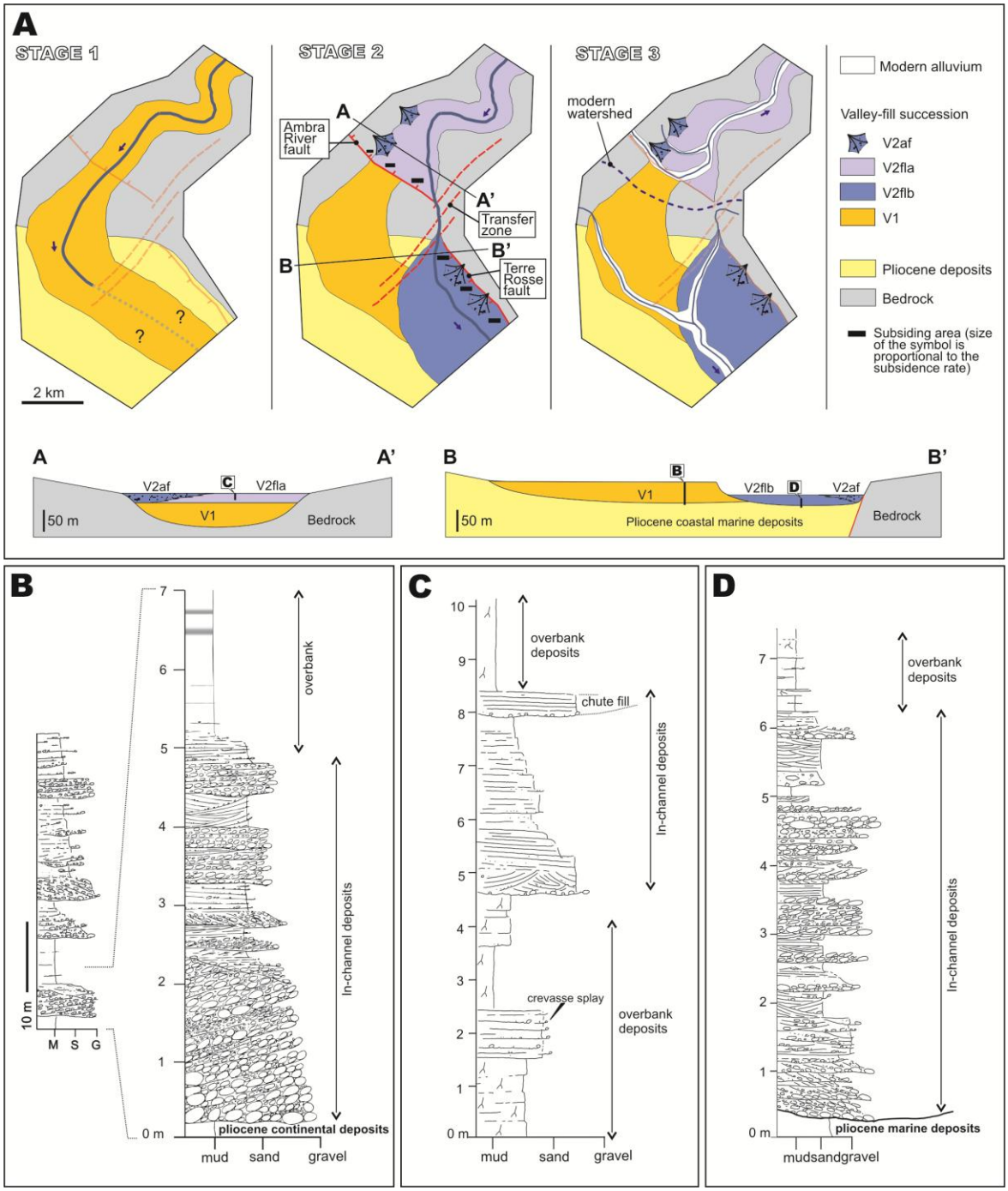

Figure 4.2: A) Tectono-sedimentary evolution of the studied area illustrated in a three-step sketch with geological cross-sections (A-A', B-B'). B) Sedimentary log showing depositional features of unit V1, with a detail of the first FU interval. C) Sedimentary log showing depositional features of unit V2fla. D) Sedimentary log showing depositional features of unit V2flb; note the FU trend.

1) Tectonic uplift of the Chianti ridge provided a pulse of sediment which caused accumulation of about 60-70 m of gravelly sand deposits within the whole valley (V1 unit; Fig. 4.2B).

2) Activation of the Ambra River Fault triggered subsidence upstream of the fault zone, with an overall decrease of fluvial transport capability and consequent accumulation of mud-rich fluvial deposits (V2fla; Fig. 4.2C) and coeval alluvial-fan gravels (V2af) at the entrance of the main tributaries into the valleys. In the uplifted area, fluvial incision progressively shifted toward the left-hand flank of the valley, in response to the SE increase in displacement of the Ambra River fault. Downstream of the uplifted zone, the activation of the Terre Rosse Fault caused an eastward shift of the fluvial system, which started to accumulate gravel and sand (V2flb) sourced from the uplifted area over the marine Pliocene succession (Fig. 4.2D).

3) The piracy of the Ambra River toward North marked the establishment of the present-day drainage configuration.

The present study focuses on the tectono-sedimentary dynamics stemming out from the interaction between the fluvial system and the Ambra River fault (Stage 2 of Fig. 4.2A).

4.2.5 Simulated processes & governing equations

Until recently, geomorphic and stratigraphic codes were generally separated. Increasing demand for solving geomorphic changes and track sedimentary record simultaneously stemmed out to the generation of new codes (e.g. CHILD: Gasparini *et al.*, (2004), or ROMS: Warner *et al.*, (2008)). LECODE (Salles & Duclaux, submitted) is one of these codes. It performs 3D parallel geomorphic and stratigraphic modelling, able to replicate surface processes and their influences on the sedimentary system through time. This modelling framework addresses large-scale landscape evolution and stratigraphic reconstruction equivalent to valley or basin scale through geological time (Salles &

Duclaux, submitted). The adopted modelling scale is suitable for the scientific community because it encompasses the results obtained from different geological disciplines, such as sedimentology, geomorphology, stratigraphy, hydrology, geodynamics and palaeoclimatology (Alexander *et al.*, 1994; Bishop, 2007; Jerolmack, 2011; Salles & Duclaux, submitted). The geomorphic and stratigraphic modelling framework used in this work, is based on a Lagrangian particle-in-cell finite difference scheme, already developed in other codes (Tetzlaff & Harbaugh, 1989; Griffiths *et al.*, 2001). The method has the advantage of allowing the flow to follow the topography in a natural way and it also offers an alternative to purely diffusive approach often used in stratigraphic models (Heimsath *et al.*, 2005). LECODE modelling code is able to reproduce several sedimentary processes that shape the surface in an innovative way. It has been implemented through: i) a parallel approach, increasing the modelling power and then accounting better the surface flow; ii) an unstructured mesh, which consists of triangulated irregular networks for discretise the surface with variable resolution, enhancing the possibility of a refinement by means of a dynamic rediscretisation (Salles & Duclaux, submitted).

LECODE solves the flow evolution using the "particle-in-cell" approach. It uses fluid elements (*flow walkers*) as passive tracers particles, which describe flow evolution through time, and with their acceleration or deceleration these flow walkers are able to erode or deposit (Harlow, 1964; Hockney & Eastwood, 1981). For every flow walker it is possible to obtain two equation sets from Newton's law of motion for incompressible fluid: i) The Navier-Stokes momentum equation and ii) the law of conservation mass (Lane & Richards, 1998). Assuming the fluid as incompressible, homogeneous and at constant temperature, in two dimension the continuity or mass conservation equation can be expressed as:

$$\frac{\partial A}{\partial t} = -\nabla * (Av) = 0$$

where A is the flow area and v is the horizontal flow velocity vector.

And the simplified depth-averaged shallow water momentum equation can be simplified as:

$$\frac{Dv}{Dt} = -gR\nabla H + \frac{c_2}{\rho}\nabla^2 v - c_1 \frac{v|v|}{h}$$

The Lagrangian derivative of horizontal flow velocity vector with respect time is function of *H* water surface elevation, *p* the fluid density, c_1 the bottom friction coefficient, c_2 the lateral friction coefficient and *gR* the specific gravity of the flow.

The bottom friction is expressed using Manning equation (Tetzlaff & Harbaugh, 1989; Griffiths *et al.*, 2001).

$$c_1 = gR\frac{n^2}{h^{\frac{1}{3}}}$$

where *n* is the Manning roughness coefficient. The values of *n* are determined empirically and are available for open channel flow (Arcement & Schneider, 1984; McCuen, 1998).

In addition the transport is simulated as a non-uniform sediment mixture and then divided into several grain-size classes (Zhang, 1989; Wu *et al.*, 2000). Wu (2007) solved a simplified sediment transport for each grain-size class *k* in a Lagrangian context:

$$\frac{Dc_k}{Dt} = -\frac{\beta_t w_{sk}}{h}(c_k - c_k^*)$$

where c_k is the depth-averaged concentration of sediment *k,* c^*_k is the equilibrium sediment concentration that involve both suspended and bed load sediments and β_t is the adaptation coefficient, proposed by Wu (2007).

In LECODE, sediment diffusion assumes that a particle moves downslope until it reaches its angle of static friction (θ), at a rate proportional to the tangent of the slope

angle. Such an assumption is simplistic because natural agents such as air and water actually move sediments at rates that are not determined solely by slope (Heimsath *et al.*, 2005; Paola *et al.*, 2009). In LECODE the slope diffusion algorithm is used associate with previously described sediment transport processes, becoming a secondary sediment transport mechanism.

4.2.6 Parameters calibration

Parameters associated with sediment size, hydrology and time-scaling are required to constrain any simulation to the case of study. The following subsections present how palaeo-hydraulic and time-scale parameters required to initialize LECODE simulations have been derived from previous field data studies.

4.2.6.1 Palaeo-hydrology

Palaeohydrological investigations were focused on gravelly deposits of unit V1 exposed in the Arcidosso area, where a specific cross-section (Fig. 4.3) allowed to measure grain size distribution of bed material and the hydraulic geometry (e.g. bankfull area, wetted perimeter, maximum and mean depths). These gravels were accumulated (Bianchi *et al.*, submitted) in lateral bars within single, relatively-sinuous channels ("wandering" *sensu* Rice *et al.*, 2009 or "pseudo-meandering" *sensu* Bartholdy & Billi, 2002).

Grain size distribution of bed material was measured in channel lag deposits stretching a tape ruler across the outcrop cliff and collecting 100 clasts tangent to the ruler dent every 50 cm. Channel lag deposits was selected since they are the most

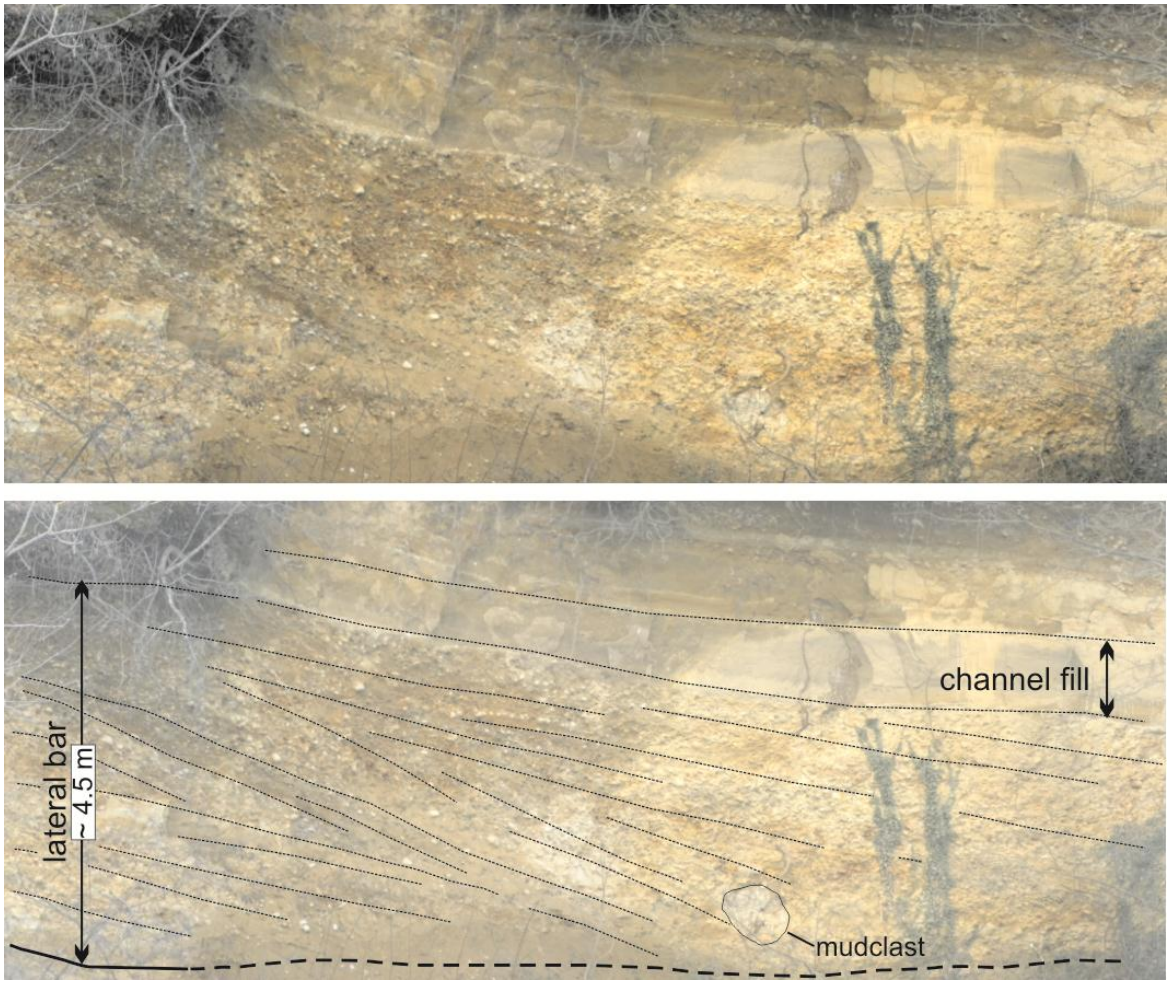

Figure 4.3: Panoramic view and relative line-drawing of the last FU interval belonging to unit V1. The sedimentary parameters to calculate the palaeohydraulic section are reported.

effective in determining the boundary flow resistance in the equations to calculate the hydraulic parameters. Grain size of bed material is shown in Table 4.1 as D_{50}, D_{84} and D_{90}. Thickness of large scale-inclined bedsets shows that the studied palaeochannel was about 4.5 m deep (Fig. 4.3 and Table 4.1). Channel-fill deposits are not entirely exposed but their lateral extent shows that the channel was at least a few tens of meters wide. The width of a 4.5 m deep single channel forming gravelly lateral bars can be estimated at about 70 m (Wb in Table 4.1) according to Leeder (1978), and its hydraulic section at about 200 m^2 (A in Table 4.1) following (McGowen & Gardiner, 1970).

Mean flow velocity (v) was calculated using the Chezy uniform flow equation

$$v = C\,(RS)^{0.5} \quad [1]$$

where R is the hydraulic radius, S the streambed gradient and C the roughness coefficient.

$$C = (8g)^{0.5}/f^{0.5} \quad [2]$$

in which g is gravity and $1/f^{0.5}$ is the Darcy-Weisbach roughness coefficient.

To calculate $1/f^{0.5}$, the following equations were used:

$$1/f^{0.5} = 1 + 2*\log\,(h/D_{84}) \text{ (Leopold \& Wolman, 1957)} \quad [3]$$

where h is mean depth and D_{84} is the grain size for which 84% of the distribution is finer;

$$1/f^{0.5} = 1.16 + 2*\log\,(R/D_{84}) \text{ (Limerinos, 1970)} \quad [4]$$

$$1/f^{0.5} = 0.82*\log\,(4.35*R/D_{84}) \text{ (Knighton, 1996)} \quad [5]$$

These equations were selected since they were developed for gravel-bed streams with grain size similar to those of the studied cross-section.

Since tectonic tilting affected the studied deposits the streambed gradient that could be eventually inferred from field exposures is considered not to be representative of the actual one.

In order to assess the streambed gradient of the studied palaeochannel, the following equations were used:

$$S = 0.002 \cdot W_b^{-0.06}\, H^{-0.91} \text{ (Williams, 1984)} \quad [6]$$

in which W_b is bankfull width and H is maximum depth

$$S = 0.0173\,*(H / D_{84})\,0.785 \text{ (Dingman \& Sharma, 1997)} \quad [7]$$

$$S = Jf / 2.58^{\,0.862} \text{ (Billi } \textit{et al.}\text{, 2014)} \quad [8]$$

where Jf is the Jamming factor of the clasts in the considered section (table 1) , which is function of channel width and grain-size (Jf = D_{90} / Wb; D_{90})

Eqs [6], [7] and [8] provided streambed gradients of 0.0004, 0.0007529 and 0.0006436, respectively (Table 4.1). Combining *C* and *v* values, we obtained the *v* values reported in Table 1. For each *v* values, bankfull discharge *Qb* was calculated

$$Qb = v / A.$$

The bankfull discharges calculated with different criteria are very close with an average value of 230 m^3s^{-1} (Table 4.1). This value is considerably similar to the discharge of the modern Arno River, which is located at about 10 km North of the study area and represents the main watercourse in the region since Piacentian (Bartolini & Pranzini, 1981).

4.2.6.2 Palaeomagnetism

In order to provide a time-constrain for the valley-fill succession we have integrated regional geological evidence with palaeomagnetic analyses, which were carried out on 56 oriented samples collected for unit V1 and V2 the Arcidosso (30) and Pian di Bari (26) area respectively (Fig. 4.1B and 4.4A). All the oriented specimens were stepwise thermally demagnetized up to a temperature of 575 °C, and the natural remanent magnetization (NRM) of the specimens was measured after each demagnetization step. A set of representative specimens from the rock-cutting residuals was used to investigate the magnetic properties of the sediments by mean thermomagnetic curves, which revealed that a mixture of goethite and maghemite dominates the magnetic particles of the sediments.

		Arcidosso
Field data	H (m)	4.5
Leeder (1977)	Wb (m)	**68.9**
Section (McGowen & Gardiner, 1970)	A (m^2)	**206.8**
Field data	D_{50} (mm)	0.0363
	D_{84} (mm)	0.0830
	D_{90} (mm)	0.1004
Billi *et al.* (2014)	Jf	0.0015
Billi et al. (2014)	**S**	**0.0006436**
Williams (1984)	**S**	**0.0004**
Dingman & Sharma (1997)	**S**	**0.0007529**
Knighton	C	15.739621
Limerinos	C	37.353591
Leopold & Wolman	C	35.936951
Knighton + Billi	V (m/s)	0.669
Knighton + Williams	V (m/s)	0.524
Knighton + Dingman & Sharma	V (m/s)	0.724
Limerinos + Billi	V (m/s)	1.588
Limerinos + Williams	V (m/s)	1.244
Limerinos + Dingman & Sharma	V (m/s)	1.718
Leopold & Wolman + Billi	V (m/s)	1.528
Leopold & Wolman + William	V (m/s)	1.197
Leopold & Wolman + Dingman & Sharma	V (m/s)	1.653
Knighton + Billi	Qb (m^3/s)	138.4
Knighton + Williams	Qb (m^3/s)	108.4
Knighton + Dingman & Sharma	Qb (m^3/s)	149.7
Limerinos + Billi	Qb (m^3/s)	328.5
Limerinos + Williams	Qb (m^3/s)	190.8
Limerinos + Dingman & Sharma	Qb (m^3/s)	263.6
Leopold & Wolman + Billi	Qb (m^3/s)	316.0
Leopold & Wolman + Williams	Qb (m^3/s)	247.5
Leopold & Wolman + Dingman & Sharma	Qb (m^3/s)	341.8
Qb total average	**Qb (m^3/s)**	**231.6**
Qb total average without Knighton	**Qb (m^3/s)**	**281.4**

Table 4.1: Parameters involved in the calculation of bankfull discharge.

Intensity of the NRM varies between $5.5x10^{-5}$ and $9.6x10^{-4}$ A/m, with an average value of $4.3x10^{-4}$ A/m. Scattered magnetic component directions are observed between room temperature and generally 150–250 °C. Characteristic magnetic component (ChRM) directions linearly trending to the origin of the demagnetization axes were isolate

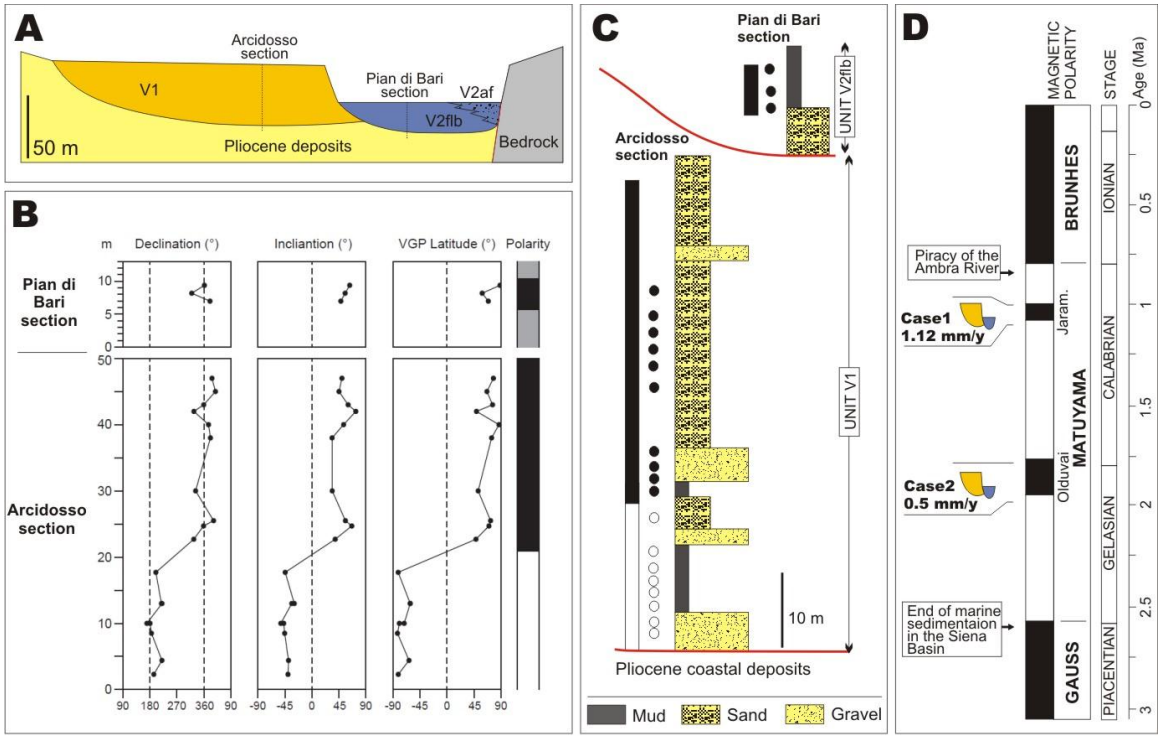

Figure 4.4: A) Schematic geological cross-section showing sites of palaeomagnetic sampling B) From left to right declination, inclination and virtual geomagnetic pole (VGP) latitude associated to each ChRM direction, plotted vs. the stratigraphic position of the samples. The relative latitude of each VGP with respect the paleomagnetic (North) pole was used to interpret the magnetic polarity: black (white) bar indicate normal (reverse) polarity. C) Representative sedimentary log with positioning of palaeomagnetic samples in the valley-fill succession. D) Palaeo-magnetic constraints on valley-fill deposition.

generally up to 450–550°C in 16 oriented specimens at Arcidosso and on 9 at Pian di Bari. At Arcidosso these directions are organized in two modes pointing Nord-and-down and South-and-up, respectively. In 2 specimens the thermal demagnetization patterns are compatible with South-pointing ChRM directions, however tracking along a great circle path. We combine these great circles with the S-and-upward pointing stable endpoint directions applying the algorithm proposed by McFadden & McElhinny (1988). After these analyses we obtained 18 ChRM directions suitable for magnetic polarity stratigraphy, 10 pointing North-and-down and 8 South-and-up. The two modes deviate from antipodality by 15.0°, passing the reversal test using the procedure suggested by Watson (1983; V_0= 5.4, $V_{critical}$= 6.5, Fig. 4.4B; see also Tauxe, 2010 for details on the method), with a class 'C'

following the classification proposed by McFadden & McElhinny (1990). At Pian di Bari all the ChRM directions point North-and-down. We have calculated the position of the virtual geomagnetic pole (VGP) for each ChRM direction, and we have used the latitude of each VGP relative to the mean palaeomagnetic (north) pole for interpreting magnetic polarity stratigraphy (Kent *et al.*, 1995; Lowrie & Alvarez, 1977). The VGP relative latitudes approaching +90° or -90° are interpreted as recording normal or reverse polarity, respectively (Fig. 4.4B). At Pian di Bari we have calculated a total of 3 VGPs averaging the samples ChRM directions from the same stratigraphic level. The Arcidosso section is characterized by reverse polarity from the base up to 26.3 m, and by normal polarity upsection, whereas the whole Pian di Bari section is characterized by normal polarity (Fig. 4.4B and C).

The termination of marine sedimentation in the Siena Basin (i.e. latest Piacentian; Bambini *et al.*, 2010; Martini *et al.*, 2011, 2013; Arragoni *et al.*, 2012) and the valley abandonment due to a piracy of the Ambra river (i.e. latest Calabrian; Bartolini & Pranzini, 1981; Fidolini *et al.*, 2013a, 2013b) allow to frame accumulation of units V1 and V2 within the Gelasian to Calabrian time span (Fig. 4.4D). Two distinct scenarios stem out therefore from palaeomagnetic analyses. In the first case (Fig. 4.4D), most of the study succession accumulated during the subchron Jaramillo, with an average sedimentation rate close to 1.1 mm/yr. In the second case, it was mainly deposited with an average sedimentation rate of about 0.5 mm/yr during subchron Olduvai (Fig. 4.4D). The sedimentation rate for the first scenario seems to be unrealistic considering the scarce elevation and uplift rate of the of the Chianti ridge during the Pliocene – Pleistocene time (Thomson *et al.*, 2010). Considering the duration of the Olduvai subchron, a time of deposition of 300 kyr will be therefore used for numerical models.

4.2.7 The experiment 1 – Ambra Valley simulation

The initial setting of Ambra Valley numerical simulation requires the definition of pre-Gelasian buried geological layers sedimentary composition and thicknesses, the reconstruction of palaeo-topography, and the assumption that tectonic was the main forcing on sedimentation, as attested by field evidence (Bianchi *et al.*, 2013; Bianchi *et al.*, submitted).

4.2.7.1 Initial geological layers

The geological layers were characterised by a volume, represented by the sedimentary layer defining the substratum geology, and the surface defined by the topography (Fig. 4.5).

The topography reconstruction was obtained by a geomorphic and geological interpretation of the early Gelasian palaeo-topography consistent with field data presented in previous chapters. To defined the palaeo topography, we used a Digital Elevation Model (DEM) of the modern topography (www.regionetoscana.com). Then this modern topography was modified in GRASS software (GIS open-source software Neteler & Mitasova, 2008) using several filters. These filters were used to create (1) a spatial tilting of the whole region, (2) an uplift flattening in correspondence to Castello di Montalto (see Bianchi *et al.*, 2013) and a localized digging within the whole valley. The DEM was tilted with a 300 m rotation toward south, necessary to contrast the modern slope and to simulate the Gelasian drainage slope, based on calculated palaeo-hydrological values (S = 0.06%). The uplifted southern portion was flattened to guarantee a continuum with the altitude of the northern portion and to provide a uniform valley

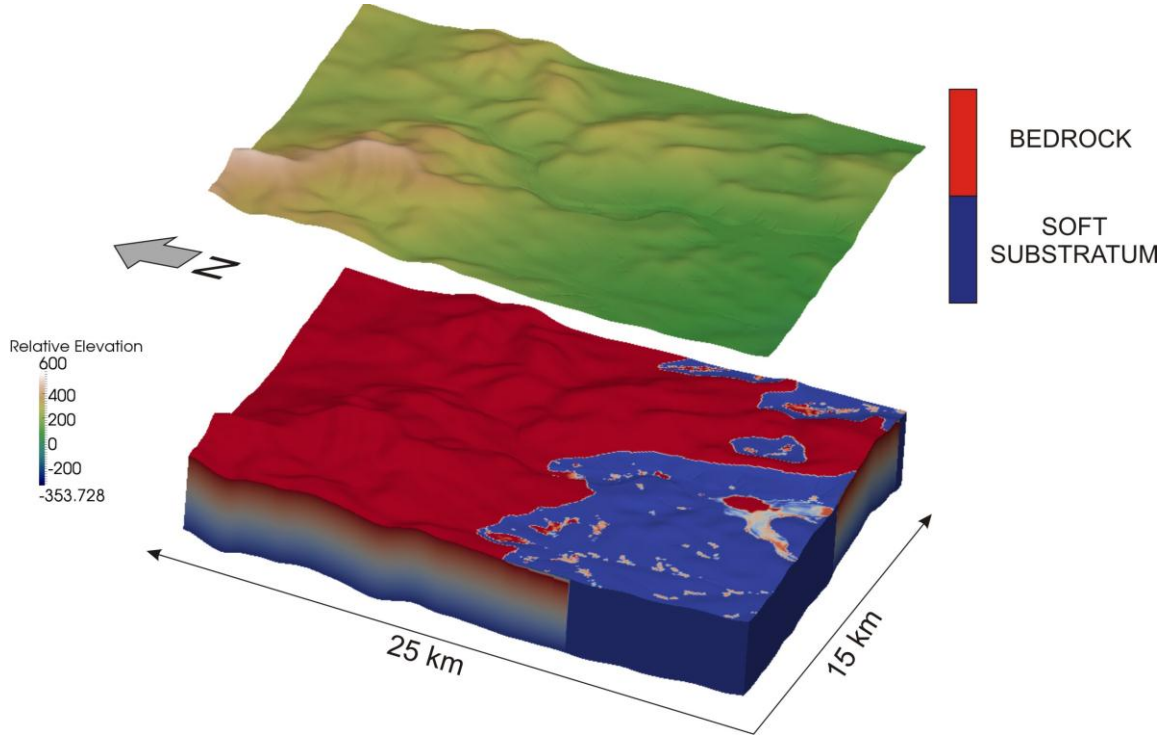

Figure 4.5: Illustration of initial layers composed by substratum geology and topography. The substratum geology is represented by a bulk made of deposits with two different hardnesses. The palaeo-topography is represented by a modified modern DEM (see the text for details).

floor, consistent with the calculated slope. The digging was performed by removing 100 m of valley deposits, through a localized subsidence within the valley.

The substratum geology was simulated using two initial underlying sedimentary layers with specific hardness and grain size distribution (Fig. 4.5), based on the valley lithological features documented in the geological map of the area (Bianchi *et al.*, 2013). Two types of substratum were considered: (1) one representing the sandstone of Macigno Fm., simulated as hard rock (h = 2, d = 0.25 mm), and (2) the second corresponding to the Pliocene marine deposits belonging to the Siena Basin infill, simulated as unconsolidated sand and clay (h = 1, d = 0.20, 0.01 mm).

4.2.7.2 River parameterisation

As explained above, in LECODE, river input is represented by flow walkers holding river information such as river discharge, velocity, flow height, sediment concentration and sediment percentages.

According to palaeo-hydrological evidence, the considered initial discharge has been set to 200 m^3/s. The velocity was directed toward South and was set to 2 m/s at the source point, according to palaeocurrent distribution (Bianchi *et al.*, 2013; Bianchi *et al.*, submitted). Flow height defines the flow walker depth at the source point; the maximum height defined in the input file is 10 m. For sediment concentration, a value of 3.5 kg/m^3 was fixed and corresponds to both suspended and bed load sediments.

As mentioned in the paragraph 4.4, LECODE uses a non-uniform sediment mixture for sediment transport calculation. For this reason it is convenient to divide the mixture in several grain-size classes (Zhang, 1989; Wu *et al.*, 2000), which are characterized also by density and angle of repose. Relatively to the source, 6 sediment classes were imposed: 4 for gravel, 1 for sand and 1 for silt-clay. The following table (Table 4.2) shows the values adopted for each sediment class.

	Gravel 1	Gravel 2	Gravel 3	Gravel 4	Sand	Silt/Clay
Diameter (mm)	10	5	2.5	1	0.23	0.01
Density (kg/m^3)	2250	2250	2250	2250	2650	2350
Angle of repose (dz/dx)	0.0070	0.0069	0.0068	0.0067	0.0065	0.0045

Table 4.2: parameters characterising the examined grain-size classes.

The choice of 4 gravelly classes was used to match with the sediment distribution cropping out in Arcidosso section (Fig. 4.1) and corresponding to the V1 deposits (Bianchi et al., 2013). To finalize the river parameterization, each grain-size class composing the source has to be allocated based on their respective percentages. It was chosen to define the following values from coarsest to finest grain-sizes: 1 %, 1.5 %, 1.25 %, 1.25 %, 37 % and 58 %.

4.2.7.3 Allogenic forcing

Two factors control sedimentation within the model: climate and tectonics (Fig. 4.6).

Since the tectonic is the main control factor, we supposed the climatic contribution steady through the simulation; consequently we used as a proxy of ancient climate a rainfall rate of 1 m/y, which corresponds to the modern average precipitations in the Tuscany region.

In order to simulate the Ambra River fault dynamics (Bianchi *et al.*, submitted), the movement of the footwall block was replicated, since the uplift can be easily spatially constrained by LECODE. The uplifting portion was displayed as a hilly area bounded to the North by a steep NW-SE trending slope mimicking the Ambra River fault plane. The maximum displacement, located in correspondence to the main valley axis, was about 100 m and occurred over 50 kys. Although Thomson *et al.* (2010) calculated the average uplift rate of Northern Apennines as 1 mm/y, with peaks of 1.4 mm/y (Mt. Falterona, NE Tuscany) and 0.5 mm/y (Valdarno, Central Tuscany), we modeled an uplift event for a limited portion and for a brief period, thus assessing an increased uplift rate of 2 mm/y. Furthermore, we impose the presence of a localized subsidence in the eastern valley flank

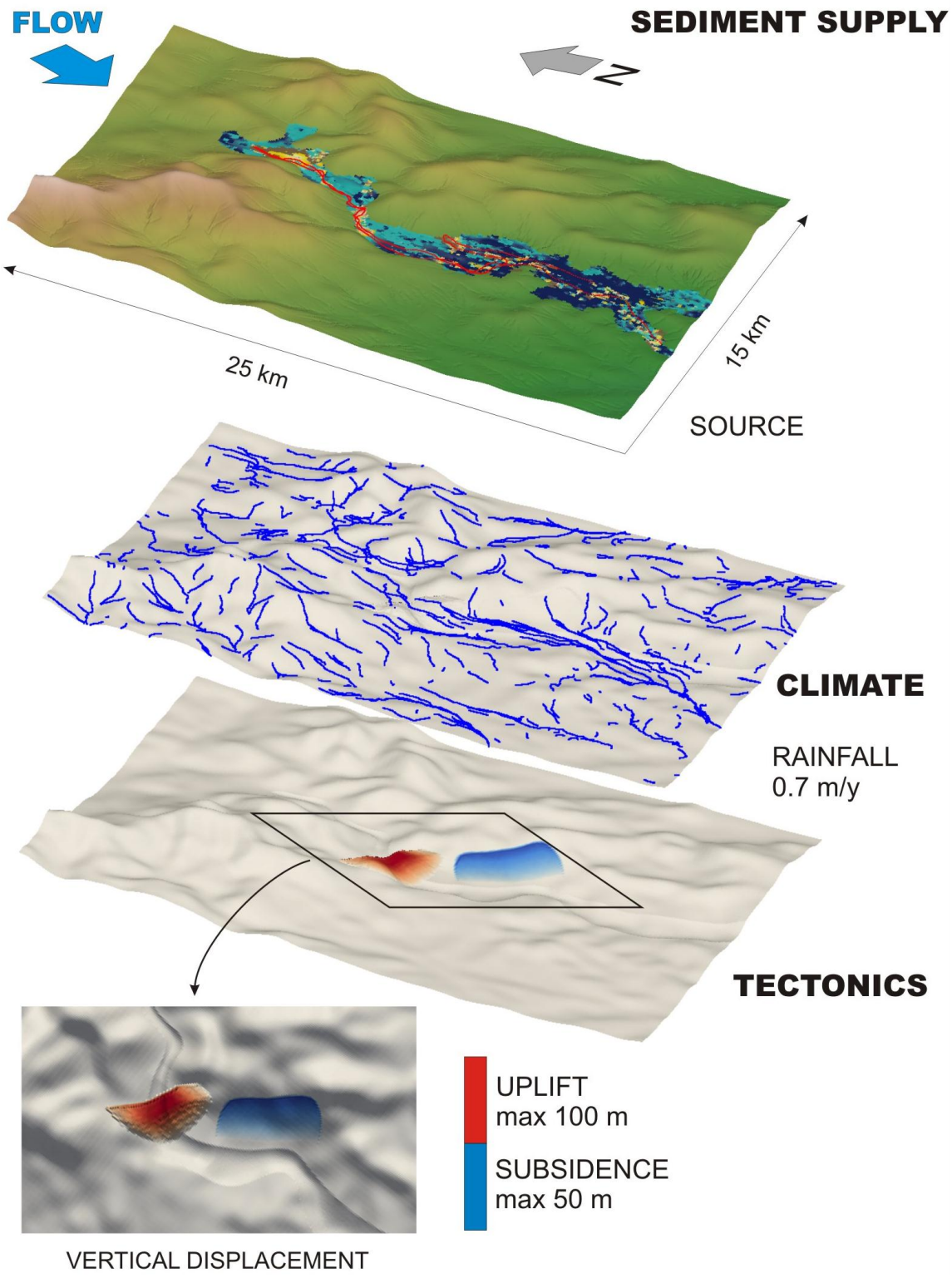

Figure 4.6: Representation of forcing parameters arranged in different layers. Vertical displacement characterised by uplift (red) and subsidence (blue); rain-derived drainage with a rainfall rate of 0.7 m/yr; flow walker and sediment relative to the source.

of the southern sector to simulate the Terre Rosse fault creating accommodation space for the input of lateral tributaries. This lineament has the same trend of the fault mentioned above.

4.2.7.4 Running phases

Three phases were defined to simulation the valley evolution. The first, pre-tectonic phase aimed at reaching the steady state of the system, the second, syn-tectonic phase focused on the monitoring of the sedimentary dynamics, while the last, post-tectonic phase consists in the adjustment of the system to reach an equilibrium corresponding a new steady state. This approach highlighted the signature of autogenic factors on sedimentation during the reaching of the pre-tectonic steady state, and allowed to avoid their disturbance during syn-tectonic sedimentation (Whipple, 2004).

The model duration is strictly linked with the bankfull discharge stemmed out from palaeo-hydraulic investigations. Although the bankfull discharge is associated to a specific return time (Dalrymple, 1960; Chow, 1964; Eagleson, 1972), it provides the most dynamic phase for channel construction (Dunne & Leopold, 1978) and it is, therefore, simulated here in a continuous virtual time. Moreover, the similarity between the inferred palaeo-discharge and the modern Arno River was considered in order to develop the model. Specifically, we assumed the bankfull discharge frequency of the modern Arno River (12h per year) as starting point for the first running tests. In this framework, assuming that the Ambra valley succession accumulated over about 300.000 years, the time arose from the flood frequency analysis could be approximated to 400 years. Unfortunately, with a discharge of 200 m^3/sec, a running time of 400 yrs is not able to: i) bring the system to a steady state; ii) develop the fluvial response to tectonic disturbance; iii) reach a second

steady state. This lack highlights that the bankfull discharge frequency was probably higher than that of the modern Arno River. Several test allowed to establish that a virtual time of 1100 yrs is adequate to allow the model to simulate the former three stages. Specifically a first simulation phase (i.e. reaching of the steady state) was run for 700 years, the second phase (i.e. fluvial response to tectonic disturbance) for 200 years and the third phase (i.e. reaching of the second steady state) for other 200 years for a total of 1100 years of virtual time. Every 100 years the model generates one sedimentary layer and every 50 years the flow walkers are released. During the syn-tectonic phase, the tectonic perturbation does not create a decreasing valley slope, as highlighted by field insights (Bianchi *et al.*, submitted). For that motive, we decrease the velocity and height of the source (V = 2 > 1.5 m/s; H = 2.25 > 1.5 m) only in the syn-tectonic phase (form 700 to 900 years), to simulate the effects of river potential energy loss (Blum & Tornqvist, 2000).

4.2.7.5 Results

To illustrate how the numerical reconstruction displays similar features of Ambra study case maps of aggradation/degradation, grain size changing, stratal architectures and valley evolution are presented in the fault zone (Fig 4.7, 4.8, 4.11).

The aggradation/degradation pattern (Fig. 4.7) shows that most of the aggradation occurred upstream of the fault, where the thickness of virtual sediments reaches 85 m. The valley evolution is displayed in the panel in fig. 4.8 and shows the fluvial valley filling by deposits derived from the lateral tributaries, enhanced by the rain, and by the source that provides most of the sediment on the area (Fig. 4.8).

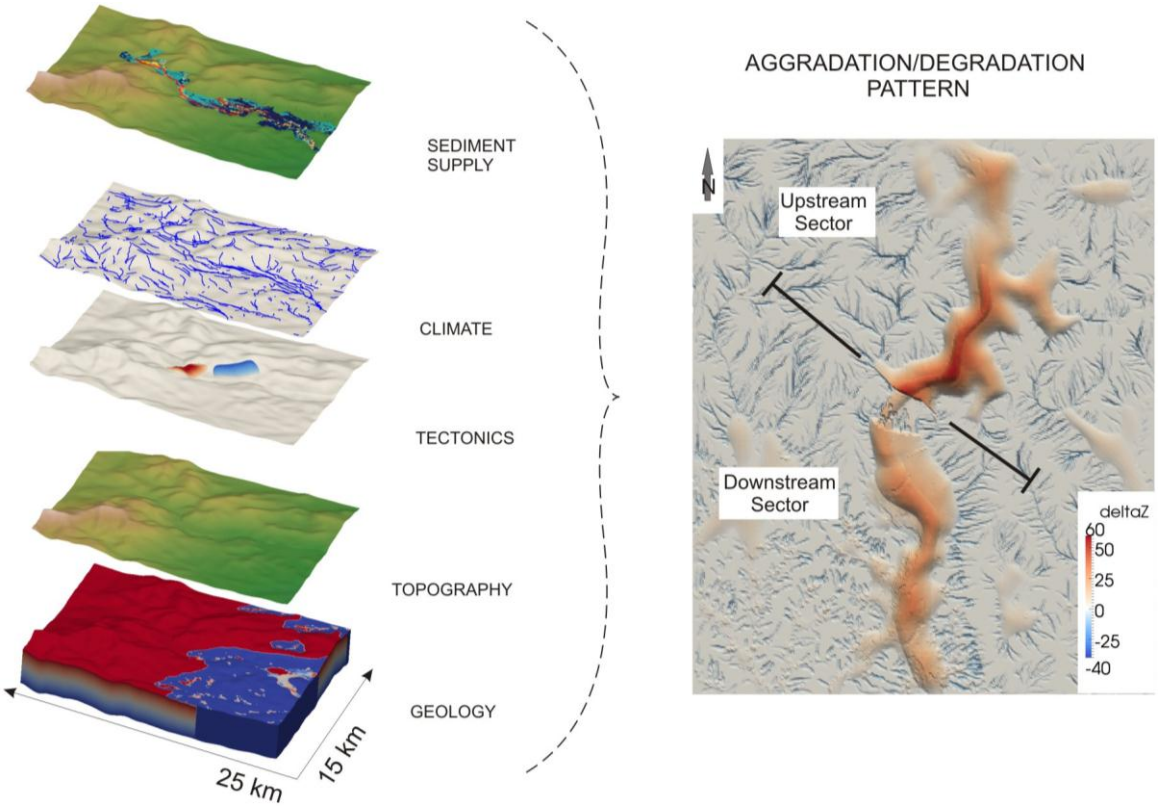

Figure 4.7: Schematic sketch describing the parameters (stacked layers) involved in the formation of aggradation/degradation pattern. Aggradation is expressed in red high relief and degradation in blue low relief.

4.2.7.5.1 Pre-tectonic phase (0 – 700 years)

In the pre-tectonic phase the valley fills (Fig. 4.9A) and reaches its steady state. The overall grain size distribution (Fig. 4.8, 4.9) shows a downstream fining sequence, whereas thickness of infill deposits varies as consequence of irregularities of the valley floor. From 0 to 500 years the system displays the fluctuating sedimentation rate (Fig. 4.9C) and it deposits thick layers (up to 15 m each), showing a sandy-gravelly coarsening-upward tendency (Fig. 4.9B). From 500 to 700 years the system is defined by a low constant sedimentation rate (0.3 cm/y, fig. 4.9C). The grain-size is mainly sandy-gravelly, with a fining-upward trend. Deposits younger than 500 years present sharp bases that incised the older deposits with almost no depositional features (Fig. 4.9B), suggesting the

development of a by-pass zone (Whipple, 2004). When the by-pass zone develops, the sedimentation rate reaches a stability pattern at about 500 years.

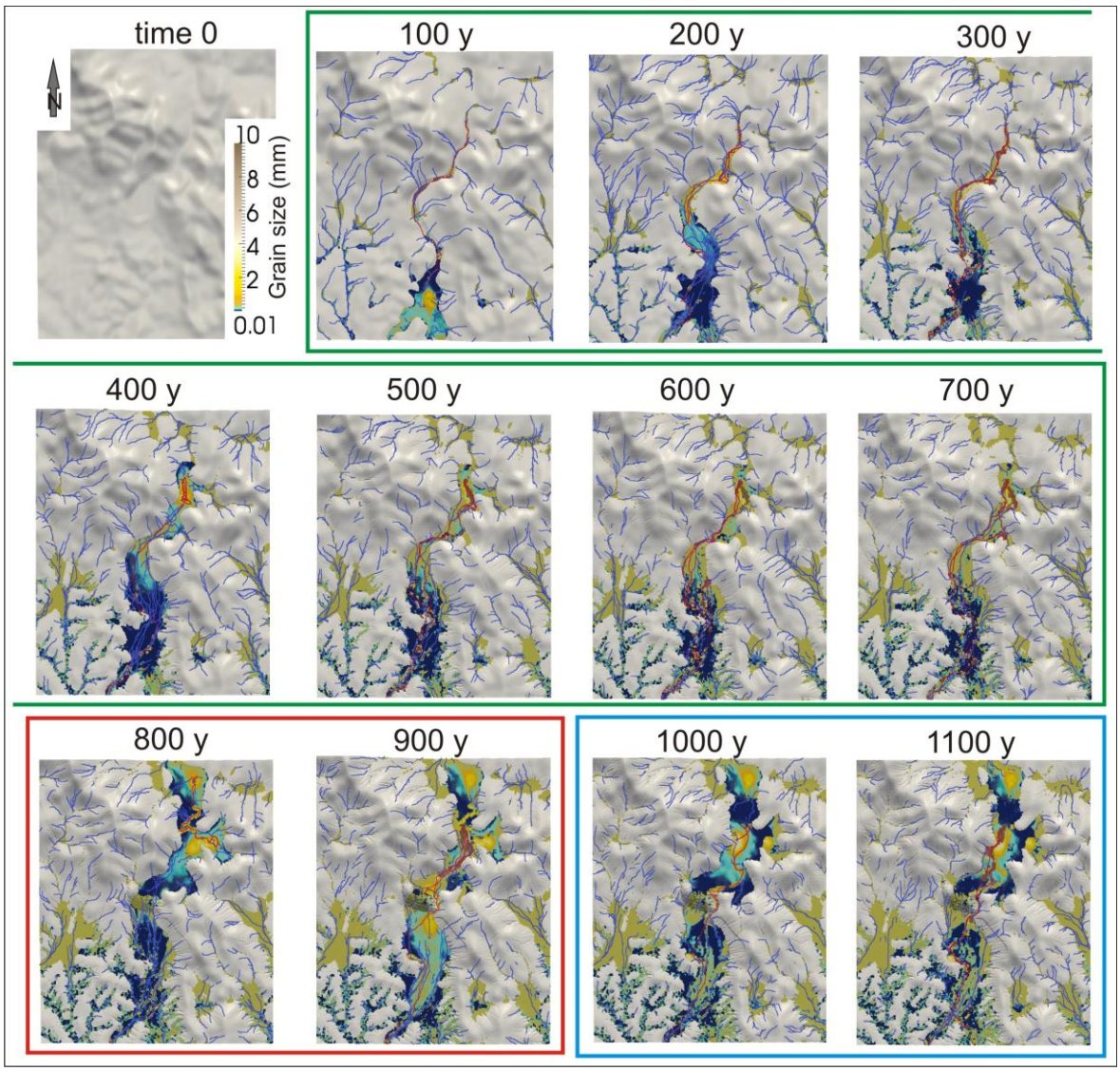

Figure 4.8: Set of frames showing the landscape evolution of the valley. Green line comprises frames belonging to the pre-tectonic phase. Red line borders frames of syn-tectonic phase. Blue line frames screenshots of post-tectonic phase.

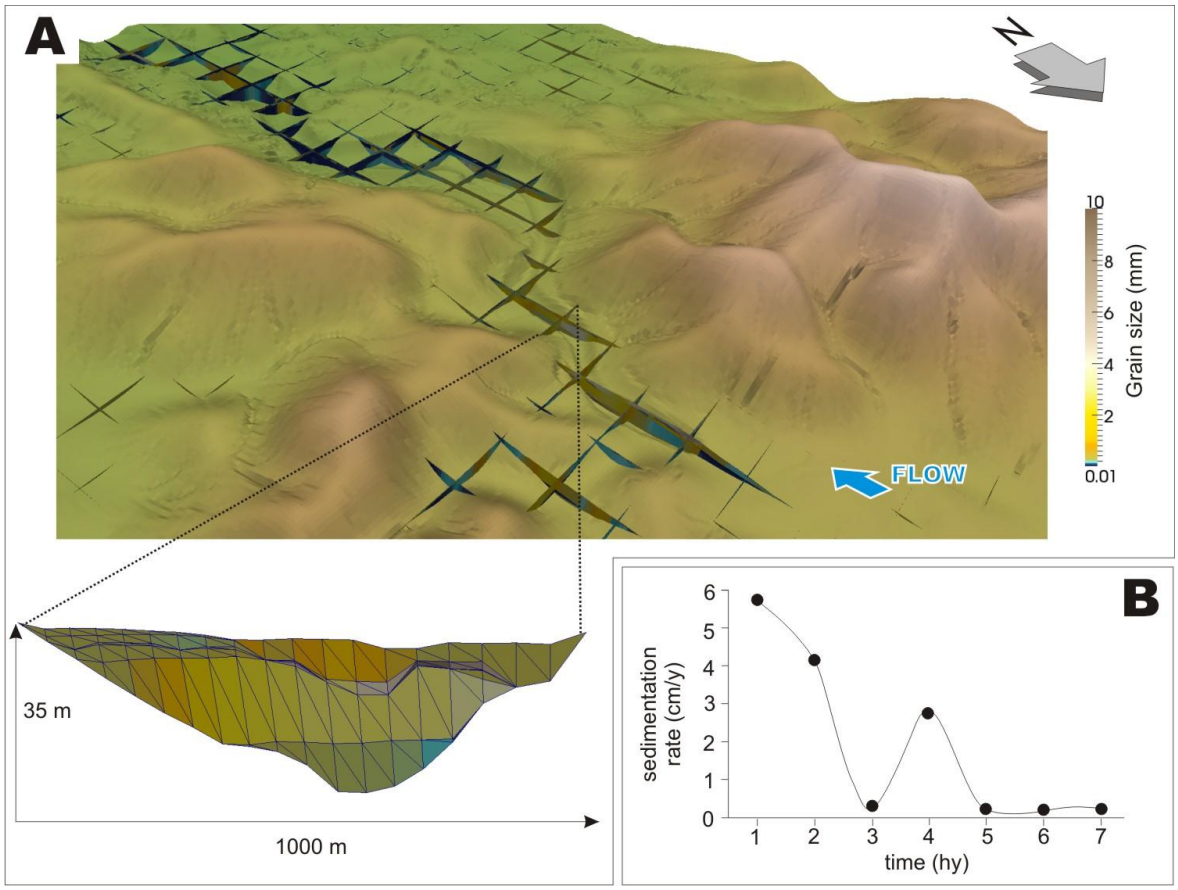

Figure 4.9: Pre-tectonic phase. A) Plan view of the area with cross section of the valley fill framed at 700 years; note the enlarged cross-section of pre-tectonic deposits, highlighting the grain size. B) Sedimentation rate graph; note the low sedimentation rate from 500 to 700 years.

4.2.7.5.2 Syn-tectonic phase (700 – 900 years)

During this phase the virtual fault displacement reaches 100 m, which is equally distributed in two distinct tectonic events (Fig. 4.10). Just after the first pulse (700-800 years), aggradation occurred upstream of the fault (Fig. 4.10A), whereas just after the second pulse (800-900 years) the river shifts eastward and leads to the aggradation of coarse sediments in the downstream part (Fig. 4.10B). This shifting form a second valley (Fig. 4.10B) sourced from the eastward tip of the fault and developed onto the rocky substrate. (Fig. 4.10C).

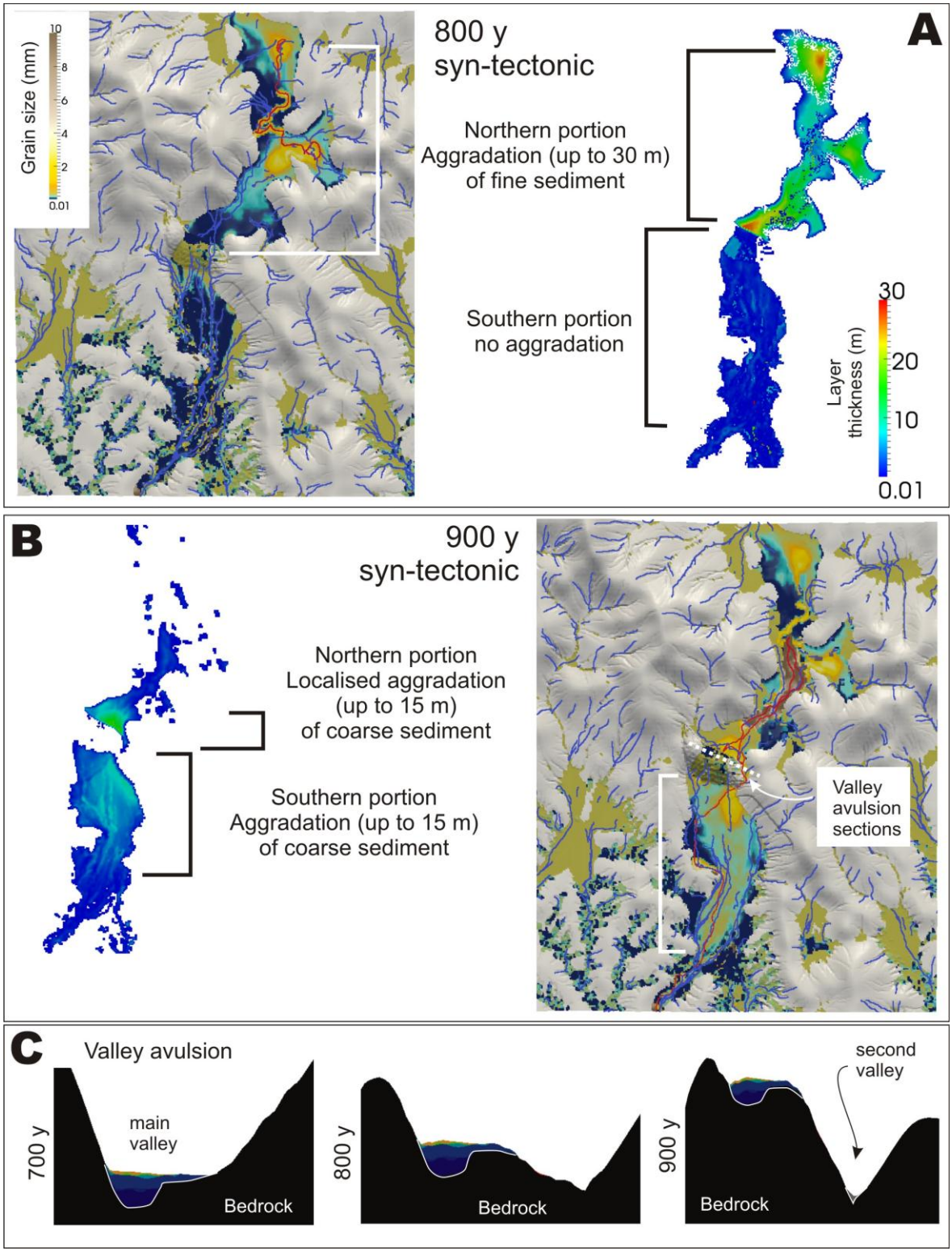

Figure 4.10: Syn-tectonic phase. A) Plan view of grain-size distribution (left-hand) at 800 years; detail of thickness distribution (right-hand) in plan view at 800 years, showing the aggradation localised in the valley upstream portion. B) Plan view of grain-size distribution (right-hand) at 900 years; highlighted in the left-hand the deposits thickness at 900 years, showing an aggradation framed in the downstream portion and spatially limited in the upstream portion. C) Cross-sections (position shown in B) concerning the valley axis shifting. Note the bedrock degradation and formation of a second valley at 900 years.

Upstream of the fault zone, cross-sections show a narrow (about 1.7 km) and deep (up to 60 m) valley (Fig 4.11A). About 30 m of muddy sediments and 10 m of sand were accumulated during the first and second tectonic pulse, respectively (Fig. 4.11A). Both these intervals tend to thin upstream. In this area sedimentation occurred with a rate of about 10 cm/yr at 800 years, then decreasing to 3 cm/yr at 900 years (Fig. 4.13A). Downstream of the fault zone, cross-sections display a wider (about 3.2 km) and shallower (about 35 m) valley than the upstream sector. Deposits are mainly gravelly, up to 10 m thick (Fig. 4.11B) and form a fan-shaped lithosome confined within the newly-formed valley (Fig. 4.10B,C). Aggradation occurred at 900 years with a rate of about 3 cm/y (Fig. 4.13B). Along-valley sections show as the layers pinch southward. The presence of the secondary Terre Rosse fault is laterally recorded by gently rollover layers architecture (Fig. 4.11B).

4.2.7.5.3 Post-tectonic phase (900 -1100 years)

During the post-tectonic phase, the river system maintains its new pathway (Fig. 4.8) and only a reduced thickness of sediments was accumulated along the valley (Fig. 4.11). Significant accumulations of bedrock-derived materials occur at the entrance of the main tributaries into the main valley, both upstream and downstream of the fault zone (Fig. 4.12). This phase was characterized by a reduced aggradation rate about 0.3 cm/y, indicating the achievement of the steady state (Fig. 4.13A, B).

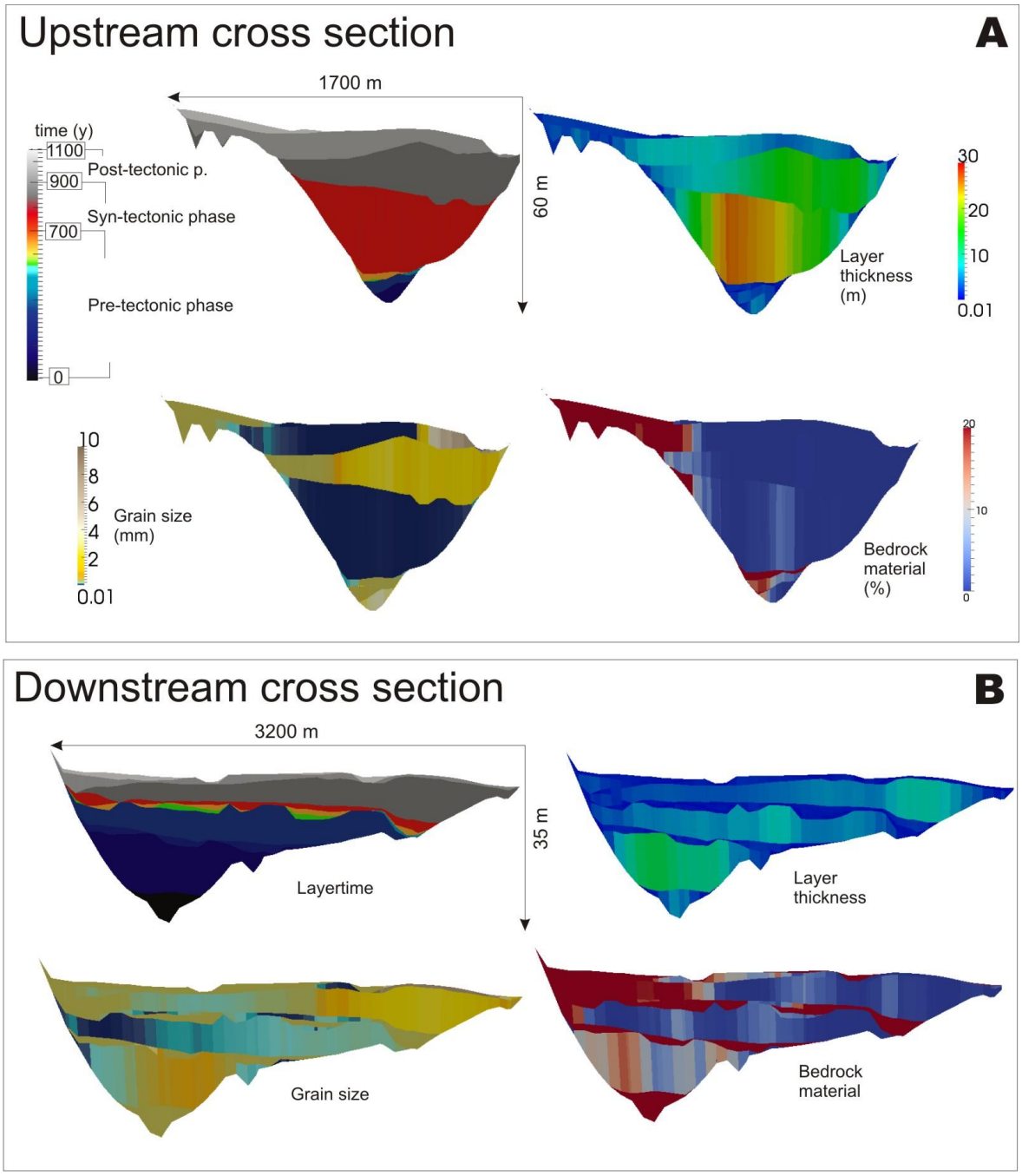

Figure 4.11: A) set of cross-sections of the upstream portion displayed on the base of different parameters; B) set of cross-sections of the downstream portion visualised through different parameters (see A for the colour scales).

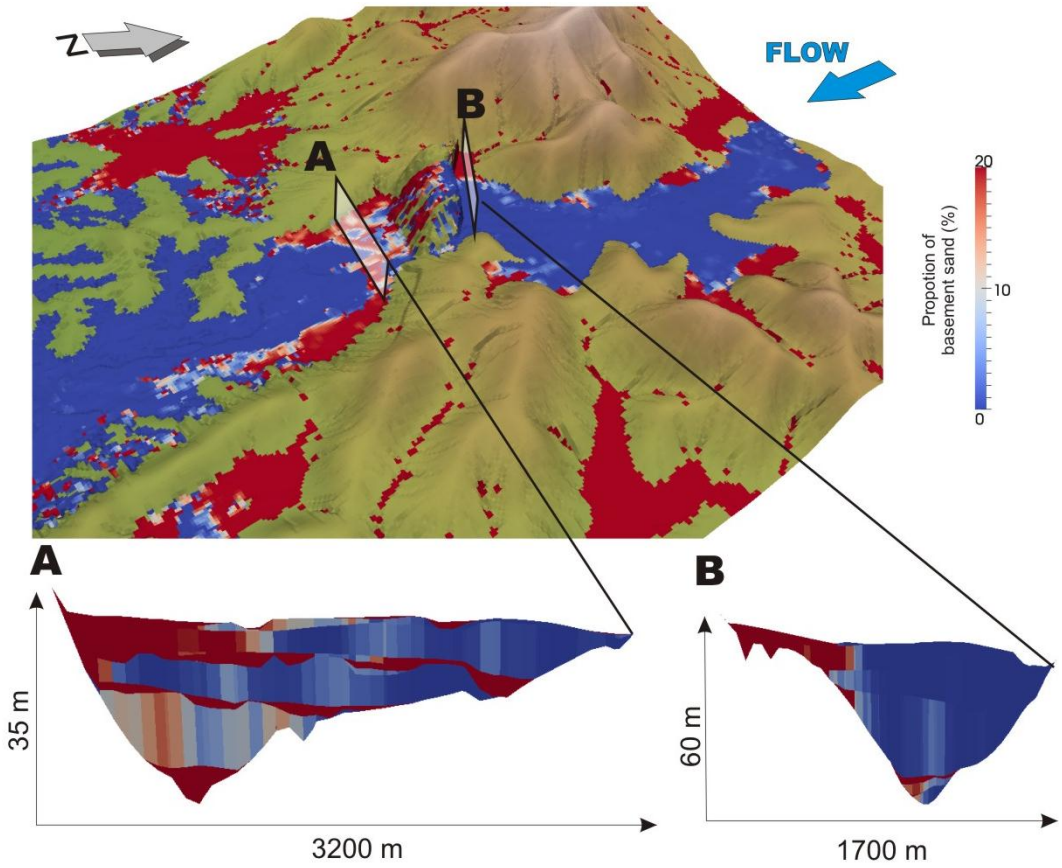

Figure 4.12: Post-tectonic phase. Plan view of the area across the fault highlighting the proportion of bedrock material. Cross-sections of the downstream area (A) and the upstream area (B) displayed on the basis of the proportion of the bedrock material, representing alluvial fan deposits.

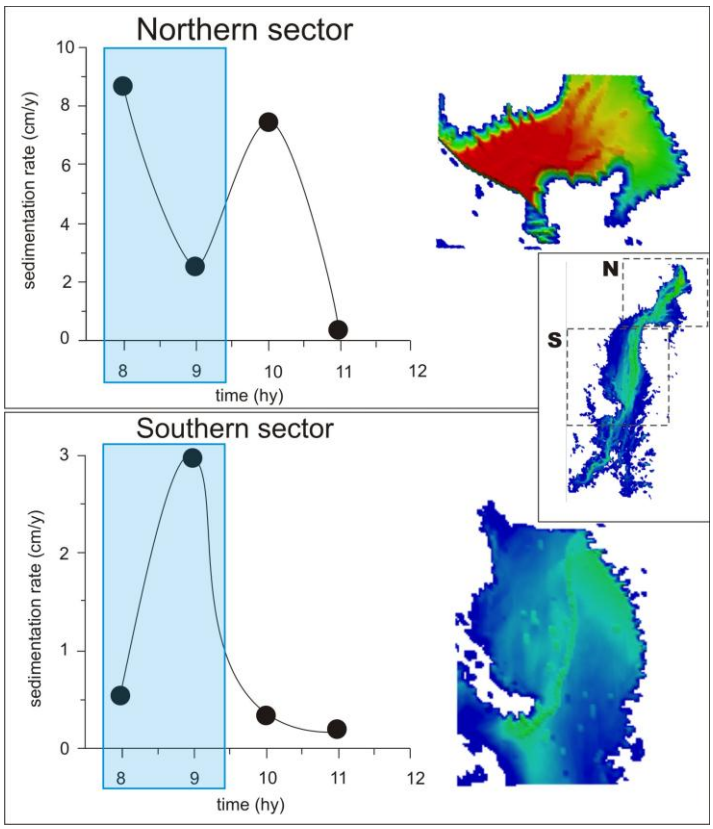

Figure 4.13: Sedimentation rate graph for the northern sector and the southern sector calculated on the basis of the instantaneous aggradation in both syn- and post-tectonic phase (from 800 to 1100 years); note the high aggradation at 800 y in the northern sector and at 900 y in the southern one. On the right-hand representative portions (for location see the inset). Note the highlighted portions in graphs, concerning the sedimentation rate during the syn-tectonic phase.

4.2.8 Experiment 2 - generic models

In this section generic models developed on the base of Experiment 1 are used to better investigate the relationship between different rate of tectonic uplift and fluvial discharge.

4.2.8.1 Experimental apparatus

The adopted stratal grid has a simplified structure of a U-shaped valley prolonged in the entire model length (Fig. 4.14A). This simplified construction is adequate to focus on the effects of selected forcing, avoiding disturbance due to a more complex topography. The initial layers have high value of hardness, simulating a bedrock succession. Finally, to focus on the effects provided by tectonic forcing only, we do not consider rainfall input. This simplified structure is dissected by an upstream-dipping, normal fault trending slightly oblique to the valley axis (Fig. 4.14B).

Three sources were simulated, all positioned on the same abscissa, and with the same characteristics. The multiple-source approach is used to fill homogenously the valley floor.

Hydraulic parameters adopted for each source are: flow height 2 m, velocity 1 m/s, sediment concentration 0.5 kg/s. Three grain-size classes are involved: 10% of gravel (2 mm of diameter), 30% of sand (0.25 mm) and 60% of silt (0.1 mm).

The examined variation of elementary parameters focuses on fluvial discharge and uplift rate. Fluvial discharge range was ranging from 3 to 150 m^3/s. The discharge frequency was not considered here, since the uplift rate strongly controls the simulation time. Uplift rate was simulated as low rate with 1 mm/y and high rate with 2 mm/y, in order to reproduce slow and rapid deformation.

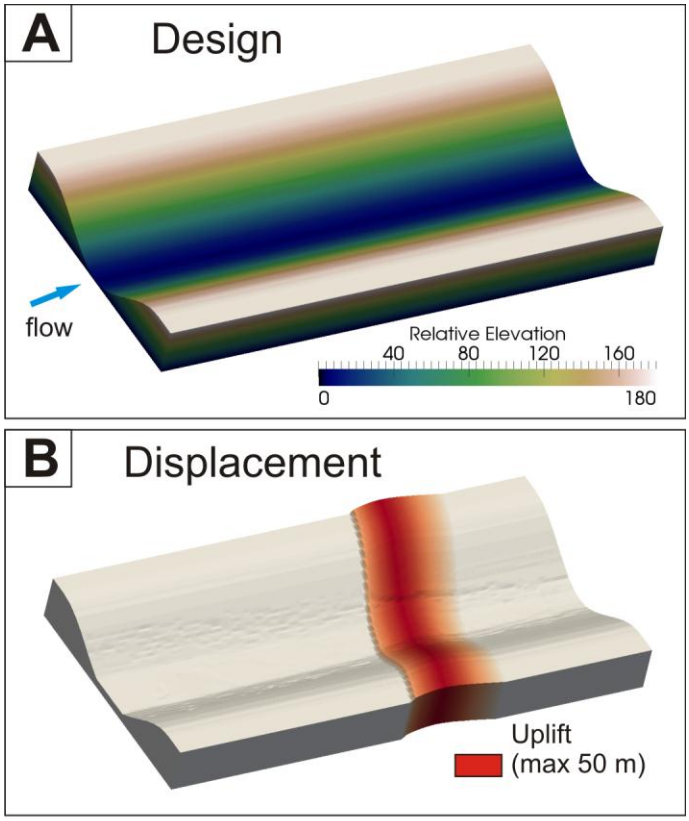

Figure 4.14: A) Representation of the simplified design used as topography. B) Localisation and shape of the uplifted portion.

From 0 to 50 ky the pre-tectonic phase run, whereas the syn-tectonic phase is from 50 ky to 75 ky for system with high uplift rate, and from 50 ky to 100 ky, for low uplift rate simulations.

According to the combination of fluvial discharge and uplift rate, we have created four possible scenarios: i) scenario 1 characterised by low discharge (3 m^3/s) and low uplift rate (1 mm/y); ii) scenario 2 with low discharge (3 m^3/s) but high uplift rate (2 mm/y); iii) scenario 3 with high discharge (150 m^3/s) and low uplift rate (1 mm/y); iv) scenario 4 characterised by high discharge (150 m^3/s) and high uplift rate (2 mm/y).

4.2.8.2 Results

Scenario 1. (Fig. 4.15 scenario 1). In the context of low rates of uplift and discharge the valley is characterised by a dominance of silty sedimentation, although downstream

of the uplifted area, sandy sedimentation occurs. Fluid elements path shows that the uplift block, which is strongly eroded, does not dam the flow. The uplift degradation is visible from the cross-sections A-A' (Fig. 4.15), whereas downstream thinning of syn-tectonic layers is shown by the layer-index cross-section B-B'. All valley-fill deposits are organised in thin layers.

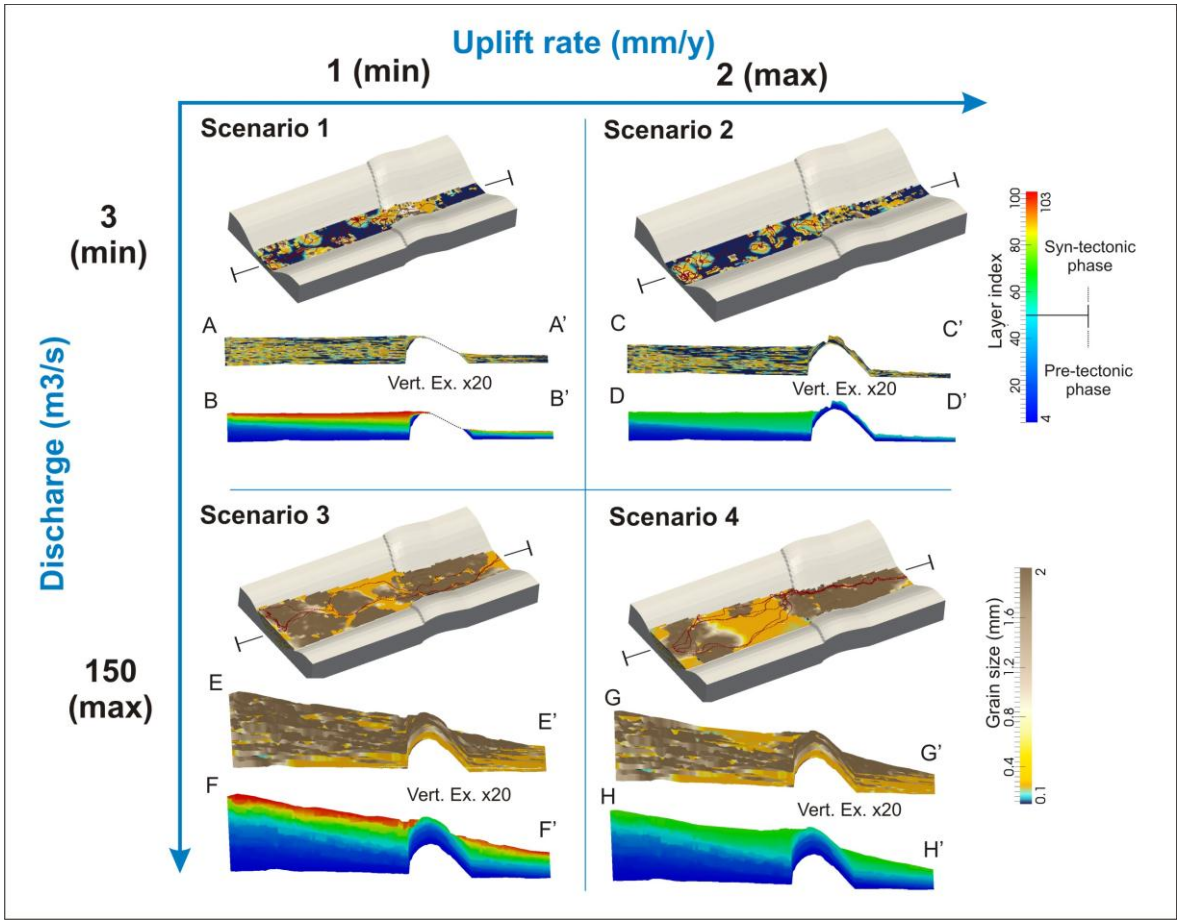

Figure 4.15: Sketch of scenarios, function of uplift rate and discharge. Every scenario corresponds to one simulation and it is displayed in plan view and two along-valley sections highlighting grain-size distribution and layer index (time). Flow is expressed in red lines. See the text for more details.

Scenario 2. (Fig. 4.15 scenario 2). The plan-view displays a dominance of muddy-sandy deposition within the valley with a coarser deposition on correspondence to the fault. Accumulation of fine-grained deposits in the upstream sector propagates upstream

in time. Moreover, the flow is dammed by the uplift, emphasised also by the lacking of syn-tectonic deposits in the downstream portion (layer-index cross-sections D-D').

Scenario 3. (Fig. 4.15 scenario 3). The plan-view shows as gravelly deposits accumulate along the whole valley trunk, although their thicknesses are reduced in the uplifted zone, where erosion is also occurring. Coarse sediments accumulated downstream of the uplifted area. Sediment distribution becomes finer when moving downstream. In this scenario the flow is able to pass over the uplifted portion (F-F' presents) and no damming effect of the fault are shown.

Scenario 4. This scenario shows a complex grain-size distribution (Fig. 4.15 scenario 4). Gravels are accumulated in the most upstream portion followed by sandy deposits just upstream of the fault. These sand are thicker close to the fault and pinch out upstream. Gravels are also accumulated across and just downstream of the uplifted zone and sediment distribution turns into sandy deposits downstream. The flow is not dammed by the uplifted block, but is shifted from the main valley axis and is confined toward the left-hand flank of the valley.

4.2.9 Discussions

4.2.9.1 The Ambra Valley simulation vs. The Ambra Valley succession

Experiment 1 provides insights to compare the virtual landscape evolution with the field study case and discuss the main steps of this evolution in terms of spatial and temporal dynamics of the alluvial system (Fig. 4.16).

During the run of the first part of the experiment (0 – 700 years), the sediment accumulated within the valley and reached the steady state after the 500 yrs, when the virtual river lost its capacity to deliver or acquire sediments and assumed an equilibrium

configuration dominated by sediment bypass (Whipple, 2004, Blum *et al.*, 2013). The period is a virtual timing required to the river for reaching this stage corresponds to 135 kyr, and can be considered as the intrinsic response time (or equilibrium time) introduced by Paola *et al.* (1992); it was thought for basin filling (Paola *et al.*, 1992), whereas Blum *et al.* (2013) extended the definition also for river system in valley. The achievement of the steady represents therefore the tendency of the inland valley system to equilibrate its local profile beyond the marine or lacustrine influence bodies (Gibling *et al.*, 2011). Since the deposits accumulated during the achievement of the steady state are thinner in respect to those of unit V1, slightly different conditions (e.g. localized subsidence, higher sediment supply) probably framed sedimentary dynamics of the Ambra River succession during the pre-tectonic phase.

During the tectonic phase, aggradation of fine-grained sediments upstream of the fault zone fits with the V2fls deposits of the Ambra succession (Bianchi *et al.*, submitted), agrees with laboratory experiments (Ouchi, 1985) and modern river examples (Holbrook & Schumm, 1999). Upstream pinching of the fine-grained deposits imitates the backfilling architecture (*sensu* Schumm, 1993) of alluvial valley fills genetically linked with relative sea-level rises (Boyd *et al.*, 2006). The edge of the uplifted block represents, in this case, the base level of the system (Blum & Tornqvist, 2000). Higher will the block will be uplifted and longer the aggradation will propagate upstream. The time needed by the fault to affect valley sedimentary dynamics is referred as time reaction and it is expressed by the simple formula (Blum *et al.*, 2013 and references therein):

$$T^* = T/T_{eq}$$

where T_{eq} is the equilibrium time for the system to reach the steady-state configuration, and T is the time scale of the tectonic forcing (Paola *et al.*, 1992; Marr *et al.*, 2000;

Swenson, 2005; Blum *et al.*, 2013). Swenson (2005) referred "slow" variation to T* >> 1, whereas "fast" variation to T* <<1. In the case of the Experiment 1, simulated fluvial system has a rapid time reaction to tectonic forcing since its T* is calculated to be 0.4. Thickness of the virtual V2fla agrees with this classification and fits with increase of overbank sedimentation due to augment of flooding events (Hole, 2011).

In the uplifted block degradation occurred (Fig. 4.16A) as documented in the Ambra River area (Bianchi *et al.*, submitted) and in similar tectono-morphological settings (Holbrook & Schumm, 1999). The narrowness valley trunk, which was cut on the uplifted bedrock, reflects that the river incision rate is comparable with the uplift rate (Whipple, 2004). The experiment highlights also that the lateral change in fault displacement is not the only forcing on valley shift across the uplifted block. This process was also influenced by the fault trend, which is not closely orthogonal to the valley axis, as observed during lateral drainage adjustment into active margin setting (e.g. Carizzo Plain, Schumm, 1986). The high incision rate in the uplifted area prevents development of terraced surfaces (Lavé & Avouac, 2001). The model show also that the eastward valley shift was probably further enhanced by the activation of the Terre Rosse fault, which generated a localized depocentre which attracted the main watercourse.

Aggradation of virtual coarse sediment downstream of the uplifted block finds its equivalent in the V2flb deposits of the Ambra River succession (Fig. 4.16A), and fits with laboratory experiments (Ouchi, 1985) and some modern examples (Holbrook & Schumm, 1999). This aggradation was triggered by a significant increase in sediment supply from a point source (i.e. uplifted block) and can be labelled as downfilling process (*sensu* Schumm, 1993), which caused shifting of the river equilibrium profile above the valley floor (Blum & Tornqvist, 2000). Although downfilling and backfilling processes are

commonly considered as typical of upstream and downstream valley reaches respectively (Schumm, 1993; Zaitlin *et al.*, 1994; Boyd *et al.*, 2006), it is noteworthy that both in the experiment and in the Ambra River case they occur with the opposite distribution (Fig. 4.16B). Although the alluvial architecture stemmed out from the experiment clearly resemble the Ambra River succession, the experiment show that aggradation of V2flb unit postdates accumulation of V2fla (Fig. 4.13). This diachrony highlights that the lowering of fluvial transport capability induced by localized uplift is followed by an immediate aggradation upstream of the deformed zone, which allow the river to reach a new equilibrium profile. On the contrary, aggradation in the downstream sectors is strictly dependent by the amount of sediments eroded from the uplifted area, which is, in turn, linked with the ratio between the rate of uplift and that of fluvial incision. This diachrony has been detected in some natural examples (e.g. New Madrid earthquake, Russ, 1982; Schumm, 1986).

The post-tectonic documents the achievement of a second steady state and occurs over 1000 years of virtual time. Upstream of the fault zone, accumulation of alluvial fan deposits along the left-hand flank of the valley occurred during the post-tectonic phase as consequence of the reduced fluvial transport capacity associated with the renewed equilibrium profile assumed by the river. Although similar deposits occurs also in the Ambra River succession (Bianchi *et al.*, submitted), this experiment highlights that alluvial fans prograded during the achievement of the post-tectonic steady state, confirming that these deposits represents the relaxation phase the upsetting of a tectonic disturbance (Sømme *et al.*, 2013; Fidolini *et al.*, 2013b).

The aggradation/degradation map (Fig. 4.7) highlighted the results of differential erosion on bedrock and unconsolidated substratum. Hard substrate promotes the

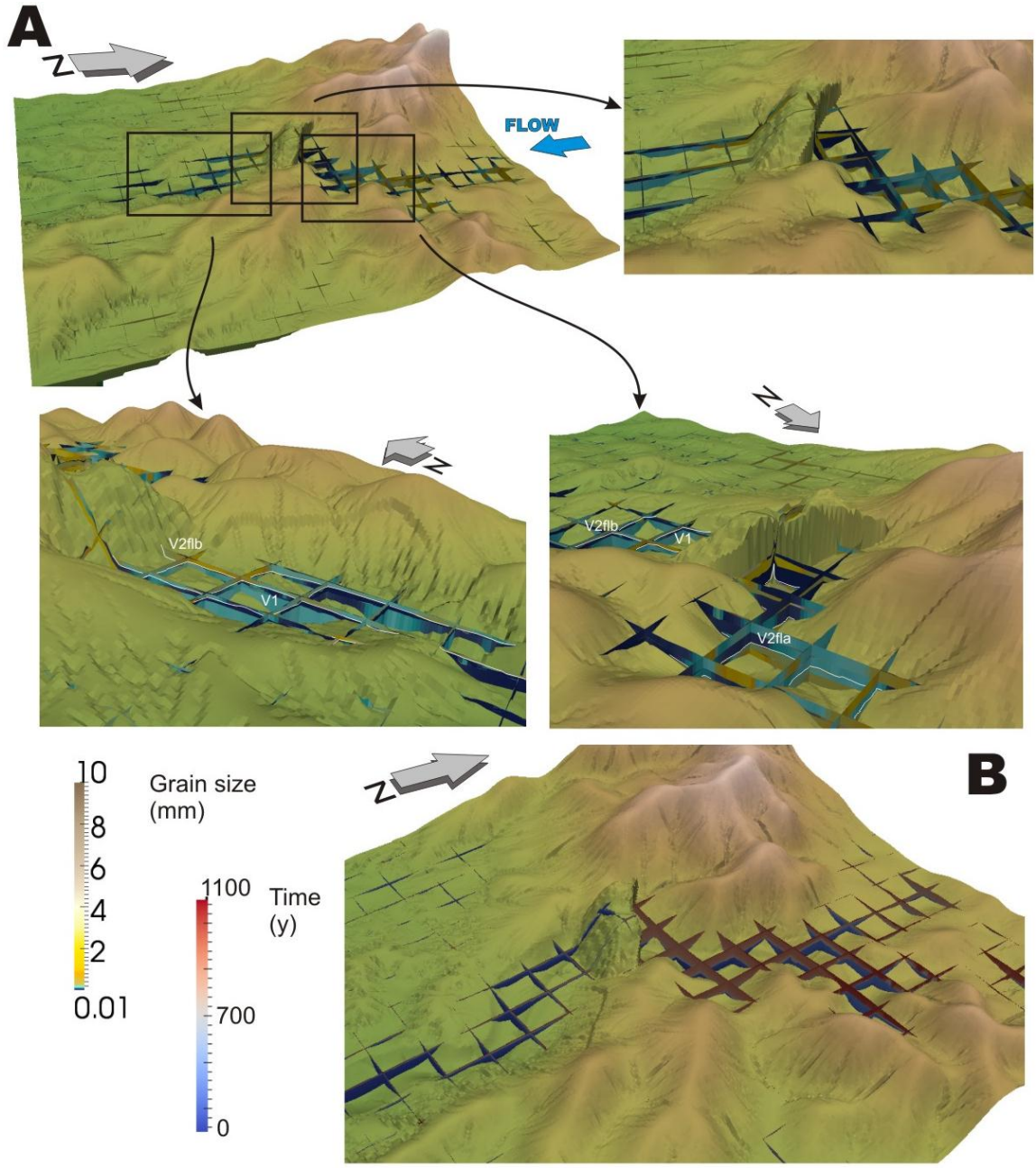

Figure 4.16: Grid of cross-sections in the valley with enlargements of portion downstream, across and upstream of the fault area., highlighting grain-size (A) and time (B). Note in B architectures in backfilling upstream and architectures in downfilling downstream.

development of narrow and deep valleys, whereas a soft substrate will lead to development of wide a shallow valley as consequence of the capacity that has a river to shift laterally (Blum *et al.*, 2013). Where the modelled valley is cut onto a rocky substrate, its W/T ratio (Gibling, 2006) is about 11.6, whereas this value rises to 175 where the

valley is cut onto the soft substrate. These two values correspond respectively to the field of "Valley Fills on Bedrock Unconformities" and "Valley Fills within Alluvial and Marine strata" as defined by Gibling (2006) and fit well with those observed for the V1 and V2 units of the Ambra Valley succession (Bianchi *et al.*, submitted).

4.2.9.2 Generic models: role of tectonics in variable-discharge systems

Experiment 2 allows to analyse and discuss the sedimentary response of a system with a tectono-morphological configuration resembling the Ambra River setting under variable fluvial discharge and fault uplift rate (Fig. 4.15). Experiment 2 shows that fluvial discharge has a remarkable control on along-valley grain size distribution (Fig. 4.15). In all the scenarios, sediments accumulated upstream of the fault are always finer that those deposited downstream, but low-discharge systems are dominated by finer sedimentation and reduced thicknesses, whereas high-discharge systems are associated with coarser sedimentation and accumulation of thick successions (Paola *et al.*, 1992; Blum & Tornqvist, 2000; scenario 3 and 4 in Fig. 4.15). Systems characterised by low discharge, are extremely sensitive to localized upwarpings, which easily induce dramatic decreases in fluvial transport capability (Doornkamp & Temple, 1966; Rasanen *et al.*, 1987; Dumont, 1992, 1993; Marple & Talwani, 1993). On the contrary, systems with high discharge are scarcely affected by tectonic perturbation with a reduced uplift rate (Holbrook & Schumm, 1999; Ethridge & Schumm, 2007), as attested by development of a reduced along-valley facies heterogeneity in scenario 3 (Fig. 4.15).

If the uplift rate increases, high-discharge rivers became able to store fine sediments (i.e. sand) upstream of the uplifted area (scenario 4 Fig. 4.15), and are also affected by a remarkable channel organization across the uplifted zone. Specifically,

under these conditions the channel network appears to be sensitive to the fault orientation (Ethridge & Schumm, 2007; Schumm, 1986) and channels tend to converge into the funnel formed between the valley flank and the uplifted block, possibly as a consequence of the scarce erodibility of the upwarped rocks (Alexander & Leeder, 1987; Bridge & Mackey, 1993; Blum & Price, 1998).

4.2.10 Conclusions

This study is based on a previous work (Bianchi *et al.*, submitted) that focused on a palaeovalley, draining the northern margin of the Siena Basin (Ambra, Northern Apennines, Italy). In particular this work aimed at monitoring the fluvial anomalies developed across a syn-depositional uplift zone, with high resolution in grain-size and sedimentary architectures. Through the numerical modelling we assessed and time-constrained the tectonic control on aggradation of the studied valley fill. The study described also the main effects of uplift rate on variable-discharge systems.

Physical and hydrological laws that constrain numerical modelling validated our tectono-sedimentary scenario, derived from field observations. The assessment is expressed in the similarity between the modelling results and sedimentary features of Ambra palaeovalley, reproducing the two differential and characteristic aggradations within the valley.

Temporal control, taking advantage of numerical modelling, highlighted that aggradations occurred time-shifted. The time span between the two aggradations results necessary for the achieving of the potential energy that leads to the required stream power, responsible of the uplift incision.

The generalisation of tectonic role on aggradation of variable-discharge systems reveals that low- and high-discharge systems respond to minor and major uplift rates, respectively. In both low- and high-discharge systems, the increasing of uplift rate promoted the facies heterogeneity, through an abrupt variation of grain-size distributed in sectors and characterised by a fining tendency moving toward the uplift.

It is important also to recognise as model uncertainties or its codified simplifications can limit the relevance of the modelling outcomes. For this reason it was necessary to provide a meticulous and continuous calibration of the parameters concerned, aiming to find of the best-fit equations between natural cases, reconstructive and predictive models.

CHAPTER 5

CONCLUSIONS

5.1 OVERVIEW

Through the integration between a "classical" field approach", which involved field mapping, facies and structural analysis and geophysical investigations, and numerical modeling, the present study discussed the tectono-sedimentary evolution of the Pliocene – Pleistocene inland Ambra paleovalley (Northern Apennines, Italy). The Ambra palaeo-valley drained the northern margin of the Siena Basin crossing a set of NW-SE and NE-SW trending extensional and transtensional active faults. This tectono-sedimentary interaction resulted in a 90 m thick fluvial valley-fill succession, which is characterized by marked downstream facies heterogenity.

5.2 THE PLIOCENE – PLEISTOCENE AMBRA VALLEY SUCCESSION

Field evidence allowed to discuss the role of longitudinal and lateral floodplain tilting as forcing on fluvial aggradation and valley avulsion. Longitudinal tilting was due to an upstream-dipping normal fault. This particular geometry encompassed fluvial aggradation both upstream and downstream of a central uplifted area, which produced instead landscape degradation. Two distinct knickpoints were stemmed out by the onset of faulting: the upstream one responds to local increase of valley slope, whereas the downstream one reacts to increased stream power due to upstream bedload trap. In the upstream zone, migration of the knickpoint triggered a progressive valley backfilling, which developed a stratal architecture similar to that of sea-level-controlled, coastal incised valleys. Downstream of the fault zone, aggradation occurred as a downfilling

related to an overwhelming sediment supply, which caused the fluvial equilibrium profile to rise above the valley floor. Lateral tilting affected the fluvial morphodynamics in distinct ways: the activity of a normal fault striking parallel to the valley axis was associated with a down-dip shift of the trunk system; lateral increase in displacement along faults striking transverse to the valley axis also involved a shift of the trunk system towards the faulted valley flank. The latter process was counter-balanced by the activation of fault-sourced, supply-dominated alluvial fans that generated positive topography and shifted back the trunk system towards the valley axis. The study case attests therefore that both backfilling and downfilling architecture can develop in inland valleys as consequence of specific tectono-sedimentary interaction, and that lateral shifts of several mechanisms can interact to cause lateral shifting of alluvial valleys and related rivers.

5.3 NUMERICAL MODELLING

Numerical modeling allowed to assess the spatial and temporal constraints concerning tectonic control on aggradation of the studied valley fill and to investigate the effect of lifting rate on variable-discharge systems.

Physical laws, on which is based the fluvial simulation, verified the tectono-sedimentary scenario, stemmed out from sedimentological investigations. Model approximations and simplifications can restrict the bearing of the modelling outcomes. For this reason it was necessary to provide a careful calibration of the parameters considered, in order to find the best-conformity equations between natural cases, reconstructive and predictive models. The confirmation is expressed by comparing the modelling outcomes with the sedimentary and architectural features of the Ambra

palaeovalley succession. Using the numerical reconstruction, we were able to understand that downstream aggradation post-dated the upstream one. The time span between them corresponds to the time required by the river to incise partially the uplifted block, leading to the valley avulsion. This incision comes out from river potential energy and stream power.

The generalisation of tectonic forcing on aggradation of variable-discharge fluvial systems reveals that low-discharge systems are sensitive to minor uplift rates, whereas high-discharge settings are influenced solely by major uplift rates. In both low- and high-discharge systems, the increasing of uplift rate develops facies heterogeneity, through an orderly pattern of grain-size characterised by a fining tendency moving toward the uplift region.

REFERENCES

Abbate, E. and **Sagri, M.** (1982) Le unità torbiditiche cretacee dell'Appennino settentrionale ed i margini continentali della Tetide. *Mem. Soc. Geol. Ital.*, **24**, 115-126.

Abbate, E., Bortolotti, V., Conti, M., Marcucci, M., Principi, G., Passerini, P. and **Treves, B.** (1986) Apennines and Alps ophiolites and the evolution of the Western Tethys. *Mem. Soc. Geol. Ital.*, **31**, 23-44.

Albianelli, A., Bertini, A., Magi, M., Napoleone, G. and **Sagri, M.** (1995) Il Bacino Plio-Pleistocenico del Valdarno Superiore: eventi de posizionali, paleomagnetici e paleoclimatici. *Il Quaternario*, **8**, 11-18.

Aldinucci, M., Ghinassi, M. and **Sandrelli, F.** (2007) Climatic and tectonic signature in the fluvial infill of a late Pliocene Valley (Siena Basin, Northern Appennines, Italy). *SEPM, J. Sediment. Res.*, **77**, 398-414.

Alexander, J. and **Leeder, M.R.** (1987) Active tectonic control on alluvial architecture. In: *Recent Developments in Fluvial Sedimentology* (Eds. F.G. Ethridge, R.M. Flores and M.D. Harvey), *SEPM Spec. Publ.*, **39**, 243-252.

Alexander, J., Bridge, J.S., Leeder, M.R., Collier, R.E.L. and **Gawthorpe, R.L.** (1994) Holocene meander-belt evolution in an active extensional basin, southwestern Montana. *J. Sediment. Res.*, **B64**, 542-559.

Allen, J.R.L. (1978) Studies in fluvial stile sedimentation: an exploratory quantitative model for the architecture of avulsion-controlled alluvial suites. *Sediment. Geol.*, **21**, 129-147.

Allen, G. and **Posamentier, H.** (1993) Sequence stratigraphy and facies model of an incised valley fill; the Gironde Estuary, France. *J. Sediment. Petrol.,* **63**, 378-391.

Arcement, Jr. G. and **Schneider, V.** (1984) Guide for Selecting Manning's Roughness Coefficient For Natural Channels and Flood Plains. *U.S. Geol. Surv., Water Supply, Pap.*, **2339**, 38 pp.

Arragoni, S., Martini, I. and **Sandrelli, F.** (2012) Facies association map of the Pliocene deposits of the central-southern Siena Basin (Tuscany, Italy). *Journal of Maps*, **8**(4), 406-412.

Aslan, A. and **Blum, M.D.** (1999) Contrasting styles of Holocene avulsion, Texas Gulf Coastal Plain. In: *Fluvial Sedimentology* (Eds. N.D. Smith and J.J. Rogers), *Fluvial Sediment. VI: IAS Spec. Publ.*, **28**, 193-209.

Baldi, A.M., Civeli, A., La Bella, M. and **Seitz, H.** (2006) The extraction of the layer of CO_2 "Torrente Ambra" in the province of Siena. 15th Int. Symp. MPES – Torino 2006.

Bambini, A.M., Brogi, A., Cornamusini, G., Costantini, A., Foresi, L.M. and **Lazzarotto, A.** (2010) Geological setting of the Rapolano Terme area (Siena, Northern Apennines). *Ital. J. Geosci.*, **129**, 457-495.

Barchi, M. (2010) The Neogene-Quaternary evolution of the Northern Apennines: Crustal structure, style of deformation and seismicity. In: *The Geology of Italy: Tectonics and life along plate margins* (Eds. M. Beltrando, A. Peccerillo, M. Mattei, S. Conticelli and C. Doglioni), *J. Virtual Explorer*, **36**(11).

Bartholdy, J. and **Billi, P. (**2002) Morphodynamics of a pseudomeandering gravel bar reach. *Geomorphology*, **42**, 293-310.

Bartolini, C. and **Pranzini, G.** (1981) Plio-Quaternary evolution of the Arno basin drainage. *Z. Geomorphol. N.F.*, **40**, 77-91.

Basilici, G. (1997) Sedimentary facies in an extensional and deep-lacustrine depositional system: the Pliocene Tiberino Basin, Central Italy. *Sediment. Geol.*, **109**, 73-94.

Bersezio, R., Pavia, F., Baio, M., Bini, A., Felletti, F. and **Rodondi, C.** (2004) Aquifer architecture of the Quaternary alluvial succession of the southern Lambro basin (Lombardy-Italy). *Il Quaternario*, **17**, 361-378.

Bianchi, V., Ghinassi, M., Aldinucci, M., Boscaini, N., Martini, I., Moscon, G. and **Roner, M.** (2013) Geological map of Pliocene-Pleistocene deposits of the Ambra and Ombrone valleys (Northern Siena Basin, Tuscany, Italy). *Journal of Maps*, **9**(4), 573-583.

Bianchi, V., Ghinassi, M., Aldinucci, M., Boaga, J, Brogi, A. and **Deiana, R.** (submitted) Tectonically-driven deposition and landscape evolution within upland incised valleys: the Ambra Valley fill, Pliocene-Pleistocene of Tuscany, Italy. *Sedimentology*.

Billi, P., Preciso, E. and **Salemi, E.** (2014) Rhythmic roughness elements and channel morphology of gravel bed rivers. *Z. Geomorphol.* DOI: http://dx.doi.org/10.1127/0372-8854/2013/0127.

Binley, A. (2008) Resistivity inversion software. Available at: http://www.es.lancs.ac.uk/people/amb/Freeware/freeware.htm. Last access: December 4, 2011. 11157.

Bishop, P. (2007) Long-term landscape evolution: linking tectonics and surface processes. *Earth Surf. Proc. Land.*, **32**(3), 329-365.

Blair, T.C. (1987) Tectonic and hydrologic controls on cyclic alluvial fan, fluvial, and lacustrine rift-basin sedimentation, Jurassic-lowermost Cretaceous Todos Santos Formation, Chiapas, Mexico. *J. Sediment. Petrol.*, **57**(5), 845-862.

Blair, T.C. and **McPherson, J.G.** (1994a) Alluvial fan processes and forms. In: *Geomorphology of Desert Environments* (Eds. A.D. Abrahams and A. Parsons), pp. 354-402. Chapman and Hall, London.

Blair, T.C. and **McPherson, J.G.** (1994b) Alluvial fans and their natural distinction from rivers based on morphology, hydraulic processes, sedimentary processes, and facies. *J. Sediment. Res.*, **64**, 451-490.

Bluck, B.J. (1980) Structure, generation and preservation of upward fining, braided stream cycles in the Old Red Sandstone of Scotland. *Transac. Roy. Soc. Edinburgh Earth Sci.*, **71**, 29-46.

Blum, M.D. and **Aslan, A.** (2006) Signatures of climate vs. sea-level change within incised valley-fill succession: Quaternary examples from the Texas Gulf Coast. *Sediment. Geol.*, **190**, 177-211.

Blum, M.D. and **Price, D.M.** (1998) Quaternary alluvial plain construction in response to interacting glacio-eustatic and climatic controls, Texas Gulf Coastal Plain. In: *Relative Role of Eustasy, Climate, and Tectonism in Continental Rocks* (Eds. K.W. Shanley and P.J. McCabe), *SEPM Spec.Publ.*, **59**, 31-48.

Blum, M.D. and **Tornqvist, T.E.** (2000) Fluvial responses to climate and sea-level change: a review and look forward. *Sedimentology*, **47**, 2-48.

Blum, M.D. and **Womack, J.H.** (2009) Climate change, sea-level change, and fluvial sediment supply to deepwater systems. In: *External Controls on Deep Water Depositional Systems: Climate, Sea-Level, and Sediment Flux* (Eds. B. Kneller, O.J. Martinsen and B. McCaffrey), *SEPM Spec. Publ.*, **92**, 15-39.

Blum, M.D., Martin, J., Milliken, K., and **Garvin, M.** (2013) Paleovalley systems: insights from Quaternary analogs and experiments. *Earth-Sci. Rev.*, **116**, 128-169.

Boccaletti, M., Ciaranfi, N., Cosentino, D., Deiana, G., Gelati, R., Lentini, F., Massari, F., Moratti, G., Pescatore, T., Ricci Lucchi, F. and **Tortorici, L.** (1990) Palinspastic restoration and paleogeographic reconstruction of the Peri-Thyrrhenian area during Neogene. *Palaeogeogr. Palaeocl. Palaeoeco*., **77**, 41-50.

Bonini, M. and **Sani, F.** (2002) Extension and compression in the Northern Apennines (Italy) hinterland: Evidence from the late Miocene-Pliocene Siena-Radicofani Basin and relations with basement structures. *Tectonics*, **21**, 1-35.

Bonini, M., Moratti, G., Sani, F. and **Balestrieri, M.L.** (2013) Compression-to-extension transition in the Late Plio-Pleistocene Upper Valdarno Basin (Northern Apennines, Italy): structural and thermochronological constraints. *Ital. J. Geosci.*, **132**, 54-80.

Bonnet, S. and **Crave, A.** (2003). Landscape response to climate change: Insights from experimental modelling and implications for tectonic versus climatic uplift of topography. *Geology*, **31**(2),123-126.

Boyd, R. and **Diessel, C.F.** (1994) The application of sequence stratigraphy to non-marine clastics and coal. 2nd High Resolution Sequence Stratigraphy Conference, pp. 13–20. Tremp, Proceedings.

Boyd, R., Dalrymple, R.W. and **Zaitlin, B.A.** (2006) Estuarine and incised-valley facies model. In: *Facies Models Revisited* (Eds. H.W. Posamentier and R.G. Walker), *SEPM Spec. Publ.*, **84**, 171-235.

Braun, J. and **van der Beek, P.** (2004). Evolution of passive margin escarpments: what can we learn from low-temperature thermochronology? *J. Geophys. Res.*, **109**. DOI: 10.1029/2004JF000147

Breda, A., Mellere, D., Massari, F. and **Asioli, A.** (2009) Vertically stacked Gilbert-type deltas of Ventimiglia (NW Italy): The Pliocene record of an overfilled Messinian incised valley. *Sediment. Geol.*, **219**, 58-76.

Bridge, J.S. (1993) Description and interpretation of fluvial deposits: a critical perspective. *Sedimentology*, **40**, 801-810.

Bridge, J.S. (2003). Rivers and Floodplains. Blackwell Scientific Publications, Oxford, 491 pp.

Bridge, J.S. and **Leeder, M.R.** (1979) A simulation model of alluvial stratigraphy. *Sedimentology*, **26**, 617-644.

Bridge, J.S. and **Lunt, I.A.** (2006) Depositional models in braided rivers. In: *Braided Rivers: Process, Deposits, Ecology and Management* (Eds. G.H. Sambrook Smith, J.L. Best, C.S. Bristow and G.E. Petts), *IAS Spec. Publ.*, **36**, 11-50.

Bridge, J.S. and **Mackey, S.D.** (1993) A theoretical study of fluvial sandstone body dimension. In: *Geological Modeling of Hydrocarbon Reservoirs* (Eds. S.S. Flint and I.D. Bryant), *IAS Spec. Publ.*, **15**, 213-236.

Brierley, G.J. (1991a) Floodplain sedimentology of the Squamish River, B.C.: relevance of element analysis. *Sedimentology*, **38**, 735-750.

Brierley, G.J. (1991b) Bar sedimentology of the Squamish River, British Columbia: definition and application of morphostratigraphic units. *J. Sediment. Petrol.*, **61**, 211-225.

Brogi, A. (2008). The Triassic and Palaeozoic successions drilled in the Bagnore Geothermal field and Poggio Nibbio area (Monte Amiata, Northern Apennines, Italy). *Boll. Soc. Geol. Ital.*, **3**, 599-613.

Brogi, A. (2011a) Bowl-shaped basin related to low-angle detachment during continental extension: The case of the controversial Neogene Siena Basin (central Italy, Northern Apennines). *Tectonophysics*, **499**, 131-148.

Brogi, A. (2011b) Variation in fracture patterns in damage zones related to strike-slip faults interfering with pre-existing fractures in sandstone (Calcione area, southern Tuscany, Italy). *J. Struct. Geol.*, **33**, 644-661.

Brogi, A. and **Liotta, D.** (2008) Highly extended terrains, lateral segmentation of the substratum and basin development: The middle-late Miocene Radicondoli Basin (Inner Northern Apennines, Italy). *Tectonics*, **27**, 1-20.

Brogi, A., Lazzarotto, A., Liotta, D. and **Ranalli, G.** (2003) Extensional shear zones as imaged by reflection seismic lines: the Larderello geothermal field (central Italy). *Tectonophysics*, **363**, 127-139.

Brogi, A., Lazzarotto, A., Liotta, D. and **CROP 18 Working Group** (2005) Structural features of southern Tuscany and geological interpretation of the CROP18 Seismic Reflection Survey (Italy). *Boll. Soc. Geol. Ital.*, **3**, 213-236.

Brogi, A., Liotta, D., Meccheri, M. and **Fabbrini, L.** (2010) Transtensional shear zones controlling volcanic eruptions: the Middle Pleistocene Monte Amiata volcano (inner Northern Appennines, Italy). *Terra Nova*, **22**, 137-146.

Brogi, A., Fidolini, F. and **Liotta, D.** (2013) Tectonic and sedimentary evolution of the Upper Valdarno Basin: new insights from the lacustrine Santa Barbara Basin. *Ital. J. Geosci.*, **132**, 81-97.

Brown, J.L. (1993) Sedimentology and depositional history of the Lower Paleocene Tullock Member of the Fort Union Formation, Powder River Basin, Wyoming and Montana: depositional style of fluvial deposits during initiation of a Laramide foreland basin. US Government Printing Office, 42 pp.

Bruni, P., Cipriani, N., Nebbiai, M. and **Papini, M.** (2007) Dati litostratigrafici e petrografici delle arenarie silicoclastiche del complesso di Canetolo affiorante tra le Cinque Terre e la Val di Magra (Paleocene-Oligocene sup., Appennino Settentrionale). *Boll. Soc. Geol. Ital*., **126**, 557-565.

Bryant, M., Falk, P. and **Paola, C.** (1995) Experimental study of avulsion frequency and rate of deposition. *Geology*, **23**, 365-368.

Burnett, A.W. and **Schumm, S.A.** (1983) Alluvial river response to neotectonic deformation in Louisiana and Mississippi. *Science*, **222**, 49-50.

Carmignani, L., Decandia, F.A., Fantozzi, P.L., Lazzarotto, A., Liotta, D. and **Meccheri, M.** (1994). Tertiary extensional tectonics in Tuscany (Northern Apennines, Italy). *Tectonophysics*, **238**, 295-315.

Carmignani, L., Decandia, F.A., Disperati, L., Fantozzi, P.L., Lazzarotto, A., Liotta, D. and **Oggiano, G.** (1995) Relationship between the tertiary structural evolution of the Sardinia-Corsica-Provencal domain and the Northern Apennines. *Terra Nova*, **7**(2), 128-137.

Carmignani, L., Decandia, F.A., Disperati, L., Fantozzi, P.L., Kligfield, R., Lazzarotto, A., Liotta, A. and **Meccheri, M.** (2001). Inner Northern Apennines. In: *Anatomy of an Orogen. The Apennines and adjacent Mediterranean basins* (Eds. G.B. Vai and I.P. Martini), pp. 197-214. Kluwer Academic Publisher, London.

Cassiani, G., Bruno, V., Villa, A., Fusi, N. and **Binley, A.M.** (2006) A saline tracer test monitored via time-lapse surface electrical resistivity tomography. *J. Appl. Geophys.*, **59**, 244-259.

Castellarin, A., Eva, C., Giglia, G. and **Vai, G.B.** (1986) Analisi strutturale del fronte Appenninico padano. *Giorn. Geol.*, **47**, 47-76.

Chang, K.H. (1975) Unconformity bounded stratigraphic units. *Geol. Soc. Am. Bull.*, **86**, 1544-1552.

Chatelain, J.L., Guiller, B., Cara, F., Duval, A., Atakan, K., P.-Y. Bard and **WP02 SESAME TEAM** (2007) Evaluation of the influence of experimental conditions on H/V results from ambient noise. *Bull. Earthq. Eng.*, **6**, 33-74.

Chow, V.T. (1964) Handbook of Applied Hydrology. McGraw-Hill Book Company, New York, NY, 1481 pp.

Collinson, D.J. (1986) Alluvial sediments. In: *Sedimentary Environments and Facies* (Ed. H.G. Reading), 2nd ed., pp. 20-62. Blackwell Scientific Publications, Oxford.

Cornamusini, G., Ielpi, A., Bonciani, F., Callegari, I. and **Conti, P.** (2012) Geological map of the Chianti Mts (Northern Apennines, Italy). *Journal of Maps*, **8**(1), 22-32.

Costantini, A., Lazzarotto, A. and **Sandrelli, S.** (1982) Il Graben di Siena: conoscenze geologico- strutturali. *CNR, Progetto Finalizzato Energia, Rapporto Finale*, **9**, 11-33.

Costantini, A., Mazzanti, R. and **Sandrelli, F.** (1995) La val d'Ambra, appendice del lago superiore del Valdarno Superiore nel Pleistocene medio e attuale punto di contatto incerto nello spartiacque tra i bacini dell'Arno e dell'Ombrone. *Mem. Atti Soc. Tosc. Scienze Naturali, Serie A*, **102**, 177-184.

Currie, B.S. (1997) Sequence stratigraphy of nonmarine Jurassic–Cretaceous rocks, central Cordilleran foreland-basin system. *Geol. Soc. Am. Bull.*, **109**, 1206-1222.

Daily, W., Ramirez, A., Binley, A.M. and **LaBrecque, D.** (2004) Electrical resistivity tomography. *The Leading Edge*, **23**, 438-442.

Dales, G.T. (1966) The decline of the Harappans. *Sci. Am.*, **214**, 92-100.

Dallmeyer, R.D. and **Liotta, D.** (1998) Extension, uplift of rocks and cooling ages in thinned crustal provinces: the Larderello geothermal area (inner Northern Apennines, Italy). *Geol. Mag.*, **135**(2), 193-202.

Dalrymple, R.W. (2006) Incised valleys in time and space: an introduction to the volume and an examination of the controls on valley formation and filling. In: *Incised Valleys in Time and Space* (Eds. R.W. Dalrymple, D.A. Leckie and R.W. Tillman) *SEPM Spec. Publ.*, **85**, 5-12.

Dalrymple, R.W., Boyd, R. and **Zaitlin, B.A.** (1994) History of research, types and internal organization of incised-valley systems: Introduction to the volume. In: *Incised-Valley Systems: Origin and Sedimentary Sequences* (Eds. R.W Dalrymple, R.Boyd and B.A. Zaitlin), *SEPM Spec. Publ.*, **51**, 3-10.

Dalrymple, T. (1960) Flood-frequency analyses. *U.S. Geol. Surv., Water Supply, Pap.*, **1543-A**.

Davis, W.M. (1899) The Geographical Cycle. *Geogr. J.*, **14**, 481-504.

De Castro, C. and **Pilotti, C.** (1933) I giacimenti di lignite della Toscana. Mem. Descr. Carta Geol. Italia, Regio Ufficio Geologico d'Italia, Roma, 224 pp.

Deiana, R., Cassiani, G., Villa, A., Bagliani, A. and **Bruno, V.** (2008) Model calibration of a water injection test in the vadose zone of the Po River plain using GPR cross-hole data. *Vadose Zone J.*, **7**, 215-226.

Dietrich, W.E., Bellugi, D., Heimsath, A.M., Roering, J.J., Sklar, L. and **Stock, J.D.** (2003) Geomorphic transport laws for predicting the form evolution of landscapes. In: *Prediction in Geomorphology* (Eds. P. Wilcock and R. Iverson), pp. 103-132. Am. Geophys. Union, Washington, DC.

Dingman S.L. and Sharma, K.P. (1997) Statistical development and validation of discharge equations for natural channels. *J. Hydrol.*, **199**, 13-35.

Dolson, J.C., Muller, Dave, Evetts, M.J. and **Stein, J.A.** (1991) Regional paleotopographic trends and production, Muddy Sandstone (Lower Cretaceous), central and northern Rocky Mountains. *Am. Assoc. Petr. Geol. Bull.*, **75**, 409-435.

Doornkamp, J. and **Temple, P.H.** (1966) Surface drainage and tectonic instability in part of southern Uganda. *Geogr. J.*, **132**, 238-252.

Dumont, J.F. (1992) Rasgos morfoestructurales de la llanura Amazonica del Peru: efecto de la Neotectonica sobre los cambios fluviales y la delimitacion de las provincias morfologicas. *Bull. Inst. Fr. Etud. Andines*, **21**(3), 801-833.

Dumont, J.F. (1993) Lake patterns as related to neotectonics in subsiding basins. The example of the Ucamara Depression, Peru. *Tectonophysics*, **222**, 69-78.

Dumont, J.F. and **Hanagarth, W.** (1993) River shifting and tectonics in the Beni Basin (Bolivia). Proc. 3rd Int. Conf. Geomorph., 23–29 August, 1993, Hamilton, ON.

Dunne, T. and **Leopold, L.B.** (1978) Water in environmental planning. W.H. Freeman and Co, New York, 818 pp.

Eagleson, P.S. (1972) Dinamics of Flood Fraquency. *Water Resour. Res.*, **8**(4), 878-898.

Einsele , G. (1992) Sedimentary Basins: Evolution, Facies and Sediment Budget. Springer, Berlin Heidelberg New York, 628 pp.

Elter, P., Giglia, G., Tongiorgi, M. and **Trevisan, L.** (1975) Tensional and compressional areas in the recent (Tortonian to present) evolution of the Northern Apennines. *B. Geofis. Teor. Appl.*, **17**, 3-18.

England, P. and **Molnar, P.** (1990) Surface uplift, uplift of rocks, and exhumation of rocks. *Geology*, **18**, 1173-1177.

Ethridge, F.G. (1985) Modern alluvial fan and fan deltas. In: *Recognition of Fluvial Systems and Their Resource Potential* (Eds. R.W. Flores, F.G. Ethridge, A.D. Miall, W.E. Galloway and T.D. Fouch), *SEPM, Short Course*, **19**, 101-126.

Ethridge, F.G. and **Schumm, S.A.** (2007) Fluvial seismic geomorphology: a view from the surface. *Geol. Soc., London, Spec. Publ.*, **277**, 205-222.

Ethridge, F.G., Jackson, T.J. and **Youngberg, A.D.** (1981) Flood-basin sequences in fine-grained meander belt subsystems: the coal bearing Lower Wasatch and Upper Fort Union Formations, Powder River Basin, Wyoming. In: *Recent and Ancient Nonmarine Depositional Environments: Models for Exploration* (Eds. F.G. Ethridge and R.M. Flores), *SEPM Spec. Publ.*, **31**, 191-212.

Esu, D., Girotti, O. and **Kotsakis, T.** (1993) Palaeobiogeographical observations on Villafranchian continental molluscs of Italy. *Scripta Geol., Spec. Vol.*, **2**, 101-119.

Fidolini, F., Ghinassi, M., Magi, M., Papini, M. and **Sagri, M.** (2013a). The Plio-Pleistocene, fluvio-lacustrine Upper Valdarno basin (central Italy): Stratigraphy and Basin fill evolution. *Ital. J. Geosci.*, **132**, 13-32.

Fidolini, F., Ghinassi, M., Aldinucci, M., Billi, P., Boaga, J., Deiana, R. and **Brivio, L.** (2013b) Fault-sourced alluvial fans and their interaction with axial fluvial drainage: An example from the Plio-Pleistocene Upper Valdarno Basin (Tuscany, Italy). *Sediment. Geol.*, **289**, 19-39.

Field, E.H. and **Jacob, K.H.** (1993) The Theoretical Response of Sedimentary Layers to Ambient Seismic Noise. *Geophys. Res. Lett.*, **20**, 2925-2928.

Fielding, C.R., LaGarry, H.E., LaGarry, L.A., Bailey, B.E. and **Swinehart, J.B.** (2007) Sedimentology of the Whiteclay Gravel Beds (Ogallala Group) in northwestern Nebraska, USA: Structurally controlled drainage promoted by Early Miocene uplift of the Black Hills Dome. *Sediment. Geol.*, **202**, 58-71.

Galgaro, A., Boaga, J. and **Rocca, M.** (2013) HVSR technique as tool for thermal-basin characterization: a field example in N-E Italy. *Environ. Earth Sci.*, DOI: 10.1007/s12665-013-2838-5.

Gasparini, N. M., Tucker, G. E., and Bras R. L. (2004) Network-scale dynamics of grain-size sorting: implications for downstream fining, stream-profile concavity, and drainage basin morphology. *Earth Surf. Proc. Land.*, **29**(4), 401-421.

Ghinassi, M. (2011) Chute channels in the Holocene high sinuosity-river deposits of the Firenze plain, Tuscany, Italy. *Sedimentology*, **58**, 618–642.

Ghinassi, M., Magi, M., Sagri, M. and **Singers, B.S.** (2004) Arid climate 2.5 Ma in the Plio-Pleistocene Valdarno Basin (Northern Apennines, Italy). *Palaeogeogr. Palaeocl. Palaeoeco.*, **207**, 37-57.

Ghinassi, M., Libsekal, Y., Papini M., and **Rook, L.** (2009) Palaeoenvironments of the Buia Homo site: High-resolution facies analysis and non-marine sequence stratigraphy in the Alat formation (Pleistocene Dandiero Basin, Danakil depression, Eritrea). *Palaeogeogr. Palaeocl. Palaeoeco.*, **280**, 415-431.

Ghinassi, M., Fidolini, F., Magi, M. and **Sagri, M.** (2013). Depositional environments of the Plio-Pleistocene Upper Valdarno Basin (Tuscany, Italy). *Ital. J. Geosci.*, **132**, 33-53.

Gibling, M.R. (2006) Width and thickness of fluvial channel bodies and valley fills in the geological record: A literature compilation and classification. *J. Sediment. Res.*, **76**, 731-770.

Gibling, M.R., Fielding, C.R. and **Sinha, R.** (2011) Alluvial valleys and alluvial sequences: towards a geomorphic assessment. In: *River to Rock Record: the preservation of fluvial sediments and their subsequent interpretation* (Eds. S.K. Davidson, S. Leleu and C.P. North), *SEPM Spec. Publ.*, **97**, 423-447.

Gilbert, G.K. (1895) Sedimentary measurement of Cretaceous time. *J. Geol.*, **3**(2), 121-127.

Greb, S.F. and **Chesnut, D.R.** (1996) Lower and lower Middle Pennsylvanian fluvial to estuarine deposition, central Appalachian basin: effects of eustasy, tectonics, and climate. *Geol. Soc. Am. Bull.*, **108**(3), 303-317.

Griffiths, C.M., Dyt, C., Paraschivoiu, E. and **Liu, K.** (2001) Sedsim in hydrocarbon exploration. In: *Geologic Modeling and Simulation* (Eds. D. Merriam and J.C. Davis) pp. 71-97. Kluwer Academic, New York.

Guiseppe, A.C. and **Heller, P.L.** (1998) Long-term river response to regional doming in the Price River Formation, central Utah. *Geology*, **26(3)**, 239-242.

Harlow, F.H. (1964) The particle-in-cell computing method for fluid dynamics. *Method. comput. Phys.*, **3**, 319-343.

Hasbargen, L.E. and **Paola, C.** (2000) Landscape instability in an experimental drainage basin. *Geology*, **28**, 1067-1070.

Heimsath, A.M., Furbish, D.J. and **Dietrich W.E.** (2005) The illusion of diffusion; field evidence for depth-dependent sediment transport. *Geology*, **33**(12), 949-952.

Hengesh, J.V. and **Lettis, W.R.** (2002) Tectonic setting and geological effects of the Mw 7.7 2001 Bhuj Earthquake. *EERI Spec. Publ. on the Bhuj earthquake.*

Hickson, T.A., Sheets, B.A., Paola, C. and **Kelberer, M.** (2005) Experimental test of tectonic controls on three-dimensional alluvial facies architecture. *J. Sediment. Res.*, **75**, 710-722.

Hockney, R.W. and **Eastwood, J.W.** (1981) Computer Simulation Using Particles. McGraw-Hill, New York, 540 pp.

Holbrook, J.M. (2001) Origin, genetic interrelationships, and stratigraphy over the continuum of fluvial channel-form bounding surfaces: An illustration from middle Cretaceous strata, southeastern Colorado. *Sediment. Geol.*, **144**, 179-222.

Holbrook, J.M. and **Schumm, S.A.** (1999) Geomorphic and sedimentary response of rivers to tectonic deformation: a brief review and critique of a tool for recognizing subtle epeirogenic deformation in modern and ancient settings. *Tectonophysics*, **305**, 287-306.

Holbrook, J.M. and **White, D.W.** (1998) Controls on lithofacies distribution and sequence architecture by low-relief intraplate uplift: examples from the Lower Cretaceous of northeastern New Mexico. In: *Relative Role of Eustasy, Climate, and Tectonism in Continental Rocks* (Eds. K.W. Shanley and P.J. McCabe), *Soc. Sediment. Geol. Spec. Publ.*, **59**, 123-132.

Hole, J.A. (2011) Rivers, rifts and ruptures. *Nat. Geosci.*, **4**, 428-429.

Howard, R.H. and **Whitaker, S.T.** (1988) Hydrocarbon accumulation in a paleovalley at Mississippian–Pennsylvanian unconformity near Hardinville, Crawford County, Illinois: a model paleogeomorphic trap. *Illinois State Geol. Surv., Illinois Petrol.*, **129**, 26 pp.

Ielpi, A. (2013) Frequency-reliant correlative patterns of asymmetric lacustrine-paralic sequences: A genetic approach to the late Miocene Bithynia Marlstones of the southeastern Volterra Basin, Italy. *J. Sediment. Res.*, **83**, 377-394.

International Subcommission On Stratigraphic Classification (1987) Unconformity bounded stratigraphic units. *Geol. Soc. Am. Bull.*, **98**, 232-237.

Jackson, R.G. (1976) Depositional model of point bars in the lower Wabash River. *J. Sediment. Petrol.*, **46**, 579-594.

Jerolmack, D.J. (2011). Causes and effects of noise in landscape dynamics. *EOS, Trans AGU*, **92**, 385-386.

Jones, S.J., Frostick, L.E. and **Astin, T.R.** (2001) Braided stream and flood plain architecture: the Rio Vero Formation, Spanish Pyrenees. *Sediment. Geol.*, **139**, 229-260.

Kent, D.V., Olsen, P.E. and **Witte, W.K.** (1995) Late Triassic-Early Jurassic geomagnetic polarity sequence and paleolatitudes from drill cores in the Newark rift basin (Eastern North America). *J. Geophys. Res.*, **100**, 14965-14998.

Knighton, A.D. (1996) Fluvial Forms and Processes. Arnold Publishers, London, pp.

Konno, K. and **Ohmachi, T.** (1998) Ground-motion characteristics estimated from spectral ratio between horizontal and vertical components of microtremor. *Bull. Seismol. Soc. Am.*, **88**, 228-241.

Kooi, H. and **Beaumont, C.** (1994) Escarpment evolution on high-elevation rifted margins: insights derived from a surface process model that combines diffusion, advection, and reaction. *J. Geophys. Res.*, **99**, 12191-12209.

Kooi, H. and **Beaumont, C.** (1996) Large-scale geomorphology: classical concepts reconciled and integrated with contemporary ideas via a surface process model. *J. Geophys. Res.*, **101**, 3361-3386.

Koons, P.O. (1989) The topographic evolution of collisional mountain belts: a numerical look at the Southern Alps, New Zealand. *Am. J. Sci.*, **289**, 1041-1069.

Koons, P.O. (1994) Three-dimensional critical wedges: tectonics and topography in oblique collisional orogens. *J. Geophys. Res.*, **99**, 12301-12315.

LaBrecque, D.J., Miletto, M., Daily, W.D., Ramirez, A.L. and **Owen, E.** (1996) The effects of noise on Occam's inversion of resistivity tomography data. *Geophysics*, **61**, 538-548.

Lague, D., Crave, A. and **Davy, P.** (2003) Laboratory experiments simulating the geomorphic response to tectonic uplift. *J. Geophys. Res.*, **108**(B1), ETG 3 – 1- ETG 3 – 20.

Lane, E.W. (1955) The importance of fluvial morphology in hydraulic engineering. *Am. Soc. Civil Eng. Proc.,* **81**(745), 1-17.

Lane, S.N. and **Richards, K.S.** (1998) Two-dimensional modelling of flow processes in a multithread channel. *Hydrol. Process.*, **12**, 1279-1298.

Lavé, J. and **Avouac, J-P.** (2001) Fluvial incision and tectonic uplift across the Himalayas of central Nepal. *J. Geophys. Res.*, **106**, 26561-26592.

Lazzarotto, A., Costantini, A., Sandrelli, F., Brogi, A. and **Foresi, M. L.** (in press). Carta Geologica d'Italia alla Scala 1:50.000, Foglio 297-Asciano. ISPRA, Servizio Geologico d'Italia, Roma.

Leeder, M.R. (1978) A quantitative stratigraphic model for alluvium, with special reference to channel deposit density and interconnectedness. In: *Fluvial Sedimentology* (Ed. A.D. Miall), *Mem. Can. Soc. Petrol. Geol*, **5**, 587-596.

Leeder, M.R. (1993) Tectonic controls upon drainage basin development, river channel migration and alluvial architecture: implications for hydrocarbon reservoir development and characterization. In: *Characterization of Fluvial and Aeolian Reservoirs* (Eds. C.P. North and D.J. Prosser), *Geol. Soc., London, Spec. Publ.*, **73**, 7-22.

Leeder, M.R. and **Gawthorpe, R.L.** (1987) Sedimentary models for extensional tilt block/half-graben basins. In: *Continental Extensional Tectonics* (Eds. M.P. Coward, J.F. Dewey, P.L. Hancock), *Geol. Soc., London, Spec. Publ.*, **28**, 139-152.

Legarreta, L. and **Uliana, M.A.** (1998) Anatomy of hinterland depositional sequences: upper Cretaceous fluvial strata, Neuquen Basin, West-Central Argentina. In: *Relative Role of Eustasy, Climate, and Tectonism in Continental Rocks* (Eds. K.W. Shanley and P.J. McCabe), *SEPM Spec. Publ.*, **59**, 83-92.

Leopold, L.B. and **Wolman, M.G.** (1957) River channel pattern: braided meandering and straight. *U.S. Geol. Surv. Prof. Pap.*, **282**, 39-85.

Lewin, J. (1976) Initiation of bed forms and meanders in coarse-grained sediment. *Geol. Soc. Am. Bull.*, **87**, 281-285.

Li, C., Wang, P., Fan, D. and **Yang, S.** (2006) Characteristics and formation of Late Quaternary incised-valley-fill sequences in sediment-rich deltas and estuaries: a case study from China. In: *Incised Valleys in Time and Space* (Eds. R.W. Dalrymple, D.A. Leckie and R.W. Tillmann), *SEPM Spec. Publ.*, **85**, 141-160.

Limerinos, J.T. (1970) Determination of the Manning coefficient from measured bed roughness in natural channels. *Geol. Surv., Water Supply, Pap.*, 1898-B, 55 pp.

Liotta, D. (1991) The Arbia-Val Marecchia Line, Northern Apennines. *Eclogae Geol. Helv.*, **84**, 413-430.

Liotta, D., Cernobori, L. and **Nicolich, R.** (1998) Restricted rifting and its coexistence with compressional structures: Results from the CROP03 traverse (Northern Apennines, Italy). *Terra Nova*, **10**, 16-20.

Lowrie, W. and **Alvarez, W.** (1977) Late Cretaceous geomagnetic polarity sequence: detailed rock and palaeomagnetic studies of the Scaglia Rossa limestone at Gubbio, Italy. *Geophys. J. Internat.*, **51**(3), 561-581.

Lunt, I. A. and **Bridge, J. S.** (2004) Evolution and deposits of a gravelly braid bar, Sagavanirktok River, Alaska. *Sedimentology*, **51**, 415-432.

Lunt, I.A., Bridge, J.S. and **Tye, R.S.** (2004) A quantitative, three-dimensional depositional model of gravelly braided rivers. *Sedimentology*, **51**, 377-414.

Mackey, S.D. and **Bridge, J.S.** (1995) Three-dimensional model of alluvial stratigraphy: theory and application. *J. Sediment. Res.*, **B65**, 7-31.

Mack, G.H. and **James, W.C.** (1993) Control of basin symmetry on fluvial lithofacies, Camp Rice and Palomas Formations (Plio-Pleistocene), southern Rio Grande rift, USA. In: *Alluvial Architecture* (Eds. M. Marzo and C. Puigdefàbregas), *IAS Spec. Publ.*, **17**, 439-449.

Magi, M. (1992) Depositi fluviali e di conoidi alluvionali del Pleistocene nell'alta Valle dell'Ombrone (Siena). *Soc. Geol. Ital., 76° Riunione Estiva, Riass.*, 183 pp.

Manganelli, G., Aldinucci, M., Capezzuoli, E. and **Benocci, A.** (2007) Strobilopsid land snails (Gastropoda: Polmonata, Strobilopsidae) from late Messinian-early Pliocene (?) of Balze di Caspreno (central Italy). *Boll. Soc. Paleontol. Ital*., **46**, 101-106.

Manganelli, G., Spadini, V. and **Martini, I.** (2010) Rediscovery of an enigmatic Euro-Mediterranean Pliocene nassariid species: Nassarius crassiusculus Bellardi, 1882 (Gastropoda: Nassariidae). *Boll. Soc. Paleontol. Ital*., **49**, 195-202.

Manganelli, G., Martini, I. and **Benocci, A.** (2011) A new Janulus species (Gastropoda, Pulmonata, Gastrodontidae) from the Zanclean (early Pliocene) of Tuscany (central Italy). *Boll. Soc. Paleontol. Ital.*, **50**(3), 165-173.

Marple, R.T. and **Talwani, P.** (1993) Evidence of possible tectonic upwarping along the South Carolina coastal plain from an examination of river morphology and elevation data. *Geology*, **21**, 651-654.

Marr, J.G., Swenson, J.B., Paola, C. and **Voller, V.R.** (2000) A two-diffusion model of fluvial stratigraphy in closed depositional basins. *Basin Res.*, **12**, 381-398.

Martini, I., Aldinucci, M., Foresi, L. M., Mazzei, R. and **Sandrelli, F.** (2011). Geological map of the Pliocene succession of the Northern Siena Basin (Tuscany, Italy). *Journal of Maps*, **220**, 193-205.

Martini, I., Arragoni, S., Aldinucci, M., Foresi, L. M., Bambini, A. M. and **Sandrelli, F.** (2013). Detection of detached forced-regressive nearshore wedges: A case study from the central-southern Siena Basin (Northern Apennines, Italy). *Int. J. Earth Sci.*, **6**(5), 1467-1489.

Martini, I.P. and **Sagri, M.** (1993). Tectono-sedimentary characteristics of the late Miocene-Quaternary extensional basins of the Northern Appennines, Italy. *Earth-Sci. Rev.*, **34**, 197-233.

Martini, I.P., Sagri, M. and **Colella, A.** (2001) Neogene-Quaternary Basins of the Inner Apennines and Calabrian Arc, Italy. In: *Anatomy of an Orogen: the Apennines and adjacent Mediterranean basins* (Eds. G.B. Vai and I.P. Martini), pp. 375-400. Kluwer Academic Publisher, London.

Martinsen, O.J., Ryseth, A., Helland-Hansen, W., Flesche, H., Torkildsen, G. and **Idil, S.** (1999) Stratigraphic base level and fluvial architecture, Ericson Sandstone (Campanian), Rock Springs Uplift, W. Wyoming, USA. *Sedimentology*, **46**, 235-260.

McCuen, R.H. (1998) Hydrologic Analysis and Design. Prentice Hall, Upper Saddle River, NJ, 2nd ed., 814 pp.

McFadden, P.L. and **McElhinny, M.W.** (1988) The combined analysis of remagnetization circles and direct observations in palaeomagnetism. *Earth Planet. Sci. Lett.*, **87**, 161-172.

McFadden, P.L. and **McElhinny, M.W.** (1990) Classification of the reversal test in palaeomagnetism. *Geophys. J. Int.*, **103**, 725-729.

McGowen, J.H. and **Garner, L.E.** (1970) Physiographic features and stratification types of coarse-grained point bars: modern and ancient examples. *Sedimentology*, **14**, 77-111.

Miall, A.D. (1977) A review of the braided-river depositional environment. *Earth-Sci. Rev.*, **13**(1), 1-62.

Miall, A.D. (1985) Architectural-element analysis: a new method of facies analysis applied to fluvial deposits. *Earth-Sci. Rev.*, **22**, 261-308.

Miall, A.D. (1996) The Geology of Fluvial Deposits. Heidelberg, Springer-Verlag, 582 pp.

Minissale, A. (2004) Origin, transport and discharge of CO2 in central Italy. *Earth-Sci. Rev.*, **66**, 89-141.

Miola, A., Bondesan, A., Corain, L., Favaretto, S., Mozzi, P., Piovan, S. and **Sostizzo, I.** (2006) Wetlands in the Venetian Po Plain (northeastern Italy) during the Last Glacial Maximum: an interplay between vegetation, hydrology and sedimentary environment. *Rev. Palaeobot. Palyno.*, **141**, 53-81.

Nakamura, Y. and **Samizo, M.** (1989) Site Effect Evaluation of Surface Ground using Strong Motion Records (in Japanese). Proc. 20th JSCE Earthq. Eng. Symp., pp. 133-136.

Nanson, G.C. (1980) Point bar and floodplain formation of the meandering Beatton River, northeastern British Columbia, Canada. *Sedimentology*, **27**, 3-29.

Nemec,W. (1996). Principles of Lithostratographic Logging and Facies Analysis. Short Course Lecture Notes, Univ. of Bergen. 35 pp.

Nemec, W. and **Muszynski, A.** (1982) Volcaniclastic alluvial aprons in the Tertiary of Sofia district (Bulgaria). *Ann. Soc. Geol. Pol.*, **52**, 239-303.

Nemec W. and **Postma G. (**1993) Quaternary alluvial fans in southwestern Crete: sedimentation processes and geomorphic evolution. In: *Alluvial Sedimentation* (Eds. M. Marzo and C. Puigdefàbregas), *IAS Spec. Publ.*, **17**, 235-276.

Nemec, W. and **Steel, R.J.** (1984) Alluvial and coastal conglomerates: their significant features and some comments on gravelly mass-flow deposits. In: *Sedimentology of gravels and conglomerates* (Eds. E.H. Koster and R.J. Steel), *Mem. Can. Soc. Petrol. Geol.*, **10**, 1-31.

Neteler, M. and **Mitasova, H.** (2008) Open Source GIS : a GRASS GIS approach (3rd ed.). Springer, New York, 420 pp.

Nicolich, R. (2001) Deep seismic transects. In: *Anatomy of an Orogen. The Apennines and adjacent Mediterranean basins* (Eds. G.B. Vai and I.P. Martini), pp. 47-52. Kluwer Academic Publisher, London.

Nogoshi, M. and **Igarashi, T.** (1970) On the propagation characteristics of the microtremors. *J. Seism. Soc. Japan*, **23**, 264-280.

North American Commission On Stratigraphic Nomenclature (1983) North American stratigraphic code. *AAPG Bull.*, **67**, 841-875.

Ouchi, S. (1985) Response of alluvial rivers to slow active tectonic movement. *Geol. Soc. Am. Bull.*, **96**, 504-515.

Paola, C. (2000) Quantitative models of sedimentary basin filling. *Sedimentology*, **47**, 121-178.

Paola, C., Heller, P.L. and **Angevine, C.L.** (1992) The large-scale dynamics of grain-size variation in alluvial basins, 1: theory. *Basin Res.*, **4**, 73-90.

Paola, C., Straub, K., Mohrig, D. and **Reinhardt, L.** (2009) The "unreasonable effectiveness" of stratigraphic and geomorphic experiments. *Earth-Sci. Rev.*, **97**, 1-43.

Pascucci, V., Martini, I. P., Sagri, M. and **Sandrelli, F.** (2007) Effects of the transverse structural lineaments on the Neogene–Quaternary basins of Tuscany (inner Northern Apennines, Italy). In: *Sedimentary processes, environments and basins - A tribute to Peter friend* (Eds. G. Nichols, C. Paola and E.A. Williams), *IAS Spec. Publ.*, **38**, 155-183.

Pazzaglia, F.J. and **Brandon, M.T.** (2001) A fluvial record of long-term steady-state uplift and erosion across the Cascadia forearc high, western Washington State. *Am. J. Sci.*, 301, 385-431.

Peakall, J. (1995) The Influence of Lateral Ground-Tilting on Channel Morphology and Alluvial Architecture. Ph.D. Dissertation, University of Leeds, Leeds, 320 pp.

Pivnik, D.A. and **Johnson, G.D.** (1995) Depositional response to Pliocene–Pleistocene foreland partitioning in northwest Pakistan. *Geol. Soc. Am. Bull.*, **107**(8), 895-922.

Posamentier, H.W. and **Allen, G.P.** (1999) Siliciclastic Sequence Stratigraphy – Concepts and Applications. *SEPM, Concepts Sedimentol. Paleontol.*, **7**, 210 pp.

Posamentier, H.W. and **Vail, P.R.** (1988) Eustatic controls on clastic deposition II – sequence and system tract models. In: *Sea-Level Changes: An Integrated Approach* (Eds. C.K. Wilgus, B.S. Hastings, C.G.C. Kendall, H.W. Posamentier, C.A. Ross and J.C. Van Wagoner), *SEPM Spec. Publ.*, **42**, 125-154.

Posamentier, H.W., Jervey, M.T. and **Vail, P.R.** (1988) Eustatic controls on clastic deposition I – conceptual framework. In: *Sea-Level Changes: An Integrated Approach* (Eds. C.K. Wilgus, B.S. Hastings, C.G.C. Kendall, H.W. Posamentier, C.A. Ross and J.C. Van Wagoner), *SEPM Spec. Publ.*, **42**, 109-124.

Rasanen, M.E., Salo, J.S. and **Kaliola, R.J.** (1987) Fluvial perturbance in the western Amazon river basin: regulation by long term sub-Andean tectonics. *Science*, **238**, 1398-1401.

Reading, H.G. (1996) Sedimentary Environments: Processes, facies and Stratigraphy (3rd ed.). Blackwell Scientific Publications, 654 pp.

Rice, S.P. and **Churchs, M. (**2010) Grain-size sorting within river bars in relation to downstream fining along a wandering channel. *Sedimentology*, **57**, 232-251.

Rice, S.P., Churchs, M., Wooldridge, C.L. and **Hickin, E.J. (**2009) Morphology and evolution of bars in a wandering gravel-bed river; lower Fraser river, British Colimbia, Canada. *Sedimentology*, **56**, 709-736.

Russ, D.R. (1982) Style and significance of surface deformation in the vicinity of New Madrid, Missouri. *U.S. Geol. Surv. Prof., Pap.*, **1236**(H), 95-114.

Sacco, F. (1935) Le direttrici tettoniche trasversali nell'Appennino settentrionale. *Atti R. Acc. Lincei*, **2**, 371-375.

Salles T. and **Duclaux, G.** (submitted) Combined hillslope and channel processes simulation applied to landscape and alluvial system modelling. *Earth Surf. Proc. Land*.

Salvador, A. (1987) Unconformity bounded stratigraphic unit. *Geol. Soc. Am. Bull.*, 98, 232-237.

Salvador, A. (1994) International Stratigraphic Guide. A Guide To Stratigraphic Classification, Terminology and Procedure. IUGS, Boulder, CO, 213 pp.

Schumm, S. A. (1986). Alluvial river response to active tectonics. In: *Active Tectonics*, pp. 80–94. National Academy Press, Washington, D.C.

Schumm, S.A. (1993) River response to base-level change: Implications for sequence stratigraphy. *J .Geol.*, **101**, 279-294.

Schumm, S.A., Dumont, J.F. and **Holbrook, J.M.** (2000) Active Tectonics and Alluvial Rivers. Cambridge University Press, Cambridge, U.K., 276 pp.

Schwartz, R. (1982) Broken Early Cretaceous foreland basin in southwestern Montana: sedimentation related to tectonism. In: *Geologic Studies of the Cordilleran Thrust Belt* (Ed. R.B. Powers), pp. 159-183. Rocky Mountain Association of Geologists, Denver, CO.

SESAME (2004) Guidelines for the implementation of the H/V spectral ratio technique on ambient vibrations. Measurements, processing and interpretation, WP12 European commission - Research general directorate, project no. EVG1-CT-2000-0026 SESAME, report D23.12.

Shanley, K.W. and **McCabe, P.J.** (1991) Predicting facies architecture through sequence stratigraphy: an example from the Kaiparowits Plateau, Utah. *Geology*, **19**, 742-745.

Shanley, K.W. and **McCabe, P.J.** (1994) Perspectives on the sequence stratigraphy of continental strata: report of working group at the 1991 NUNA Conference on High Resolution Sequence Stratigraphy. *AAPG Bull.*, **74**, 544-568.

Signorini, R. (1935) Linee tettoniche trasversali nell'Appennino settentrionale. *Rendiconti R. Accad. Naz. Lincei*, **21**, 42-45.

Simms, A.R., Anderson, J.B., Taha, Z.P. *and* **Rodriguez, A.B**. (2006) Overfilled versus underfilled incised valleys: examples from the Quaternary Gulf of Mexico. *In: Incised Valleys in Time and Space (Eds*. R.W. Dalrymple, D. Leckie *and* R. Tillman*), SEPM Spec. Publ.,* **85***, 117-139.*

Smith, G.A. (1986) Coarse-grained nonmarine volcaniclastic sediments: terminology and depositional process. *Geol. Soc. Am. Bull*, **97**, 1-10.

Smith, N.D. (1971) Transverse bars and braiding in the lower Platte River, Nebraska. *Geol. Soc. Am. Bull.,* **82**, 3407-3420.

Sohn, Y.K., Rhee, C.W. and **Kim, B.C.** (1999) Debris flow and hyperconcentated flood-flow deposits in an alluvial fan, northwestern part of the Cretaceous Yongdong Basin, central Korea. *J .Geol*., **107**, 111-132.

Sømme, T.O., Jackson, C.A.L. and **Vaksdal, M.** (2013). Source-to-sink analysis of ancient sedimentary systems using a subsurface case study from the Møre-Trøndelag area of southern Norway: part 1-depositional setting and fan evolution. *Basin Res*. **25**(5), 489-511.

Swenson, J.B. (2005) Fluviodeltaic response to sea level perturbations: Amplitude and timing of shoreline translation and coastal onlap. *J. Geophys. Res. Earth Surf.*, **110**(F3), 2003-2012.

Tauxe, L. (2010) Essentials of paleomagnetism. Berkeley. University of California Press, **723**, 512 pp.

Tetzlaff, D. and **Harbaugh, J.** (1989) Simulating clastic sedimentation. Van Nostrand Reinhold, New York, 222 pp.

Thomson, S.N., Brandon, M.T., Reiners, P.W., Zattin, M., Isaacson, P.J. and **Balestrieri, M.L.** (2010) Thermochronologic evidence for orogen-parallel variability in wedge kinematics during extending convergent orogenesis of the northern Apennines, Italy. *Geol. Soc. Am. Bull.*, **122**(7-8), 1160-1179.

Thorne, C.R., Zevenbergen, L.W., Pitlick, J.C., Rais, S., Bradley, J.B. and **Julien, P.Y.** (1985) Direct measurements of secondary currents in a meandering sand-bed river. *Nature*, **315**, 746-747.

Todd, S.P. and **Went, D.J.** (1991) Lateral migration of sand-bed rivers: examples from the Devonian GlashabegFormation, SW Ireland and the Cambrian Alderney Sandsone Formation, Channel Islands. *Sedimentology*, **38**, 997-1020.

Tucker, G. and **Hancock, G.** (2010) Modelling landscape evolution. *Earth Surf. Proc. Land.*, **35**, 28-50.

Turowski, J. M., Lague, D., Crave, A. and **Hovius, N.** (2006) Experimental channel response to tectonic uplift. *J. Geophys. Res.*, **111**(F3), DOI: 10.1029/2005JF000306.

Twidale C.R. (1971) Structural Landforms. Australian National University Press, Canberra, 247 pp.

Vail, P.R., Mitchum, R.M. and **Thompson, S.** (1977) Seismic stratigraphy and global changes of sea level, part 4: global cycles of relative changes of sea level. *Mem. Am. Petrol. Geol.*, **26**, 83-97.

Van Wagoner, J.C., Mitchum, R.M., Campion, K.M. and **Rahmanian, V.D.** (1990) Siliciclastic sequence stratigraphy in well logs, cores, and outcrops: concepts of high-resolution correlation of Time and Facies. *AAPG., Methods in Exploration Series 7*, 55 pp.

Vincent, S.J. (2001) The Sis palaeovalley: a record of proximal fluvial sedimentation and drainage basin development in response to Pyrenean mountain building. *Sedimentology*, 48, 1235-1276.

Warner, J.C., Sherwood, C.R., Signell, R.P., Harris, C.K. and **Arango, H.G.** (2008) Development of a three-dimensional, regional, coupled wave, current, and sediment-transport model. *Comput. Geosci.*, **34**(10), 1284-1306.

Watson, G. (1983) Large sample theory of the Langevin distribution. *J. Stat. Plan. Inference*, **8**, 245-256.

Whipple, K.X. (2004) Bedrock rivers and the geomorphology of active orogens. *Annu. Rev. Earth Planet. Sci.*, **32**, 151-185.

Williams, G.P. (1984) Paleohydrologic equations for rivers. In: *Developments and Applications of Geomorphology* (Eds. J.E. Costa and P.J. Fleisher), pp. 343-367. Springer Berlin Heidelberg.

Willgoose, G. (2005) Mathematical modeling of whole-landscape evolution. *Annu. Rev. Earth Planet. Sci.*, **33**, 443-459.

Wright, V.P. and **Marriot, S.B.** (1993) The sequence stratigraphy of fluvial depositional systems: the role of floodplain sediment storage. *Sed. Geol.*, **86**, 203-210.

Wright, V.P. and **Marriott, S.B.** (2007) The dangers of taking mud for granted: lessons from Lower Old Red Sandstone dryland river systems of South Wales. *Sediment. Geol.*, **195**(1), 91-100.

Wu, W. (2007) Computational River Dynamics. Taylor and Francis, 494 pp.

Wu, W., Wang, S.S. and **Jia, Y.** (2000) Nonuniform sediment transport in alluvial rivers. *J. Hydraul. Res.*, **38**(6), 427-434.

Zaitlin, B.A. and **Schultz, B.C.** (1984) An estuarine-embayment fill model from the Lower Cretaceous Mannville Group, west-central Saskatchewan. In: *Mesozoic of Middle North America* (Eds. D.F. Stott and D.J. Glass), *Mem. Can. Soc. Petrol. Geol.*, **9**, 455-469.

Zaitlin, B.A., Dalrymple, R.W. and **Boyd, R.** (1994) The stratigraphic organization of incised valley systems associated with relative sea-level change. In: *Incised-Valley Systems: Origin and Sedimentary Sequences* (Eds. R.W. Dalrymple, R. Boyd and B.A. Zaitlin), *SEPM Spec Publ*, **51**, 45-60.

Zhang, R.J. (1989) Sediment dynamics in rivers. Water Resources Press.

Acknowledgments

I want to thank all the people that, scientifically and morally, helped me to keep going in the PhD and thesis period.

In particular I want to express my eternal gratitude to my supervisor Dr. Massimiliano Ghinassi, for supporting me ever, for being always present and for teaching me the best road to follow in geology and research. Thank to you this PhD was a fantastic adventure! I want to say thank you not because this is the end (because it's not), but because however you deserve it.

Million thanks to my co-supervisor Dr. Tristan Salles for giving me the awesome Australian opportunity, for helping me and introducing me in the modeling world. Thanks to you and Guillaume Duclaux for giving me the opportunity to use LECODE and to work with you, guys!

Special thanks go to Andrea Brogi for his structural support and regional advises.

I thank Mauro Aldinucci for reviewing with attention my papers.

Edoardo Dallanave, Paolo Billi, Rita Deiana and Jacopo Boaga for the data provided me for achieving the best success of my work.

Ivan Martini, Alessandro Ielpi and Katarina Gobo for helping me with the english translations and during the field-work and for sharing with me the PhD in sedimentology.

There are no words to thank FEDE the partner of my life to be my love, my best friend and my best fan and believe and support my soul, for giving me always the energy to improve me and to aim high. Without your love, your glee and your smile this goal could not have the same taste. Thanks also for your surprises.

Special and sincere thanks Paola and Franco, my parents to instill on me self-esteem, positivity and power. Never tired to cheer me up, to support (through words and facts) my goals and me and to advise the best for me. You are the best life example that a daughter can have!! I deeply love you.

Marcella Roner is here expressly thanked for her material (indispensable) and psychological support, always traceable and never tired! You look and behave like an angel!

Special thanks are for Benedetta Andreucci that taught me the right way to work and act, as an elder sister. Giant thanks also for Ada Castelluccio for her vivacity and smile, always good for a laugh. You, girls, are the best office mate, ever! Last thesis days were awesome with you!

Thanks to Giovanni Gattolin and Laura Parisio for share with me the hard thesis period with irony and laughters.

Thank you "flag-rising company", Marcella with Giorgia Moscon and Nicola Boscaini, to start with me the Ambra adventure (world center).

Thanks to the Geology Family (Cogno, Bosca, Ire, Fabri, Paolo, Manu, Marcy, Gio, La) to start with me Geology courses. This is the crowning of our passion.

Thanks to my sista Cly, Cristina, Zorro, Ziamariella, Zioggianni…for worring about me every day and for cheer me up!

Thanks to all the coffee-pod company for their congeniality.

This goal and all of these people helped me to grow.

Geological Map of the Pliocene-Pleistocene deposits of Ambra and Ombrone valleys: (Northern Siena Basin, Tuscany, Italy)

Bianchi V.(1), Ghinassi M.(1), Aldinucci M.(2), Boscaini N.(3), Martini I.(4), Moscon G.(1), Roner M.(1)

1 Geosciences Department, University of Padova, 35124 Padova, Italy
2 Weatherford Petroleum Consultants AS, 5147 Bergen, Norway
3 via J.F. Kennedy, 14, Sant'Ambrogio di Valpolicella, 37010 Verona, Italy
4 Department of Environment, Earth and Physical Sciences, University of Siena, 53100 Siena, Italy

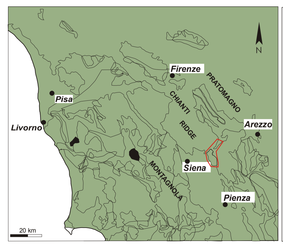

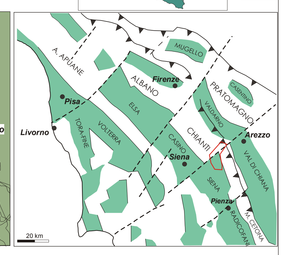

Holocene deposits

(fl) Cross to plane-parallel stratified pebbly sand with gravelly lenses. *Fluvial environment*

(ac) Well-stratified to massive silty to gravelly sand. *Alluvio-colluvial environment*

(cl) Massive cobble- to pebble-sized subangular gravel. *Colluvial environment*

Ionian deposits

Terraced deposits. Cross to plane-parallel stratified sand with subordinated gravelly lenses. Massive, pedogenized silty sand.

Terraced deposits of Ombrone Creek | **Terraced deposits of the Ambra Creek (II order)** | **Terraced deposits of the Ambra Creek (I order)**

Calabrian deposits (Allounit 2)

(V2pl) Massive, organic-rich mud containing abundant *Bythinia* gastropods shells. Pedogenized mud layers with roots traces. *Shallow lake to palustrine environment.*

(V2fla) Massive, pedogenized mud with organic-rich horizons and isolated, lensoid sandy bodies floored by clast-supported gravel. Sand is medium to coarse and ranges from plane parallel- to cross-stratified. *Fluvial environment.* Relict of floodplain morphology.

(V2af) Pebble to cobble sized gravel with medium to fine sand. Gravel forms erosive-based lensoid units ranging from massive to cross-stratified. Sand forms tabular, plane-parallel stratified beds locally bearing root traces. *Alluvial fan environment.*

(V2flb) Cross- to plane-parallel stratified pebbles with subordinate sand. Gravel is clast-supported and forms erosive-based lensoid bodies. Sand ranges from plane-parallel stratified to ripple-cross laminated. *Fluvial environment.*

Gelasian-Calabrian deposits (Allounit 1)

(V1) Cross- to plane-parallel stratified pebbles to cobbles with subordinate sand and mud. Gravel is clast-supported and forms erosive-based lensoid bodies. Sand ranges from cross- to plane-parallel stratified. Mud is massive and bear pedogenized horizons. *Fluvial environment.*

Zanclean-Piacenzian deposits

(Pl) Medium to fine sand with mud and subordinate gravel. Sand is bioturbated and bears abundant marine shells and shell fragments. Mud contain scattered shells. Gravel is planar- to cross-stratified and forms erosive-based lenses. *Coastal shallow-marine to alluvial environment.*

Pre-Neogene bedrock

(TU) *Tuscan Unit.* Macigno Fm., Scaglia toscana

(ELU) *External Ligurian Unit.* S. Fiora, Monte Morello

(SU)*Subligurian Unit.* Canetolo Fm., Groppo del Vescovo Gr., M.Senario Fm.

Certain/inferred fault
Thrust fault
Syn-sedimentary fault/fault zone
Bedding
Alluvial fans
Fossiliferous site
Well-core data

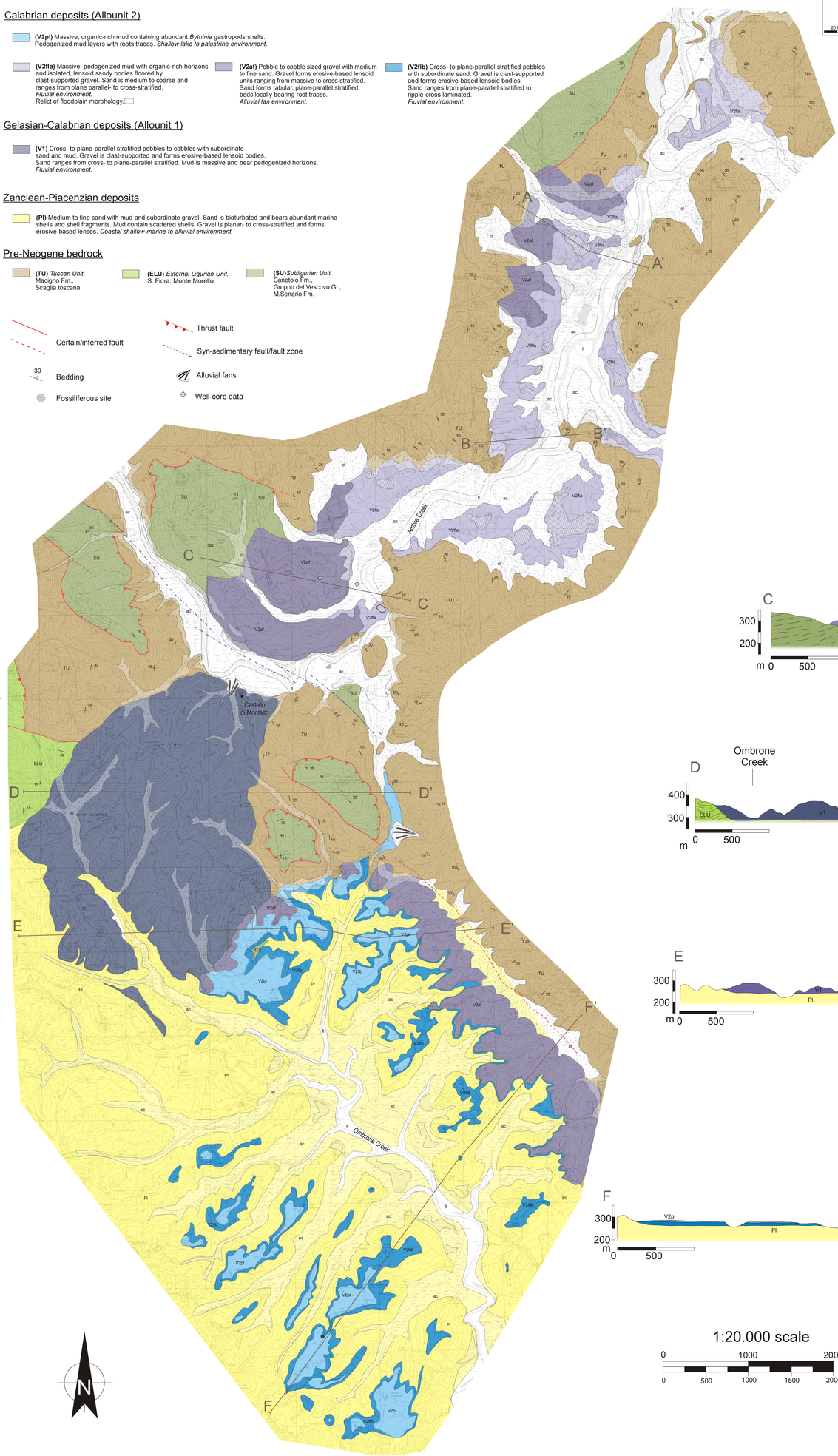

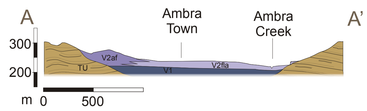

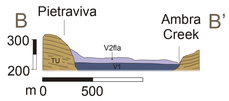

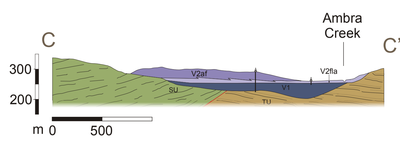

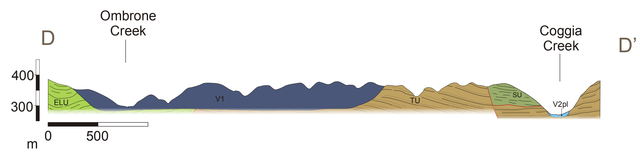

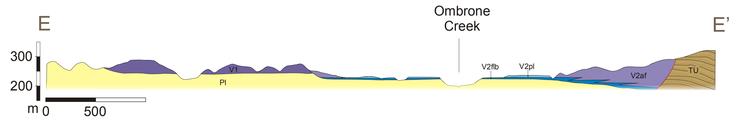

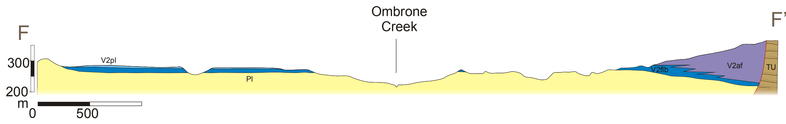

1:20.000 scale

0 1000 2000 m
0 500 1000 1500 2000

GEOGRAPHICAL CHARACTERISTICS OF THE GEOLOGICAL MAP

Topographic base: CTR map (287, 288, 297 sheets)
Coordinate System: Gauss-Boaga
Projection: Transverse Mercator
Datum: Roma40 western zone
Units: Meter